Final Report

U.S. DOT
Pipeline and Hazardous Materials Safety Administration

Competitive Academic Agreement Program (CAAP)

Contract #: *DTPH56-16-H-CAAP03*

Development of New Multifunctional Composite Coatings for Preventing and Mitigating Internal Pipeline Corrosion

Department of Civil and Environmental Engineering
North Dakota State University, Fargo, ND 58105

Technical Information Page

Organization Name:	*Department of Civil and Environmental Engineering* *North Dakota State University (NDSU)* *Fargo, ND 58105 (https://www.ndsu.edu/cee/)*
Contact Information	*Zhibin Lin, PhD, P.E.* *Associate Professor* *NDSU Dept #2470, Fargo, ND 58108, Tel: 701-231-7204, Fax: 701-231-6815, Email: Zhibin.lin@ndsu.edu* *Co-PIs: Dr. Dante Battocchi (NDSU), Dr. Xiaoning Qi (NDSU)*
Program Area:	*Preventing or Mitigating Pipeline Corrosion*
Title:	*Development of New Multifunctional Composite Coatings for Preventing and Mitigating Internal Pipeline Corrosion*
Contract #:	*DTPH56-16-H-CAAP03*
Main Objective:	*High performance protective coatings for pipeline*
Original Proposal Abstract:	*Corrosion is one of the leading causes of failures of metallic pipelines in the United States and worldwide. Severe corrosion-induced pipeline accidents in recent years have raised more widespread attention to safety issue that brings high risk to people's life, and surrounding environments. This study aims to develop and implement new high-performance multifunctional composite coatings, striving for lifetime preventing and mitigating internal pipeline corrosion for onshore gas and liquid transmission pipelines. By taking advantage of the unique properties of high performance polymer primers and nanoparticles and nanofibers as additives, the new functionalized high-performance composite coatings will significantly reduce interrelated corrosion-fouling-wear issues, effectively elongate the performance life of metallic pipelines and ultimately protect them under severe corrosive environments.* *The new multifunctional composite coating will be highly paid off for next-generation pipelines lifetime protection in terms of superior ant-fouling resistance and abrasive resistance, and long-lasting corrosion resistance, thereby introducing tremendous economic benefits. The development and utilization of the coating technologies can dramatically enhance operational safety in metallic pipelines in terms of reduction of coating maintenance and repaint costs, as well as corrosion-related accidents, injuries, fire and delays, and will have a significant impact on U.S. PHMSA operations, support and implement corrosion control practices and will ultimately improve the quality and thus structural safety of constructed pipe structures.*

Table of Contents

SUMMARY OF ACCOMPLISHMENTS

Technical Accomplishments (patents, invited talks and keynotes, publications, awards)

(I) Patents

1. Zhibin Lin, Xingyu Wang (2020), Robust Self-Cleaning Nanoparticle-Polymer Coatings
   IP Disclosed to North Dakota State University, No. 63/045,426*, 06/29/2020 Patent pending Attorney Docket No. 016.0043-PR00*

(II) Invited talks and keynotes

1. **(Keynote)** "Machine learning, data analytics and information fusion for structural health monitoring", *2019 International Conference on Artificial Intelligence, Information Processing and Cloud Computing, Dec. 19-21,* Sanya, China.

2. **(Invited Talk)** "Design and Characterization of Functional Nanoengineered Epoxy-Resin Coatings for Pipeline Corrosion Control ", *Coating Trends and Technologies 2019, Sept. 10-11,* Rosemont, IL, USA.

(III) Publications

Peer-Reviewed Journal Publications (: corresponding author)*

1. Xingyu Wang**,** Zhibin Lin* (2020) "Robust Self-Cleaning Nanoparticle-Polymeric Coating for Metallic Structure Application" ***ACS Applied Materials & Interfaces (submitted)***

2. Xingyu Wang**,** Zhibin Lin* (2020) "Robust, Superhydrophobic Anti-corrosion Coating Prepared by PDMS Modified Epoxy Composite with Graphene/Nano-silica Hybrid Nanofillers" ***Surface and Coatings Technology (submitted)***

3. Xingyu Wang**,** Zhibin Lin* (2020) "Mechanical, Electrochemical, and Tribological Properties of New Multifunctional GNP/NS Binary-Filler-Based Nanocomposite Coatings" ***Progress in Organic Coatings, Accepted.***

4. Xingyu Wang**,** Zhibin Lin* (2020) " Enhanced Protection Properties for Polymeric Coatings Reinforced by Carbon-based Nanoparticles for AISI 1018 Low-Carbon Steel Weldment" ***ASCE Journal of Materials in Civil Engineering, Accepted.***

5. Xingyu Wang**,** Matthew Pearson, Hong Pan, Mingli Li, Zi Zhang, Zhibin Lin* (2020) "Nano-Modified Functional Composite Coatings for Metallic Structures: Part I-Electrochemical and Barrier Behavior" ***Surface and Coatings Technology,*** 126286.

6. Xingyu Wang**,** Fujian Tang, Qi Cao, Xiaoning Qi, Hong Pan, Zhibin Lin* and Dante Battocchi (2020) "Nano-Modified Functional Composite Coatings for Metallic Structures: Part II-Mechanical and Damage Tolerance " ***Surface and Coatings Technology,*** 126274.

7. Xingyu Wang, Fujian Tang, Qi Cao, Xiaoning Qi, Matthew Pearson, Mingli Li, Hong Pan, Zi Zhang, and Zhibin Lin* (2020) "Comparative study of carbon nanotubes, graphene, and fullerene C60 additives for enhanced carbon-based polymer nanocomposites." ***Nanomaterials***, Vol. 10, p.838.

8. Xingyu Wang, Xiaoning Qi, Zhibin Lin*, Dante Battocchi, and Xi Chen (2019) "Enhanced Protective Coatings Based on Nanoparticle fullerene C60 for Oil & Gas Pipeline Corrosion Mitigation." ***Nanomaterials***, Vol. 9, p.1476.

9. Xingyu Wang, Fujian Tang, Xiaoning Qi, and Zhibin Lin* (2019) "Mechanical, Electrochemical, and Durability Behavior of Graphene Nano- Platelet Loaded Epoxy-Resin Composite." ***Composites Part. B: Engineering***, Vol. 176, p.107103

10. Xingyu Wang, Xiaoning Qi, Zhibin Lin*, and Dante Battocchi. (2018) "Graphene-Reinforced Composites for Protective Coatings for Oil and Gas Pipelines." ***Nanomaterials***, Vol. 8, p. 1005.

Peer-Reviewed Conference Publications and Posters (: corresponding author)*

1. Xingyu Wang, Fujian Tang, Qi Cao, Xiaoning Qi, and Zhibin Lin* (2020) "Nanoparticles for improved functional composite coatings for corrosion control of underground and marine civil infrastructure systems" *International Conference on Bridge Maintenance, Safety and Management 2020, June 28-July 2,* Hokkaido, Japan.

2. Xingyu Wang[+], Fujian Tang, Xiaoning Qi, Matthew Pearson, Zhibin Lin*, and Dante Battocchi (2020) "High-Performance Anti-Corrosion Coatings Based on the Inclusion of Nanomaterials", *Corrosion 2020, March 15-19,* Houston, TX, USA.

3. Xingyu Wang[+], Xiaoning Qi, Dante Battocchi, Zhibin Lin*, and Matthew Pearson (2020) " Corrosion behavior of weldment with and without coatings", *Corrosion 2020, March 15-19,* Houston, TX, USA.

4. Xingyu Wang[+], Xiaoning Qi, Mingli Li, Zhibin Lin*, and Dante Battocchi (2019) "Characterization of Graphene Reinforced Epoxy Coatings for Internal Surface of Oil and Gas Pipelines ", *ASCE Pipelines 2019 Conference, July 21-24,* Nashville, TN, USA. & *ASCE Pipelines 2020 Conference, Aug. 9-12,* San Antonio, TX, USA

5. Xingyu Wang[+], Xiaoning Qi, Matthew Pearson, Mingli Li, Zhibin Lin*, and Dante Battocchi (2019) "Characterization of Nano-Particle Reinforced Epoxy Coatings for Structural Corrosion Mitigation", *Bridge Engineering Institute Conference 2019, July 22-25,* Honolulu, HI, USA.

6. Xingyu Wang[+], Xiaoning Qi, Matthew Pearson, Zhibin Lin*, and Dante Battocchi (2019) "Nano-Modified Protective Coatings for Pipeline Corrosion Control and Mitigation", *2019 TechConnect World Innovation Conference, June 17-19,* Boston, MA, USA (abstract and poster).

(IV) Awards

Zhibin Lin, Research of the Year, College of Engineering | 2018
North Dakota State University, ND, USA.

Xingyu Wang, Nominated for Doctoral Dissertation Fellowship | 2020
North Dakota State University, ND, USA.

Xingyu Wang, Winner of Graduate Research Assistance of the Year | 2020
North Dakota State University, ND, USA.

Education Accomplishments (student recruitment, outreach activities)

(I) Student recruitment
Doctoral Dissertation
Student: Xingyu Wang
Title:

"High-performance Carbon-based Nanocomposite Coatings: Fabrication, Characterization, and Their Application for Metallic Infrastructures" North Dakota State University, Department of Civil & Environmental Engineering

Estimated graduation date: May 2021

Master's Thesis

Student: Matthew Pearson

Title:

"Delamination Characterization of Nanocomposite Epoxy Coatings by Incorporating Acoustic Emission" North Dakota State University, Department of Civil & Environmental Engineering

Estimated graduation date: May 2021

(II) Outreach activities

Mentoring over eight high-school students working on related research for ND Governor high school summer program | 2016-2019

Milestones

In this project, one primary deliverable aims to develop a high-performance coating for the internal surface of oil & gas pipelines. According to the experimental study, the new high-performance coating has a significant advantage over existing coatings when tailored to provide multifunctional protection for extended long-term pipeline performance against corrosion fouling-wear issues, which cannot be offered by other systems in the market.

Results revealed that the integration of these reinforcements had improved the coating's overall performance, as the coating consisted of outstanding anti-corrosion performance, wear resistance, mechanical strength, water-repellency property, and damage tolerance. Moreover, the facile fabrication method and simple application procedure exhibited its potential toward large-scale commercialization for metallic infrastructures.

By investigating the performance and micro/nano level characterization, the research offered an opportunity to understand the relationship between the deposition parameters and the coating functionality, the mechanical properties of the coating will be. The research work comparatively evaluates the influence of these nanofillers on nano-reinforcement, primarily, an experimental investigation of the tribological, mechanical and electrochemical properties.

For single & hybrid filler nanocomposites, even literature reviews demonstrated that the investigations on these nanofiller/polymer composites, due to widely varied composite designs, different dispersion procedures, and experiment methods, limited and inconsistent conclusions could be made that hindered evaluating the effects of various nanofillers on their tribological, mechanical and electrochemical performance. As a result, without a comparative experiment design and consistent criteria, there was no clear information available to guide scientists and engineers on how to properly select different nanofillers and how to effectively design promising nanocomposites. Especially when specific properties are desired, this report is an opportunity to make a comparison between additives by taking the advantage of experimental results.

Furthermore, this research work offered an excellent solution for mitigating corrosion and understanding the performance of advanced materials and practical guidelines for their implementation in the durability of civil infrastructure. The proposed study will also overcome the limitations of existing methods and the research findings can significantly benefit civil engineering fabricators, designers, and contractors, States and U.S. department of transportations.

In summary, the highlights of this research work include:

(a) New high-performance nanocomposite coatings exhibited superior anti-corrosion resistance, water-repellency, mechanical and tribological properties, thereby enabling protecting metallic oil/gas pipelines in long term.

(b) A systematic experimental and analytical investigation used for the development and characterization of nano-modified high-performance composite coatings provide scientists and engineers with the opportunity to select different nanofillers and design promising nanocomposites effectively properly.

CHAPTER 1. INTRODUCTION

1.1 BACKGROUND

1.1.1 Corrosion of oil/gas metallic pipelines

The United States consists of over 2.6 million miles of gas and oil pipelines. Pipeline spill or explosion accidents occurred in recent years, as shown in Fig. 1, while corrosion is one of the leading causes of failures of these metallic pipelines in the United States.

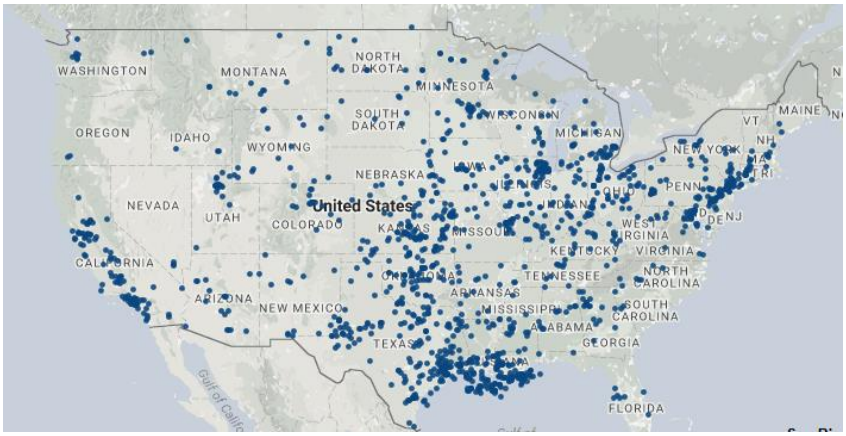

Figure 1.1: Pipeline accidents in the United State
(Photos from http://projects.propublica.org/pipelines/)

Corrosion of onshore gas and liquid transmission pipelines were responsible for over $7 billion cost. PHMSA data revealed that corrosion still maintains as high as over 20% of all pipeline failure causes in the past thirty years since 1980. Take North Dakota as an example, North Dakota has become the second-leading oil-producing state in the nation, while there are ever-increasing pipeline accidents over the last decade, as listed in Table 1.1. Some statistics data worldwide have also demonstrated that corrosion or corrosion-induced damages/defects were mainly blamed, which eventually caused the tragedies. Apart from huge financial losses due to damaged assets, corrosion or corrosion-induced damages/defects causes catastrophic failures, accidents and loss of precious lives. These severe corrosion-induced pipeline accidents in recent years have raised more widespread attention to safety issue that brings high risk to people's life, and surrounding environments.

Table 1.1: Pipeline accidents in recent years at North Dakota.

Accident	Location	Year	Loss
Pipeline spill	Tioga	2014	One gas pipeline exploded and burned
Pipeline spill	Tioga	2013	865,000 gallons
Pipeline spill	Sargent County	2011	Spilling 400 barrels of crude oil
Pipeline spill	Neche	2010	Releasing 3,784 barrels of crude oil
Pipeline spill	Mantador	2004	Residents were evacuated, and a rail line was shut down
Pipeline spill	Barnes County	2003	Releasing 9,000 barrels of propane

Pipeline ruptured	Bottineau	2001	1.1 million US gallons (4,200 m^3) of gasoline burned
Pipeline spill	Harwood	2001	Spilling 40 barrels of fuel oil

1.1.2 Internal corrosion of oil/gas metallic pipelines

Internal pipe surface is vulnerable to corrosion damage. Examples of this are the pipeline ruptures in Alberta, Michigan and BP's Prudhoe Bay, Alaska, pipeline that was shut down due to multiple sections losing 70% or more of wall thickness as a result of internal corrosion. The U.S. Department of Transportation Office of Pipeline Safety estimates that internal corrosion causes approximately 15% of all incidents occurring in oil and gas transmission pipelines with an annual industry cost of almost $15 billion US dollar per year. Studies conducted in the United Kingdom and the Middle East have come to similar conclusions. In some areas, as clearly illustrated in Fig. 1.2, the internal pipe corrosion could dominantly account for 51% of total corrosion-related breakdowns.

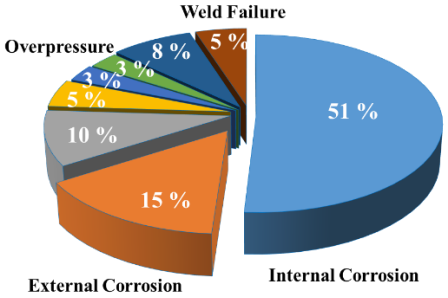

Figure 1.2: Dominant internal pipe corrosion (data from Nalli, 2012)

One of the main challenges facing the pipeline industry with respect to managing pipeline corrosion is the difficulty in predicting internal corrosion. Internal corrosion on onshore gas and liquid transmission pipelines often initiates when pipe surface locally reacts with a combination of contaminants, including moisture, oxygen, carbon dioxide, chlorides or sulfur compounds present in gas/liquid. As identified early, corrosion is also caused and sustained due to combined effects from fouling/microorganisms and local erosion on the internal pipe surface. As clearly illustrated in Fig. 1.3, localized pitting is responsible for 79% of all corrosion mechanisms. Such localization could be responsible for combined/interrelated effects due to pitting, fouling, and wear. As a result, existing technologies face a challenge in designing favorable protective coatings for harsh environment.

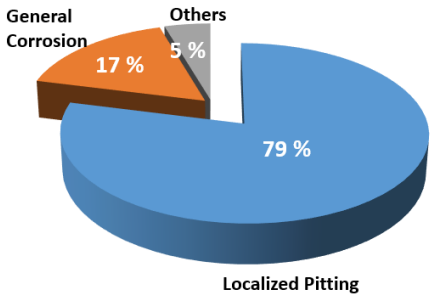

Figure 1.3: Detailing in pipeline corrosion (data from PHMSA 2010-present)

1.1.3 Protective coatings of oil/gas metallic pipelines

Protective coatings act as barriers between the steel substrate and the environment in order to resist the transport of water, oxygen, ions and other aggressive species to the coating metal interface. Protective coatings for internal corrosion control have a wide variety of types, including single or dual-layer fusion bonded epoxy coatings (FBE), coal tar, asphalt enamels, Epoxy Resin lining, Polyurethane/Polypropylene (PE/PP) lining, and other fiber-reinforced polymer (FRP) linings.

1.1.4 Challenges for existing protective coatings

As typically observed in performance of protective coating in pipelines, the percolation of afore mentioned aggressive species leads to coating delamination and under-film corrosion, and the loss of corrosion protective function. Therefore, lessons from major failure modes of coating systems in pipelines can attribute to valuable information for selection of suitable coating systems. Our review of past cases studies and practices indicates that the failure of coatings focuses on:

1) Low mechanical and damage tolerance. Coatings with insufficient damage tolerance often end up with premature degradation and eventually failure. Lab-proven coatings often not perform well in the field. Local coating imperfections and mechanical damage during shipping and handling or operation at in-service stage often causes disbondment and under-film corrosion. Wear is another key factor affecting the performance of the coatings, and low mechanical abrasion of a coating could fail prematurely as a pipeline often suffers from erosion due to flow change, even though the coating is designed with a high corrosion resistance. Thus, there is a huge demand for an alternatively cost-effective coating system for production of engineering components with excellent corrosion resistivity, as well as high damage tolerance.

2) Low long-term durability. The protective coatings used in the oil/gas metallic pipelines is often exposed to frequent cycles of surface abrasion and wear as well as varying operational environments. This is a partial explanation of the common observation that the initially-proved coatings with a high corrosion resistance could not perform well in the long run, as initially predicted. Thus, design of a protective coating with long-term performance could really extend their service life for their real-world applications.

3) Low anti-fouling resistance. Among all factors contributing to the failure of coatings and their protected metallic substrate, the water uptake process is important since water is the medium for the diffusion of oxygen and ions, and it also nucleates coating delamination and blistering. Water and other liquid/biological fouling often accelerate failure of the coating. Thus, effectively isolating wetness away from the coatings can extend their lifespan and thereby truly protect metallic substrate (pipe walls), which yields the motivation in this study for seeking new concept of a superhydrophobicity.

4) Low resistance to combined effects of corrosion, fouling, and wear. Most existing coatings are often designed in one specific function, either high corrosion resistance or anti-fouling capacity. However, lack of protective coatings has incapability of resisting combined effects: corrosion, fouling and wear/erosion, where internal pipe surface may suffer from.

This understanding drives us to propose new high-performance composite coatings in this project that may be possible to reduce internal corrosion even further. The new high-performance coating

is expected to have a significant advantage over existing coatings when it is tailored to provide multifunctional protection for extended long-term pipeline performance against corrosion fouling-wear issues, which cannot be offered by other systems in the market.

1.2 OBJECTIVES

As the high-performance anti-corrosion coatings have been gaining increasing attention in oil and gas pipeline application, this research work intends to develop new multifunctional coatings to fulfill these demands. To be able to effectively protect the metallic substrate against the harsh corrosive environments in the oil and gas pipelines, the desirable properties for the multi-functionality of composite coatings include but not limited to:

- Excellent corrosion protection properties
- Excellent abrasion-resistance
- Excellent mechanical properties
- Excellent long-term durability and damage tolerance
- Reduced cost and time consumption
- Environment-friendly

1.3 ORGANIZATION OF THE REPORT

This report is organized into sixteen chapters as follows: the first part includes the introduction and background about protective coatings in Chapters 1 and 2. A review of existing practices and research on coatings is provided in Chapter 2. The experimental methodology and techniques employed in this research work is proposed in Chapter 3. Chapter 4 aimed for polymer screening process for nanocomposite coatings and a polyamine cured bisphenol-A epoxy coating was selected in this work. Chapter 5 is to explore evaluation of the overall performance coating reinforced by single nanofillers. Chapter 6 is to evaluate the overall performance coating that reinforcement by hybrid nanofillers, and select the optimal composition. Chapter 7 aims to propose the enhancement of the selected nanocomposite coatings for pipeline application. Chapter 8 is to explore the robust, high-performance multifunctional coatings for pipeline applications. Chapter 9 is to unveil the failure mechanism of coatings. Chapter 10 tends to explore the performance of the coating on the weldment. Chapter 11 is to briefly summarize the education and outreach activities associated with this project. Conclusions are summarized in Chapter 12.

CHAPTER 2. LITERATURE REVIEW

2.1 BACKGROUND

Polymeric coatings are widely accepted for protecting metallic structures in civil, mechanical, and aerospace engineering by forming a barrier on top of the metallic substrate against aggressive chemicals and environmental attack. While a wide number of protective polymeric coatings have been developed for engineering applications, the biggest challenges for most protective coatings are their long-term durability and damage tolerance.

As an emerging technology, high-performance composite coatings through the inclusion of nanoparticles as additives have recently demonstrated great potential and attracted significant interest in engineering applications. Recent studies revealed that the inclusion of nanomaterials in polymer matrix led to various enhancements. The nanoparticles reinforced polymer has been studied and became one of the most relevant applications for nanoparticles since the discovery of carbon nanotube in the 1990s [1]–[3]. The use of polymer reinforcement is one of the most promising applications for nanoparticles due to the unique properties provided by nanoparticle reinforcement. [2]. The nanocomposites have displayed excellent mechanical, thermal and electronic attribution which made them as advanced multifunctional material [4]. Thus, this chapter aims to present a literature study for the research work in this project, which includes: 1) single filler reinforced nanocomposite, 2) hybrid filler reinforcement nanocomposite, 3) dispersion of nanofiller in the polymeric matrix, and 4) modification of polymeric resin.

2.2 OVERVIEW OF PROTECTIVE COATINGS

2.2.1 Single Nanofiller Reinforcement

The nanoparticles has been studied by many researchers, and this topic became one of the most relevant applications for nanoparticles since the discovery of carbon nanotube in the 1990s [1]–[3]. The nanofillers can be defined as zero, one, or two-dimensional materials which indicate there are 0, 1, or 2 dimensions are larger than 100nm, correspondingly. Graphene (GNP), carbon nanotubes (CNT) and nanosilica (NS) are typical 2D, 1D, and 0D materials; thus, their unique shapes and sizes will provide a different combination of properties [1], [5].

Polymer reinforcement is one of the most promising applications for nanoparticles as the unique properties of nanomaterials can be used to develop multi-functional composites [6]. Recent studies have found out that adding different carbon nanomaterials into a polymer matrix will lead to various enhancements. For example, the addition of nanodiamond (ND) particles leads to excellent biological properties, Carbon nanotubes (CNT) will significantly increase the mechanical and electrical properties, and improvements of thermal and mechanical properties by adding graphene nanoplatelets have also been investigated. [3], [7]–[12]

Graphene (GNP), a two-dimensional carbon nanomaterial with the building block of natural graphite, is currently the strongest known material [13]. It is a planar monolayer of carbon atoms with the C=C bond length of 0.142 nm.[14] Researchers' studies have shown that graphene has many extraordinary electrical, mechanical, thermal, and optical properties with high electron mobility (250,000 cm^2/Vs at room temperature), thermal conductivity (5000 $W\ m^{-1}\ K^{-1}$), and Young's modulus of 1 TPa [15]–[17]. Moreover, some derivatives of graphene, such as graphene

oxide (GO) and reduced graphene oxide (RGO), can also serve as effective barriers to ionic transport and abrasive-resistance enhanced additives in coatings.

Many researchers have been studied the anti-corrosion performance and barrier properties of graphene/polymer coatings [2], [18]–[21]. Liu et al. [18] fabricated graphene/epoxy coatings with two different contents, 0.5 and 1.0 wt.%. Their results showed that the presence of GNPs enhanced the corrosion resistance of the epoxy coating and the coating with 0.5 wt.% graphene exhibited the better performance. Chang et al. [19] discussed the impacts of the dispersion of graphene on the coating performance. Liu et al. [2] investigated the tribological and anticorrosion properties of epoxy coating reinforced by graphene nanoparticles. They observed that dramatic material degradation occurred when the content of graphene was higher than 0.5 wt.%, due to the agglomeration of the nanoparticles. Different from previous work [2], Yu et al. [20] found that higher content of graphene nanoparticles still provided high performance in resistance to corrosion and gas barrier. They evaluated the nanocomposites with varied contents of graphene from 0.5 to 2.0 wt.%, and they concluded that 2.0 wt. % of GNP additions achieved great improvement of anti-corrosion performance and gas barrier properties. Monetta et al. [21] experimentally evaluated the performance of graphene/epoxy coating with 1.0 wt.% of graphene nanoparticles. Their results indicated graphene improved the anticorrosion properties of polymers. They also pointed out that the curing process of epoxy was not affected by the addition of graphene, and no significant changes were found in adhesion and water repellency of the cured coating.

The studies have shown carbon nanotubes are also very strong with a high flexibility due to its C=C bonds which is similar to graphene nanoplatelets [13]. As discussed early, carbon nanotubes are described as a 1D carbon nanomaterial. A rolled- up narrow strip of monolayer graphene in a cylinder form is called single-wall carbon nanotube (SWNT). Multiwall carbon nanotubes (MWNT) can be obtained by adding many rolled-up concentric cylinders.[22] The diameters of single-walled carbon nanotubes can be around 0.4-2 nm with empty internal space. Carbon nanotubes have been observed excellent mechanical, thermal, and electric properties. The properties of carbon tubes will be different between SWNT and MWNT. For example, Young's modulus of SWNTs can be 1.25TPa and MWNTs can be as high as 1.8 TPa [13].

For example, when considering the CNT/polymer composites, much research work has been conducted to evaluate the mechanical properties and electrical conductivity of the composites. Jeon et al. [23] fabricated CNT/epoxy coating with three different contents, 0, 0.25, and 0.5 wt.%. Their results showed that an increase in adhesion strength of the coating, but a decrease impedance modulus. Zhang et al. [24] has prepared CNT/epoxy coating with higher content of CNT which was up to 40 wt.%, and observed that incorporation of CNT led to a decrease in impedance as well, hence, the conductive behaviors was increased. Cui. et al. [25] discussed the impacts of functionalized CNT in the tensile strength of epoxy coatings, and the tensile strength has increased by 57% compared with neat epoxy. Wernik and Meguid [26] evaluated the mechanical properties of CNT/epoxy with varied contents of CNT from 0.5 to 3.0 wt.%, and they concluded that 1.0 wt.% CNT additions gained the highest improvement of tensile strength, strain, and adhesion. Different from previous work, Zabet et al. [27] found the addition of CNT caused a reduction in mechanical properties due to the curing process was affected. Their results indicated the hardness and elastic modulus were significantly reduced in the samples with 2.8 wt.% of CNT. Moreover, Hernández-Pérez et al. [28] experimentally evaluated the tensile properties and conductivity of

CNT/epoxy. They found the addition of CNT enhanced the conductivity of the composite; however, very limited improvement of tensile properties was observed.

Moreover, there are many nano-phase materials could be used for assembling nanocomposite coatings. Successful applications of incorporating nano silica into polymers have been made by many researchers [29]–[34]. For NS/polymer composites, comprehensive studies were focused on tribological properties and anti-corrosion performance. Successful application of incorporating Nano silica into polymers have been made by many researchers [29]–[34]. In M. Conradi's work, 2 wt.% silica particles were dispersed into the epoxy matrix, and significantly enhanced hardness, damage resistance, adhesion, hydrophobicity, and corrosion barrier effect were observed [30]. Meanwhile, Kang pointed out that lower friction coefficient and higher water contact angle were also observed in EP/nano-SiO2 composite coatings with the proper amount of nano silica fillers [31]. Beside the surface properties, the EIS measurements indicated the corrosion barrier effect was significantly increased by incorporation of 2wt.% of nano silica particles [32]. The composites with a high volume of silica nanoparticles (up to 20wt.%) have been studied in Halder and Johnsen [33], [34]. The highest increase of tensile strength was observed in 5 wt.% of nanoparticles. Degradation was observed when a higher concentration of nano silica was added, which is attributed to larger sized agglomeration.

2.2.1 Hybrid Nanofiller Reinforcement

As discussed in the previous report, nanoparticles reinforced polymer has been studied by many researchers can be used to develop multi-functional composite coatings. The addition of CNT will significantly increase the mechanical and electrical properties, and improvements of thermal and mechanical properties by adding graphene nanoplatelets have also been investigated [3], [7]–[12]. However, researchers have pointed out that there are limitations of using one type of nanofillers in polymer matrices, for example, strong van der Waals forces between fillers lead to poorly dispersion and agglomeration. Furthermore, a hybrid filler system, which is synergized by the integration of different nanofillers, could be used to fabricate nanocomposites with a better dispersion state and stability. Moreover, better mechanical, electrical and thermal properties of composites were observed in these nanocomposites. [35], [36].

The combination of Carbon nanotubes and graphene nanoplatelets at different mix ratios were dispersed into the epoxy matrix, and the influence of mechanical and electrical properties was investigated in Yue's work. The presence of GNP has improved the dispersion of the CNT, and the hybrid filler forms a more robust network in the polymer matrix. Better interaction between nanofillers and epoxy matrix were observed. Meanwhile, the hybrid filler system leads to higher improvement of flexural properties and reduce the electrical percolation threshold [36].

The experimental study of hybrid nanofillers with CNT and GNP, CNT and nano silica, GNP and nano-silica at different mix ratios were performed in this study, and the results were presented in Chapter 5. The improvement of corrosion barrier properties, abrasion resistance, strength could be observed in these tested groups, but the bonding strength between the coating and steel substrate was significantly reduced regardless the types and mixing ratios of hybrid nanofillers which the low surface roughness of the nanocomposites could be the reason. Researchers have done many investigations to increase the adhesion between epoxy adhesive and steel substrate by incorporating nanofillers. Many successful works have pointed out that introducing the nano-

Al_2O_3 particles into the epoxy resin can significantly increase the bonding strength [37]–[39]. The influence on adhesion by incorporating several types nanoparticles has been studied in Zhai's work [38].

2.3 DISERPSION OF NANOFILLERS

The interaction between polymer and nanomaterials depends on the polarity, shape, and size of nanoparticles, hydrophobicity, reactive groups, solvent, resin, etc. The direct mixing method is considered only if the polymer has low viscosity. Generally, there are three strategies for incorporating carbon nanomaterials into polymer matrix: in situ intercalative polymerization, solution intercalation, and melt intercalation method [40].

The in-situ interactive polymerization method usually requires heat of radiation to initiate polymerization.[41] The nanocarbon is swollen within the liquid monomer before polymerization. There are many successful studies that prepared polymer nanocomposites by using this method. In Aldosari's study, a Polymethylmethacrylate–graphene (PMMA/RGO) nanocomposites were prepared by using in situ bulk polymerization method with two different techniques. In the first technique, graphite oxide was mixed with methylmethacrylate monomers before polymerized by using a bulk polymerization method with a radical initiator. To obtain the R-(GO-PMMA) composites, a reducing agent hydrazine hydrate was added, and the mixture was reduced by microwave irradiation. In the second approach, RGO-(PMMA) was obtained by the bulk polymerization of the mixture with a free radical initiator. The result was showing that the first method, which incorporated microwave irradiation, had better morphology, dispersion and thermal stability compared with the second method [42].

The melt intercalation method requires nanocarbon materials mixed into the polymer matrix in a molten state. The advantage of this approach is no solvent is needed during the process. During the elevation of temperatures, nanocarbon is mixed mechanically with a thermoplastic polymer. Then the polymer chains are intercalated to form nanocarbon/polymer composites. This method is usually be used to prepare thermoplastic nanocomposites, and the temperature could be hundreds of degrees Celsius [40] [43].

In solution intercalation method, nanocarbon is dispersed in a solvent which the solvent will dissolve the polymer. The solvent then is evaporated after mixing is finished, and nanocomposites will be obtained after this process. This method is the most commonly used method to fabricate for nanocomposites with carbon nanotubes. [4] In general, this method will use energetic agitation (sonication, stirring, etc.) to disperse nanocarbon in a solvent solution so that these nanoparticles will be uniformly distributed in the matrix.

The three mixing methods that discussed early were the most commonly used strategies for developing nanocomposites with nanocarbon materials. Few discussions with have been done during the weekly meeting between graduate students and PIs. The solution intercalation method will be considered first due to the following reasons.

First, solution intercalation method is the most commonly used method for developing nanocarbon/polymer composites. It has been proved that nanocarbon materials can be dispersed easily in a suitable solvent, such as water, acetone, chloroform, tetrahydrofuran (THF),

dimethylformamide (DMF) or toluene.[40] Second, in situ interactive polymerization and melt intercalation methods require either radiation or high temperature, which this high-energy consumption is not suitable for the proposed new multifunctional coatings. Compare with the nanocomposites obtained from melt intercalation method; it has been pointed out that the nanocomposites obtained by the solution intercalation method have higher electrical conductivity and lower percolation threshold [43].

A comprehensive literature study of fabricating nanofiller/polymer composites by using solution intercalation method has been done, and many successful studies have been done by researchers; hence, Table 2.1 summarized some researchers' works.

Table 2.1: Nanocarbon/polymer composites obtained by solution intercalation method

Matrix	Curing Agent	Solvent	Nanocarbon filler		Dispersion		Application method	Ref
			Type	Content	Sonication	Mechanical stirring		
Polyphenylene sulfide (PPS)	PFW	Ethanol aqueous solution	Graphene	0.4, 0.8, 1.5% wt.	30 min	10 min	Spary	[44]
Epon828	PACM20	THF	ND	2,4,12,18,25% vol.	5 min	N/A	Hot-press	[45]
Epoxy resin ML-520	HA-11	THF + CTAB	Oxidized ND	0.1, 0.3,0.5% wt.	30 min	10 min	N/A	[7]
Epoxy resin	TETA	xylene, butanol (1:1)	ND and CNT	5% wt.	3 hr.	30 min.	N/A	[46]
Poly(vinyl alcohol) (PVA)	N/A	Water	GO	0.7% wt.	30 min	N/A	N/A	[47]

The summarized works are showing the possibility using nanofillers to fabricate high-performance coatings and the potential approaches to incorporate the nanomaterials into the polymer matrix. For dispersion step, the nanoparticles will be dispersed into a suitable solvent which could be water, acetone, chloroform, tetrahydrofuran (THF), dimethyl formamide (DMF) or toluene, etc. [40] Sonication and mechanical stirring is usually employed in the dispersion step so the nanoparticle will be well distributed. According to Shadlou's study, the duration of sonication can be various due to the different shapes and size of the nanoparticles, which the sonication duration of ND, CNF, GO is 30,50,60 min., respectively.[3] Then, the polymer will be added to the solution. Additional energetic agitation (sonication, stirring, etc.) can be used in this step. For applying the fabricated coating, conventional air/airless spray method can be used to coat on a metallic substrate.

2.4 MODIFICATION FOR POLYMERIC COMPOSITE

The influence on the water contact angle by modifying the morphology and incorporating hydrophobic nanoparticles has been studied by researchers [48], [49]. In their work, the epoxy adhesive was cast into an artificial biomimetic composite coating by using natural leaves as a template. The procedure includes: first; the PDMS solution was poured on a fresh, natural leaf and detached after the curing process, then the cured PDMS polymer was used as a template to cast the epoxy adhesive. This artificial surface texture has dramatically increased the hydrophobicity of the epoxy adhesive, and the contact angle was found to be 146 degrees.

Much research has been conducted in the implementation of Polydimethylsiloxane (PDMS) modified epoxy to improve the water repellency of the coating surface [50]–[53]. In order to modify epoxy resin with the PDMS, one common way is to use 3- Aminopropyltriethoxysilane (3-APS), as the coupling agent and dibutyltindilaurate as a catalyst [50], [54]. Ammar et al. [54] have incorporated PDMS with epoxy resin and the results have shown the water contact angle increased from 65 degrees (neat epoxy) to 128 degrees. Rath et al. [55] have pointed out that the mechanisms that the increased water repellency in PDMS modified epoxy resin was due to the intercalation of PDMS into epoxy would significantly reduce the surface energy. An experimental study of PDMS modified epoxy incorporated with Nano silica was studied by Ammar et al. [50]. The weight ratio between PDMS and epoxy was 10:90, with a content of Nano silica that ranged from 2 wt.% to 8 wt.%. The highest water contact angle was observed in the sample that has 6 wt.% of NS, which was 132 degrees.

2.5 SUMMARY

In summary, the literature review revealed that different protective coatings with different nanofiller additives exhibit high variation in corrosion behavior. Some studies showed that single nanofiller loaded coatings may display high corrosion resistance, but other may observe the enhancement of hybrid nanofiller reinforced coatings. Clearly, these previous studies were carried out with a focus on specific one or two properties that were responsible for nanofiller reinforcements but few published documents provided a comprehensive, systematical assessment for quantifying the impacts of each nanoparticle on tribological, mechanical and electrochemical properties, which is crucial for the development of nanocomposite. Moreover, to this date, investigations on nanofiller-polymer coatings were mostly with focus on one single type of nanofiller. Literature review demonstrated that the investigations on these nanofiller-polymer composites, due to widely varied composite designs, different dispersion procedures, and experiment methods, limited and inconsistent conclusions could be made that hindered evaluating the effects of various nanofillers on their tribological, mechanical and electrochemical performance. As a result, without a comparative experiment design and consistent criteria, there was no clear information available to guide scientists and engineers on how to properly select different nanofillers from a wide range of the nanoparticles and how to effectively design promising nanocomposites, as focused in the following chapters.

CHAPTER 3. RESEARCH STRATEGY AND METHODOLOGY FOR EXPERIMENTAL STUDY

3.1 INTRODUCTION

This chapter presents the strategy and techniques for the experimental study in this research, and Section 3.2 explained the experiment strategy for the experimental study, and the employed techniques were also summarized. Furthermore, the material and fabrication procedure for the nanocomposite coatings are summarized in Section 3.3. The details of characterization and evaluation techniques were presented in Section 3.4.

3.2 STRATEGY AND TECHNIQUES FOR EXPERIMENTAL RESEARCH

A high-efficiency experimental strategy was developed as all the tasks were possessed simultaneously but also interacted with each other. The strategy was contributed by parallel tasks: 1) nanofiller reinforcement, 2) polymer screening, and 3) modification of polymer. With this scientific method, the research challenges in this study were solved efficiently.

The experimental techniques that were used in this study are presented in Fig. 3.1. By following this flow chart, the authors were able to understand the mechanism of the developed nanocomposite coatings. The first part was sample preparation, in which the procedure of fabricating specimens is provided. After that, the samples were characterized by several techniques; thus, an experimental study was performed on both the nanofillers and nanocomposites. In the next stage, the performance of the developed coatings was evaluated by mechanical properties, hydrophobicity, corrosion resistance, and durability. The obtained results from performance testing were used to lead the direction of the experimental study. In addition, several new techniques were employed in this project, and the detailed information was presented in Section 3.3 and 3.4.

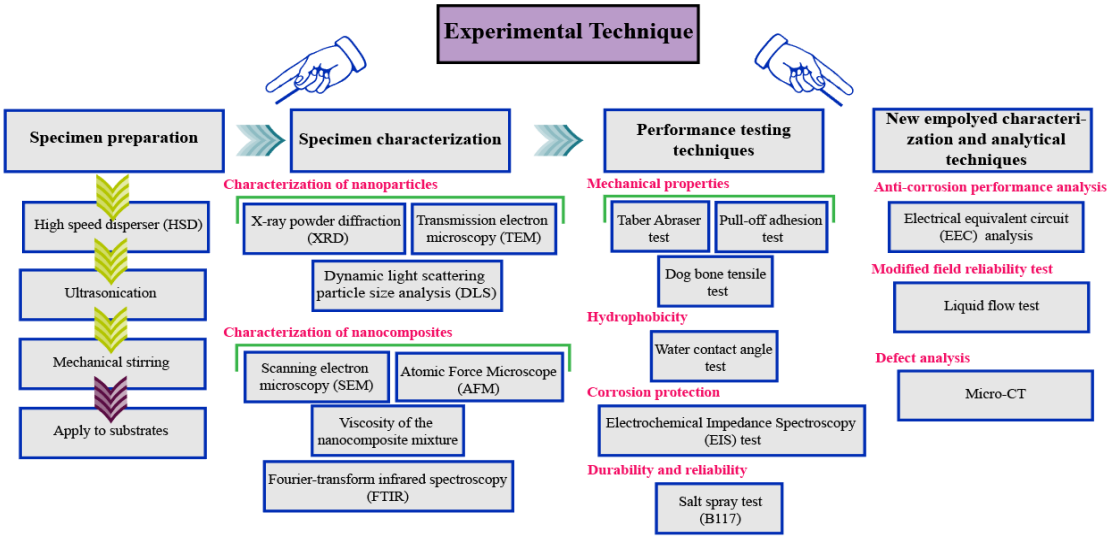

Figure 3.1: Experimental techinque

3.3 MATERIAL AND FABRICATION

3.3.1 Materials

Three nanoparticles were used in this study, and transmission electron microscopy (TEM) images of three nanoparticles were plotted in Figs. 1(a)-1(c). Commercial graphene nanoplatelets (Cheap Tubes Inc., USA), carbon nanotubes(Cheap Tubes Inc., USA), and nano-silica (Sigma-Aldrich Corp., USA) were purchased and used without any modification. The average specific surface area of the graphene is 500-700 m^2/g with an average thickness 8-12 nm. Meanwhile, the length and the outer diameter of the multi-walled carbon nanotubes are 10-50 μm and 8-15 nm, correspondingly. In addition, the silica nanopowder has a diameter between 10 and 20 nm while the surface is 175-225 m^2/g. EPON ™ resin 828 (Hexion Inc., USA), a bisphenol A liquid epoxy resin, was employed as the polymer to incorporate with nanofillers; thus, EPIIKURE™ Curing Agent 3175 (Hexion Inc., USA) was used as the hardener to cross-link with the epoxy resin.

3.3.2 Fabrication of nanocomposite coatings

The fabrication method of nanocomposites was presented in this section. Nano-filler particles were dispersed into the epoxy resin by using a high-shear disk mixer and then an ultrasonic dispersion. It is worth to mention that the ice/water batch was applied during the dispersion process to avoid overheating. The curing agent was added to the mixture followed the dispersion process, and the mole ratio between resin and curing agent was 1:1. A mechanical mixer was applied for 10 minutes, and the speed was controlled as 600 revolutions per minute. All the samples were cured at room temperature and were completely dried for several days before subjected to experimental characterization.

3.4 CHARACTERIZATION TECHNIQUES

3.4.1 Particle size distribution

The particle size distribution of the nanofillers was investigated by dynamic light scattering (DLS) with a submicron particle sizer (NICOMP 380 Particle Size Analyzers). The principle of the method is well established and understood by researchers. The test method required the nanoparticles were dispersed into a liquid, so the particles were in a suspension. By exposing the suspension to an incident light beam, such as a laser source, the particles scatter the light and broadening the laser spectra. The calculation of the particles size is based on the D the particle diffusion coefficient and λ the wavelength of light.

3.4.2 Transmission electron microscopy (TEM)

JEM-2100 high-resolution analytical TEM instrument was used to examine the morphologies and microstructures of single and hybrid nanofillers, as shown in Fig. 3.2. The nanofiller were dispersed into ethanol with a proper weight ratio before TEM observation. The size and shape of nanofillers were studied by the obtained TEM images.

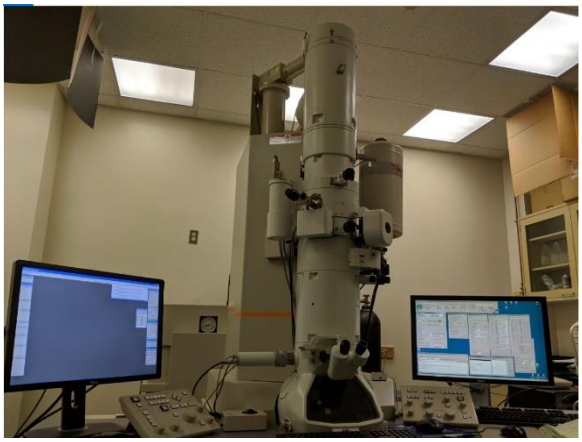

Figure 3.2: JEM-2100 high-resolution analytical TEM instrument

3.4.3 Scanning electron microscope (SEM)

The micrographs that obtained in this study were carried out by a field emission scanning electron microscope (FE-SEM), with a JSM-7600F Schottky at 2 KV. Visual assessment of the prepared samples was able to be performed with this advanced electron microscopy technique. In our study, the obtained images from the fractured surface of samples were used to study the dispersion and agglomeration of the different nanofillers at varied concentrations. Meanwhile, the SEM images of the abraded sample were used to investigate the relation between surface morphology and water repellency.

3.4.4 Powder X-Ray diffraction (XRD)

In this study, the X-Ray Diffraction (XRD) analysis was performed by using a Bruker AXS' D8 Discover multipurpose X-Ray Diffractometer, as shown in Fig. 3.3. XRD is a powerful technique to study and analyze the nanoparticle structure of the samples. The obtained results were used to characterize the nanofiller and also determine the degree of exfoliation.

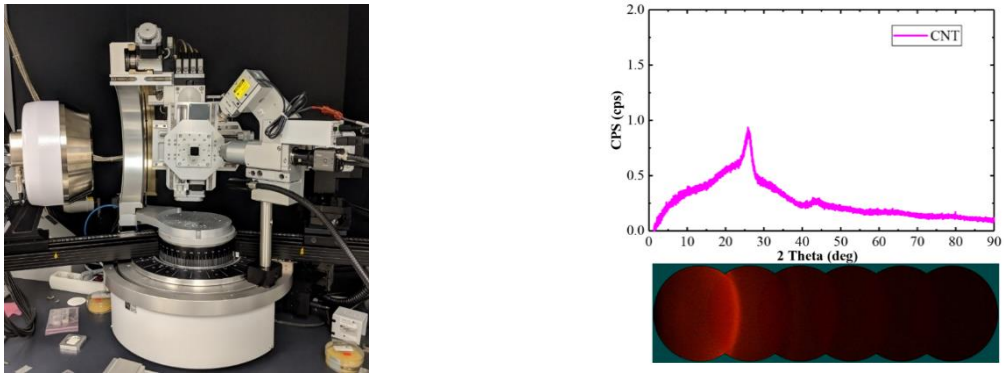

(a) (b)

Figure 3.3: (a) Bruker AXS' D8 Discover multipurpose X-Ray Diffractometer and (b) XRD test result of CNT

3.4.5 Fourier-transform infrared spectroscopy (FTIR)

FTIR analysis was conducted to the neat epoxy and nanocomposites to study reaction mechanism of epoxy resin and the nanofillers. FTIR spectra of neat epoxy, single filler, and hybrid filler composite were obtained by a Thermo Scientific Nicolet 8700 spectrometer (see Figure 3.4).

Figure 3.4: Thermo Scientific Nicolet 8700 spectrometer

3.4.6 Atomic force microscopy (AFM)

Surface roughness analysis and nanoindentation were performed with atomic force microscopy, carried out on a Nanoscope IIIa system. Both 2-D and 3-D images were collected in ‘‘tapping-mode’’. By scanning the surface of the coating with a sample-probe, the height changes were recorded, and three-dimensional images will be formed in the process. The obtained data can also be used to analyze the surface roughness of the tested samples.

3.4.7 Micro-CT

To study the interaction between nanofiller and polymer resin and the mechanism of nanofiller reinforcement, Micro-CT scan was used to evaluate the defect/voids in the coating film. As presented in Fig. 3.5, the dimensions of the scanned sample were 15*20mm, with a thickness of around 0.8mm. The analysis was performed based on the void content and the size distribution of the voids; then, the obtained results were correlated to the coating properties from previous studies.

Figure 3.5: GE v|tome|x s microCT for Micro-CT scan

3.4.8 Viscometer for viscosity

To evaluate the influence of nanofillers on the rheological properties of the polymer matrix, viscosity test was performed after nanofillers were dispersed into epoxy resin, with a Brookfield DV-II viscometer (Figure 3.6). The experiment was conducted under room temperature (23°C), and #7 spindle were selected, while the rotational speed was 50 rpm. The results are only valid while the percent torque reading is between 10 to 90%; otherwise, either the spindle or the rotational speed should be adjusted. Multiple measurements (at least 3) were taken for each sample, and the result was the average value of all the readings. Micro-CT scanning of nanocomposites.

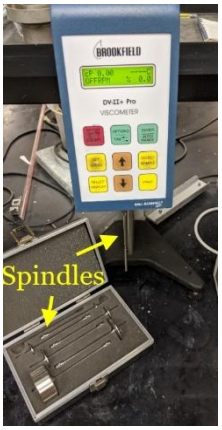

Figure 3.6: Brookfield DV-II viscometer for viscosity test

3.5 PERFORMANCE EVALUATION METHODS

3.5.1 Electrochemical impedance spectroscopy (EIS)

EIS test is used to evaluate the interface properties between a substrate and conductive electrolyte solution. Potentiostat device with counter and reference electrodes that are immersed in electrolyte solution are required to perform EIS experiments. This potentiostat is employed for applying both DC potential and small superimposed AC excitation to a working electrode which is immersed in the conductive solution. After AC and potential measurements are collected over a very wide range of frequency excitation, then the collected data of current and potential of the electrochemical cell are converted into complex impedance vs. frequency curve. DC current and potential values also should be measured. The impedance-frequency plot analysis produces useful information about metal and dielectric properties that are not available accurately or easily obtained from other electrochemical tests. The main applications of EIS test are coating performance evaluation, electrochemical mechanisms and rate analysis, and battery performance.

The test setup is shown in Figure 3.7, a 3-cm diameter O-ring glass tube with silicon joint is clamped on the test panel. A saturated calomel electrode reference electrode is used for the reference electrode; a platinum mesh is employed as the counter electrode and steel panel is worked as the working electrode. The glass tube is filled with 1% NaCl solution at all time during the test. Gamry Reference 600 Spectroscopy is used to measure the impedance vs. frequency curve and the curve will be used to study the corrosion resistance of the test coating.

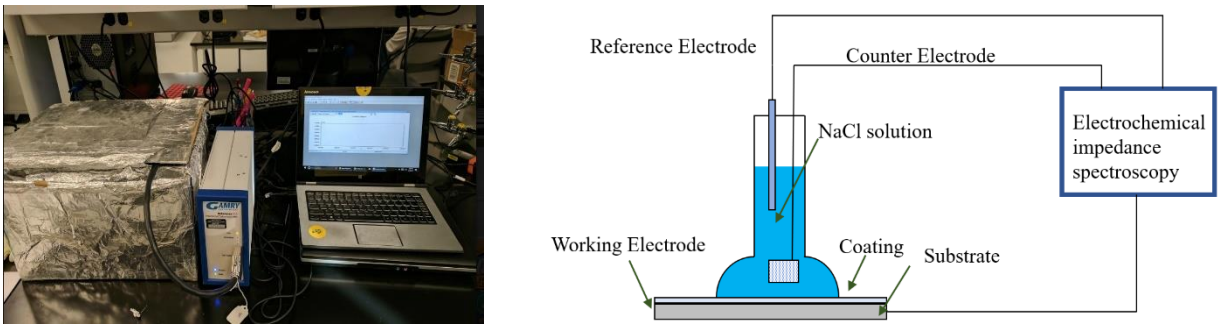

Figure 3.7: Apparatus for EIS test

3.5.2 Longer-term corrosion resistance

The influence of graphene nanoplatelets on the corrosion behavior of exposed to salt fog was evaluated by ASTM B117 Salt Fog test. The ASTM B117, Salt Fog test, is an accelerated corrosion test which the samples are exposed to a corrosive environment in a fog chamber. The samples are required to be maintained in a salt fog test environment during the test, and the salt solution should be 5% NaCl solution with a PH ranged in 6.5 to 7.2. The temperature should be maintained at 35°C (95°F).

The salt fog chamber and tested samples are shown in Fig. 3.8. After exposure, the surface of the coated sample should be cleaned by following ASTM B1654. All the corrosion products should be removed along scribe lines by either scraping, knife, paint stripper, air blow-off or power washer. Then the sample can be evaluated based on the defected areas by following the rating method from ASTM B1654.

(a) (b)

Figure 3.8: Salt Fog Chamber with tested samples

3.5.3 Electrical equivalent circuit (EEC) technique based on the EIS results

Based on literature studies, the Electrical equivalent circuit (EEC) model was widely used to interpret the EIS results [64]–[69]. The model was fitted based on the impedance and phase angle curves in the Bode plot. The corrosion phase can be classified into four stages, and each of them is represented by one EEC model, as shown in Fig. 3.9.

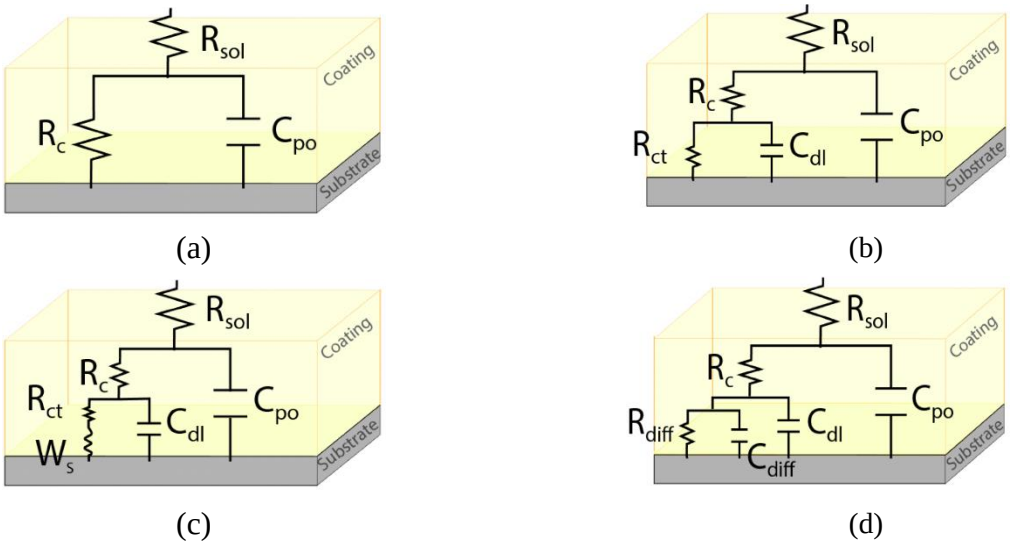

Figure 3.9: Electrical equivalent circuit models for (a) stage I, model A, (b) stage II, model B, (c) stage III, model B with Warburg element, (d) stage IV, model C

Stage I: Model A was used to present the initial stage, which the coating was an intact film and behave as an isolated protective layer for corrosion protection. At this stage, the equivalent circuit model includes R_{sol} solution resistance, R_c coating resistance, and C_{po} constant-phase element of the coating, indicating the corrosive medium could not penetrate the coating layer.

Stage II: Model B was employed to represent the initial stage of corrosion reaction, while the electrodes were able to penetrate the coating layer to contact with the metal substrate, and the corrosion reaction has been begun. Compared with model A, R_{ct} charge transfer resistance and C_{dl} constant phase element of the double-charge layer were added in the model to simulate the coating-substrate interface.

Stage III: At stage III, Model B with Warburg impedance element (W) is included in the electrochemical equivalent circuit when the diffusion effect dominates corrosion. The Warburg element indicates that the electrochemical corrosion reaction in the coating-substrate interface is diffusion-controlled.

Stage IV: The model C can be used to confirm the results, which new parameters of constant phase element of diffusion capacitance (C_{diff}) and diffusion resistance (R_{diff}) were included. At this stage, severe corrosion damage has occurred and which a thin corrosion product layer was accumulated in the coating-substrate system.

3.5.4 Abrasion resistance test

Generally, the determination of the abrasion resistance of the organic coating can be done by either Falling Abrasive method (ASTM D968) or the Taber abraser method (ASTM D4060). In this study, Taber Abraser method will be used in this study as it is able to test the wear resistance on a wide range of materials by selecting different abrading wheels and applied loads. The Taber abraser with abrading wheels and tested sample are shown in Fig. 3.10. With the applied load and the rotation of sample, a circular abrasion mark with an area of approximately 30 cm2 will be formed by the abrading wheel. The abrasion resistance is calculated as the mass loss in a specified

number of abrasion cycles with the selected loads. Each specimen was tested for a total of 1000 cycles,1000g of the load was used during the test, and the rotational speed is 72 rpm with two CS-10 abrading wheels.

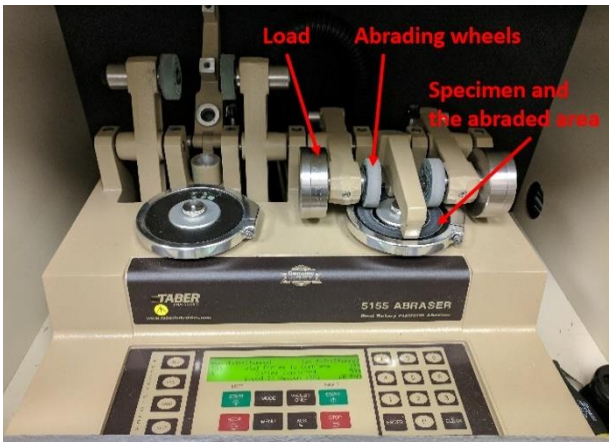

Figure 3.10: Taber abraser machine and tested specimen

3.5.5 Coupon tension test

The determination of the tensile properties of CNT reinforced polymer coating was done by the dogbone tensile test (ASTM D638). The test was performed by Shimadzu's EZ-X tester (Figure 3.11) with a testing speed of 1mm/min. The hardened dog bone specimens were clamped at two ends by the grips during the test. Tensile strength was applied to elongate the specimens during the test until the specimens were broke in the narrow cross-sectional test section. Maximum tensile strength and Young's modulus were determined for each specimen.

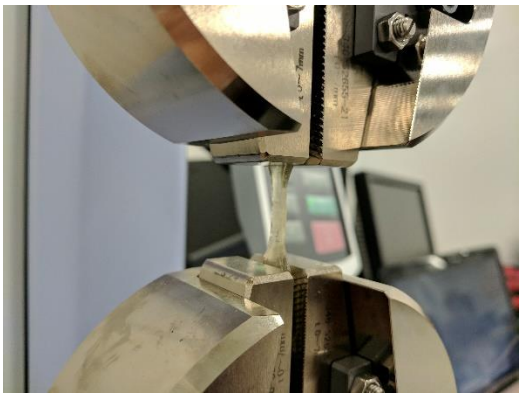

Figure 3.11: Shimadzu's EZ-X tester with specimen

3.5.6 Water contact angle test

As the discussion earlier, the contact angle test (ASTM D7334) is used to determine the anti-fouling properties indirectly which it indicates the ability of a liquid to maintain contact with the coated surface. As shown in Fig. 3.12, the dry coated sample is placed in the test area horizontally, a drop of a specific volume of water is applied by a syringe. An image is captured by the camera and processed by a computer to calculate the angle between the drop and the substrate.

The coating surface can be categorized as hydrophilic (contact angle < 450), hydrophobic (contact angle > 900), and in-between (450 < contact angle < 900) if the water is used as the test liquid. The advantages for this test are: the test can be done very fast, and it is a non-destructive test that does not require extra samples to be made for this test.

Figure 3.12: Apparatus for contact angle test

3.5.7 Adhesion property

The adhesive bonds of the coating to metal were characterized by tensile button testing. The purpose of this test is to evaluate the tensile bond strength of nano-reinforced epoxy. In order to evaluate the influences of different nanoparticles on the adhesive bonding strength, the test specimens were prepared with pure epoxy, graphene/epoxy, and CNT/epoxy.

The sample preparation procedures are described in Fig. 3.13, three dollies were glued to each specimen, and the pull-off strength was measured during the experiment. Scotch weld 460 (3M, Co.) was used to glue the dollies, and the test area was abraded with sand paper (100 grit or finer) to enhance the bonding strength between dollies and tested coatings. The test was performed 24 hours after the dollies were applied. The test area was isolated with other parts of the coating by die-cutting. An adhesion tester was used to apply tension load normal to the test surface. The pull-off strength (adhesion) was measured when the dolly was detached by the tension load.

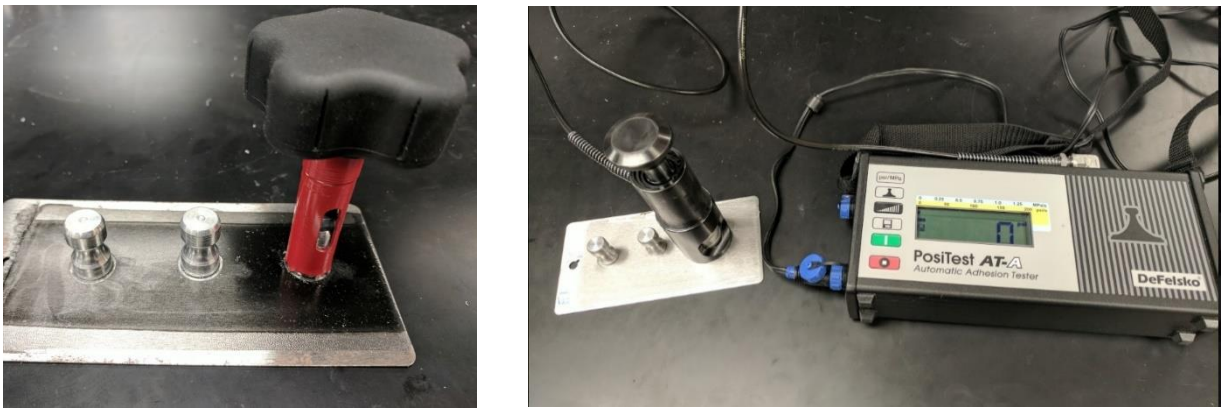

Figure 3.13: Adhesion test machine

3.5.8 Water droplet adhesion from the coating surface

In the previous study, the water contact angle was used to evaluate the hydrophobicity of coating surface. The coating surface was categorized as hydrophilic (contact angle < 45^0), hydrophobic (contact angle > 90^0), and in-between (45^0 < contact angle < 90^0) if water was used as the test liquid.

In addition, based on literature studies, it is worth to mention that the adhesion of water to the contact surface is also a major factor which contributing to the water repellency of coatings [70]–[74]. Higher adhesion indicating the water is more difficult to detach from the surface, which increase the wettability of the coating. Figure 3.14 showed a series of images taken during the water adhesion test, and a superhydrophobic surface with excellent water repellency was presented in Figure 3.14(a). The water droplet was approached and then squeezed against to the surface; after that, during the descending process, the water droplet completely detached from the surface and suspended on the tip. On the other hand, images of a surface with high adhesion were presented in Figure 3.14(b), as the water was squeezed into a cone shape during the descending process and detached from the tip in the final step. To better understand the wettability of the developed coating, the water repellency of the coating was also characterized by adhesion of water to contact surface, and the results were presented in Chapter 8.

(a)

(b)

Figure 3.14: Water ascending and descending from the coating surface

3.5.9 Modified filed reliability test with liquid flow instrument

As proposed in the project description, a long-term performance experiment was also planned to evaluate the reliability of the developed coatings. Figure 3.15 illustrated the designed accelerated flow instrument, which contained a liquid reservoir, a pump, and a flow channel. The test samples were fixed in the channel and on the bottom part of the internal surface. With the adjustable flow speed provided by the pump, the design was used to simulate the condition of the internal surface of pipelines, and the tested panels were removable so EIS test could be performed to evaluate the corrosion resistance after they were exposed to water flow.

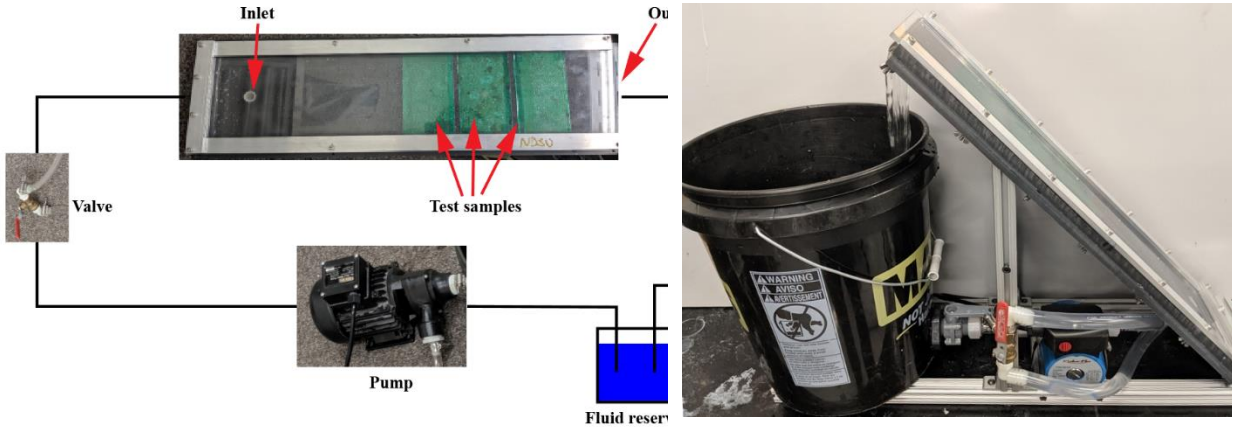

Figure 3.15: Instrument for liquid flow test

3.6 SUMMARY

In this project, a bisphenol A/epichlorohydrin derived liquid epoxy resin was selected as the baseline polymer coating, as it is a cost-effective coating and can obtain good mechanical, adhesive, dielectric, and chemical resistance properties when crosslinked with appropriate curing agents.

This section presented the experimental results for both characterization and performance of the fabricated coatings. By following the experiment strategy in Figure 3.1, the discussions will be addressed in the following chapters:

- Chapter 4 presented the results from the polymer screening process, in which a polyamine cured bisphenol-A epoxy coating was selected in this work
- Chapter 5 & 6 focused on evaluating nanofiller reinforcement of polymer coating, which explained the effects of incorporating single and hybrid nanofillers into polymetric coatings. By comparing all the nanocomposites' overall performance, the nanofiller that provided the greatest reinforcement was selected for the next step.
- Modification of polymer was conducted. Composites with different weight ratios were studied, and the modified resins were also incorporated with the selected nanofillers from the nanofiller reinforcement (Chapter 7).

- The surface modification was then incorporated with the coating that consisted of both nanofiller reinforcement and modified polymer; hence, the proposed high-performance multifunctional coating was developed, and the performance of the coating was evaluated by a comprehensive experimental study (Chapter 8).

CHAPTER 4. POLYMER SELECTION FOR NANOCOMPOSITE COATINGS

4.1 BACKGROUND

In this study, several polymeric binders have been characterized in order to select suitable resin for the project. During the polymer screening process, abrasion resistance, fouling resistance, and corrosion resistance, which was characterized by Taber abraser method (ASTM D4060), contact angle measurement (ASTM D7334), and Electrochemical Impedance Spectroscopy (EIS), correspondingly. The above tests were selected for the following reasons, 1) the corresponded properties are critical for protective coatings, and 2) the selected tests have less time cost in order to shorten the duration of polymer screening

4.2 CRITICAL FACTORS AFFECTING MATERIAL SELECTION

4.2.1 Category

The abrasion resistance, fouling resistance, and corrosion resistance of the selected organic coatings can be observed after the corresponded test. Along with the experimental results, a literature review was also incorporated during the decision-making process. The tested polymer mixtures are presented in Table 4.1, which they are either commonly used coatings or have excellent protection properties.

Table 4.1: Selected coatings during the polymer screening process

Mixture	Type	Group
Epon 828 / Epikure 3175	Epoxy / Polyamine	3175
Epon 828/Epikure 3164	Epoxy / Polyamine	3164
Lumiflon 910 /Desmodur N 3600	FEVE / Polyisocyanate	910
EPI-REZ 7510-W-60/Epikure 8535-w-50	Waterborne Epoxy	5060
EPI-REZ 7520-WD-52/Epikure 6870-w-53	Waterborne Epoxy	5253
Epon 828/Baxxodur EC 302	Epoxy / Polyether-amine	302
Epon 828/Baxxodur EC 310	Epoxy / Polyether-amine	310

4.2.2 Abrasion resistance of the selected polymer resins

Table 4.2 shows the results of the abrasion resistance of the tested polymers. The 3175 group has a mass loss of 113.5 mg at 1000 test cycles. The maximum mass loss was observed in the 5060 group, and the value is significantly higher than other groups, which indicates the abrasion resistance of this coating is much lower than other tested groups. Besides the 5060 group, the wear index of other groups various from 0.04 to 0.11. Group 310 and 3164 exhibit high abrasion resistance compared with other groups.

Table 4.2: Abrasion resistance of selected coatings

Mixture	Group	Mass loss at 1000 cycles (mg)
Epon 828 / Epikure 3175	3175	114
Epon 828/Epikure 3164	3164	46

Lumiflon 910 /Desmodur N 3600	910	63
EPI-REZ 7510-W-60/Epikure 8535-w-50	5060	455
EPI-REZ 7520-WD-52/Epikure 6870-w-53	5253	105
Epon 828/Baxxodur EC 302	302	70
Epon 828/Baxxodur EC 310	310	44

4.2.3 The contact angle of the selected polymer resins

The results of the contact angle tests are presented in the Table 4.3 and the images can be found in the appendix. The coating surface can be categorized as hydrophilic (contact angle < 45^0), hydrophobic (contact angle > 90^0), and in-between (45^0 < contact angle < 90^0) if water is used as the test liquid. It is easy to observe that most of the coatings can be categorized as in-between, which includes group 3175,3164,302, and 310. The contact angle of group 910 is slightly higher than 90^0 (see Figure 4.1), which can be categorized as a hydrophobic coating. For group 5060 and 5253, which both of them have water bone epoxy resin in the mixture, the contact angles are both close to 33^0.

Table 4.3: Contact angle of selected coatings

Mixture	Group	Contact Angle (^{0})
Epon 828 / Epikure 3175	3175	51.44
Epon 828/Epikure 3164	3164	65.65
Lumiflon 910 /Desmodur N 3600	910	90.34
EPI-REZ 7510-W-60/Epikure 8535-w-50	5060	33.35
EPI-REZ 7520-WD-52/Epikure 6870-w-53	5253	33.36
Epon 828/Baxxodur EC 302	302	60.37
Epon 828/Baxxodur EC 310	310	71.95

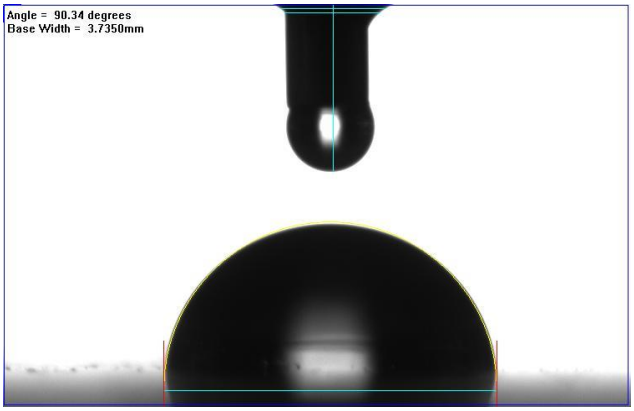

Figure 4.1: Water contact angle of 910 group

4.2.4 The corrosion resistance of the selected polymer resins

In this study, anti-corrosion performance is also an important property for evaluating polymer binders. Potentiostatic EIS test has been used to measure the impedance of each sample group. As presented in Figure 4.2, group 5060 exhibits the lowest Zmod values in all the frequency regions. For the rest of the groups, no significant difference was observed; however, group 310 has the

highest Zmod values in the high-frequency region, following by group 302. The results indicate that the impedance of the coating is enhanced by crosslinking with amine curing agents. The Zmod values of group 910 are lower than group 3164 by around half a degree of the high frequency but higher than group 5253 and 3175, about half a degree and one degree, respectively.

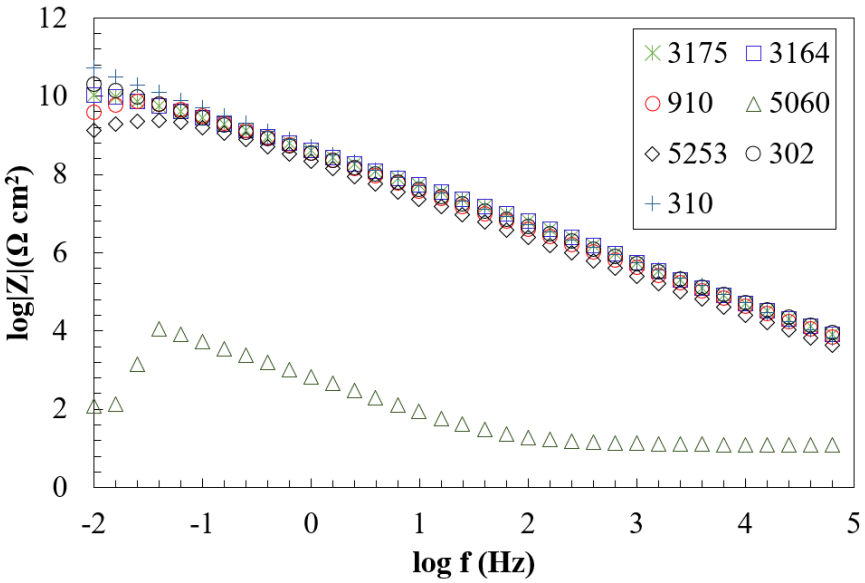

Figure 4.2: EIS results of selected coatings

4.2.5 Other considerations based on the literature study

As mentioned earlier, there are other factors that were incorporated in the decision-making process besides the obtained experimental results, as presented in Table 4.4. The considered variables include the performance of the coatings, impact to the environment, application process, etc.

Table 4.4: Additional considerations for the polymer selection process

Mixture	Group	
Epon 828 / Epikure 3175	3175	Excellent long-term corrosion resistance and chemical resistance
Epon 828 / Epikure 3164	3164	High degree of toughness and flexibility
Lumiflon 910 / Desmodur N 3600	910	Polyisocyanate is harmful if inhaled, may cause respiratory irritation
EPI-REZ 7510-W-60 / Epikure 8535-w-50	5060	Weak mechanical properties and durability
EPI-REZ 7520-WD-52 / Epikure 6870-w-53	5253	Weak mechanical properties and durability
Epon 828/Baxxodur EC 302	302	Polyether-amine is harmful in contact with skin, causes severe skin burns and eye damage
Epon 828/Baxxodur EC 310	310	Polyether-amine is harmful in contact with skin, causes severe skin burns and eye damage

4.3 SUMMARY

Considering the factors and experimental results mentioned above, the 910, 302, and 310 groups were not used in further study due to their hazardousness. On the other hand, the 5060 group was

excluded as it has the lowest corrosion resistance in the tested coatings; in addition, the 5253 group was removed due to its weak mechanical properties and durability. Compared with the 3175 group, the 3164 group has better mechanical properties, however, it is commonly known that improved mechanical properties can be easily achieved by the addition of nanofillers. In contrast, the corrosion resistance and chemical resistance are not commonly increased by nanofillers. Finally, the 3175 group was selected in the polymer screening process due to its excellent long-term corrosion resistance, which this property is desired for the oil & gas pipelines.

CHAPTER 5. SINGLE FILLER REINFORCED NANOCOMPOSITE COATINGS

5.1 BACKGROUND

Test results for single filler reinforcement were presented in this section, which included both characterization and performance of the nanocomposite coatings containing varied weight content nanoparticles. As mentioned in the previous study, carbon nanotubes, graphene nanoplatelets, and nano-silica particles were selected due to their unique geometric properties, as they are commonly used 2D (GNP), 1D (CNT), and 0D (NS) nanofillers [1], [5]. In this chapter, both the performance evaluation and mechanism study were employed to better understand the nanofiller reinforced coatings.

5.2 CHARACTERIZATION OF NANOFILLERS AND NANOCOMPOSITES

5.2.1 The Influence of Dispersion Methods for Nano-reinforced Composites

To show the significance of suitable dispersion method for nanocomposite, samples with different dispersion levels are shown in this section. Fig. 5.1 shows a graphene/epoxy sample with and without ultrasonication. Compare with the well-dispersed sample (right), poor dispersion was observed in the sample without ultrasonication (left). Due to most of the graphene was deposit at the bottom of the mixing container after mechanical stirring, the left sample did not have sufficient graphene in the matrix.

Figure 5.1: Sample with and without well-dispersed graphene nanoplatelets

In this study, a suitable dispersion method was developed, which incorporated with High-speed disk (HSD) disperser and ultrasonication. The nanofillers were dispersed into a mixture that containing EPON 828, then High-speed disk (HSD) dispersers (high-speed impellers, high-intensity mixers) was used to break down the particles by providing shear stress. Like the showing Fig. 5.2, the mixture was mixed by the high-speed disk disperser with a rotation speed 4000rpm of for 30 mins. Ultrasonication was also applied in this process after the HSD dispersion. The solution was ultrasonicated at 100% amplitude with a duration of 30 mins. Misonic S1805 sonicator with a 3/4" probe was used in this process as shown in Fig. 5.2. The sonicator was programmed to sonicate for 30 seconds and then rest 30 seconds. The ice bath was applied to avoid

overheating the sample. The curing agent was added after the mixture was cooled down to room temperature. The total solution was mixed with a10 mins mechanical stirring at 400 rpm.

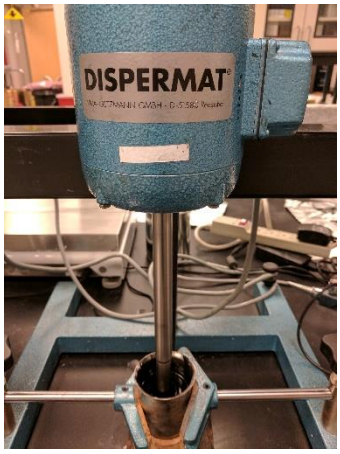

High-speed disk (HSD) disperser

High-speed disk (HSD) disperser

Ultrasonication

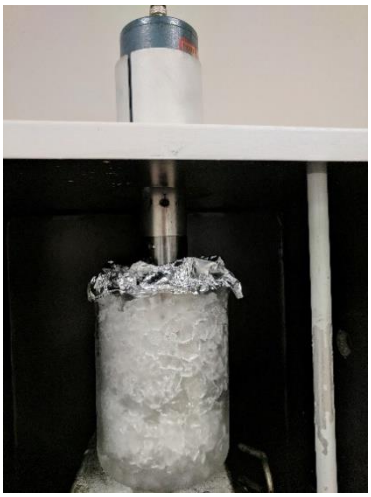

Ultrasonication

Figure 5.2: Dispersion process for nanofillers

5.2.2 Particle size distribution

One of the most important factors in the nanoparticle's reinforcement is the dispersion state of nanofillers. The size of nanoparticles can affect the reinforcement in the nanocomposites as larger aggregates create more severe defects which lead to longer microcracks [3]. The particle sizes of the nanoparticles were measured by dynamic light scattering (DLS), and it is the most effective approach to analyze the size distribution of nanomaterials [75]. The correlation of Tyndall effect and Brownian motion made it possible to obtain the particle size information in suspension. During the test, a laser beam was utilized to cross the sample, and the time-dependent scattering intensity from particles was measured while the particles were experiencing random Brownian motion [76]. The application of laser light allowed us to analyze the nanoparticles that are smaller than the wavelength of natural light.

The particle size distribution of single fillers (CNT, GNP, and NS) was illustrated in Fig. 5.3. It was observed that the particle size range was varied with the types and weight concentration (wt.%) of the nanoparticle. The average size of particles was ranged from 10^3 to 10^5, 10^2 to 10^4, and 10^1 to 10^3 for CNT, GNP, and NS, correspondingly. The results clearly indicated that, from 0.1 to 3.0 wt.%, there was no significant increase in the NS particle size. Compared with CNT and, GNP, much narrow size distribution was observed in which the particles were 10^1 to 10^3 nm in size. On the other hand, the size of GNP could be ranged from 10^2 to 10^4 nm, and the widest size distribution was obtained in CNT (10^3 to 10^5 nm). Apparently, within the tested concentration, CNT has the highest tendency to form agglomeration, followed by GNP, and NS.

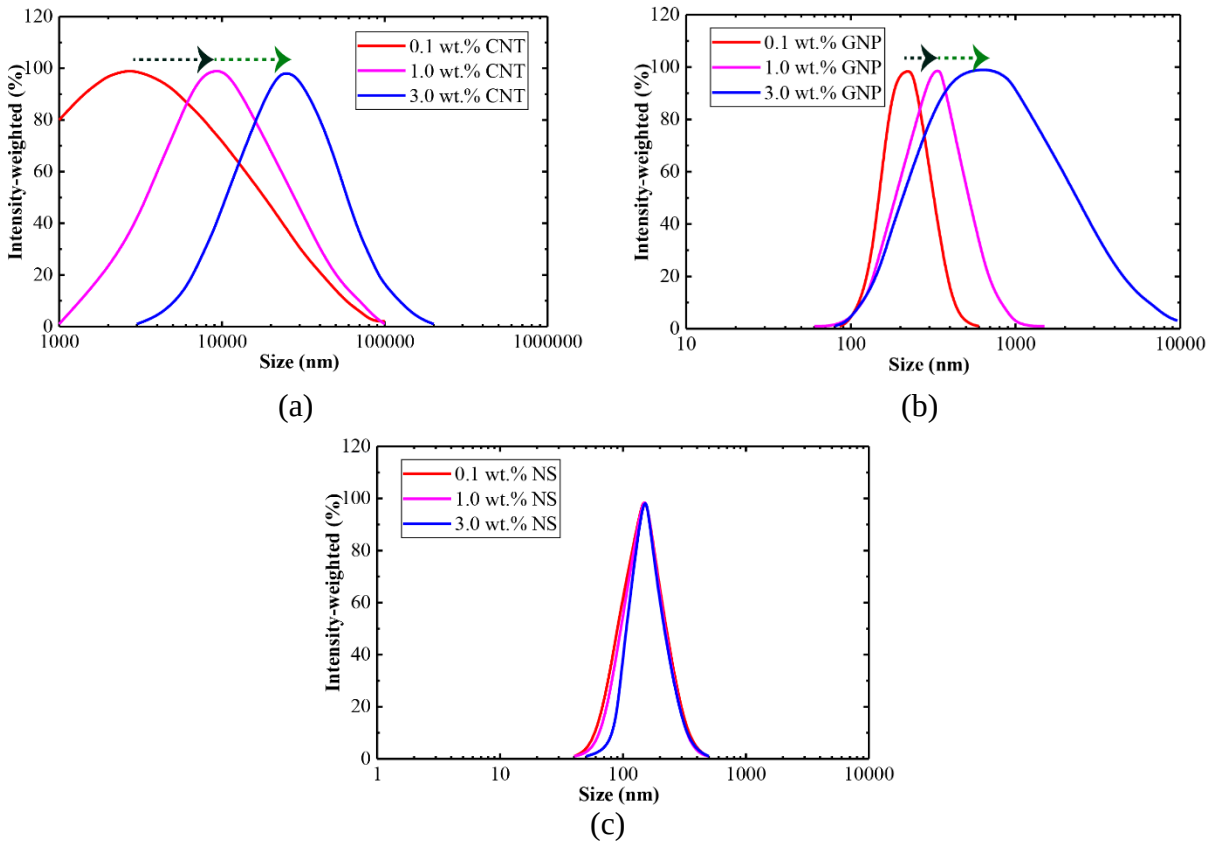

Figure 5.3: Particle size distribution of (a) CNT, (b) GNP, and (c) NS nanofillers

It was clear to observe that relations between the agglomeration size and weight concertation for CNT, GNP, and NS were completed different in the tested range. In the log scale, a nearly linear relation between average particle size and weight concentration was observed in CNT samples. The average particle size of CNT raised from 1000 to 9000 nm, while the concentration was increased from 0.1 to 1.0 wt.%. A similar tendency of agglomeration was obtained in the range of 1.0 to 3.0 wt.%, which the average size was increased from 9000 to 11000 nm. On the other hand, more severe agglomeration was observed when the concentration was greater than 1.0 wt.% in GNP samples, while particle size was slightly increased from 0.1 to 1.0 wt.%. In contrast, regardless of the weight content in the tested range, no significant difference in size distribution was observed in the NS samples.

SEM images of the cross-Sectional view of the nanocomposites through the thickness were used to visually identify the particle size of different carbon nanoparticles with varying concentrations. Figs. 5.4(a) through 5.4(i) were micrographs of 0.1, 1.0 and 3.0 wt.% three types of carbon nanoparticles in epoxy, correspondingly. The severity of aggregations directly reduced the dispersion level of nanoparticles, and the resulting defects due to the aggregates/agglomeration were mainly responsible for material degradation in the nanocomposites.

As clearly illustrated in Figs. 5.4(a)- 5.4(c), well-distributed CNTs were observed in the specimen with 0.1 and 1.0 wt.% of particles and there were no significant agglomerates observed in 1.0 wt.% CNT group. However, due to the strong van der Waals forces between fillers, severe agglomeration was observed in groups with a high content of CNT, as shown in Fig. 5.4(b). The largest the agglomerate was observed in the composites with 3.0 wt.% CNT (see Fig. 5.4 (c)). A similar tendency was observed in GNP groups, as no significant aggregate was observed in the composites with 0.1 and 1.0 wt.% particles, then stacked GNP sheets appeared in the high content groups (3.0 wt.%). Figs. 5.4(g)-5.4(i) showed the NS particles behaved differently as the samples exhibited no large agglomeration within the tested concentrations of nanoparticles. Based on the TEM images, NS particles exhibited a spherical shape, thereby leading to excellent dispersion and compatibility in the epoxy matrix.

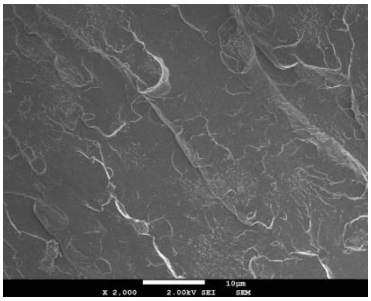

(a) 0.1 wt.% CNT/epoxy

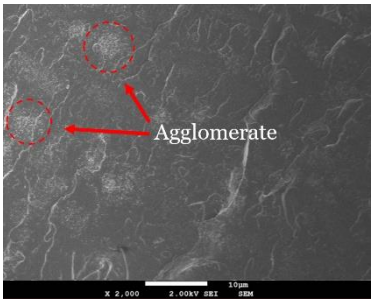

(b) 1.0 wt.% CNT/epoxy

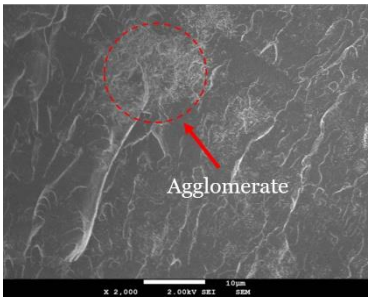

(c) 3.0 wt.% CNT/epoxy

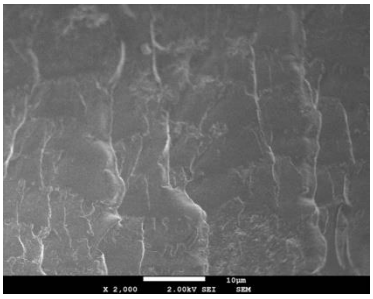

(d) 0.1 wt.% GNP/epoxy

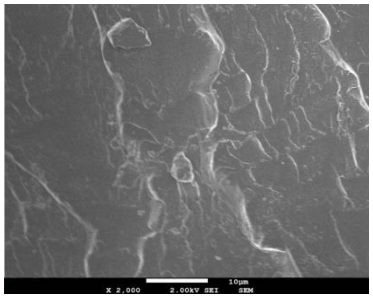

(e) 1.0 wt.% GNP/epoxy

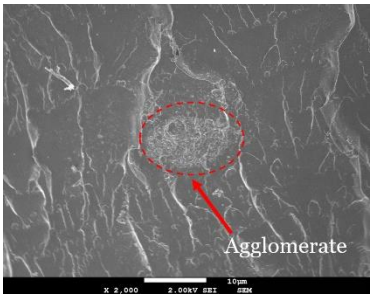

(f) 3.0 wt.% GNP/epoxy

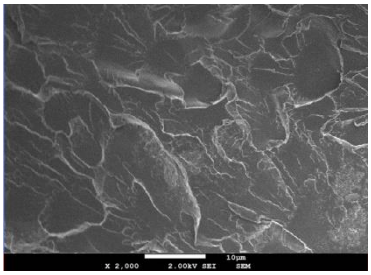

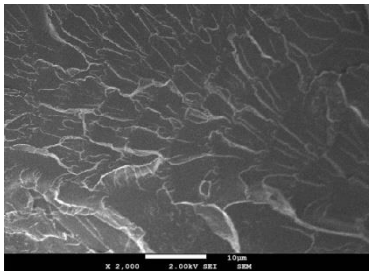

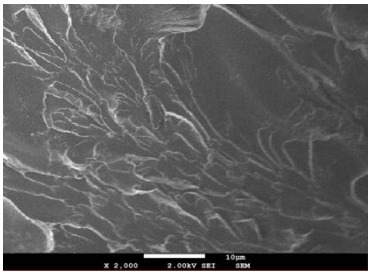

(g) 0.1 wt.% NS/epoxy (h) 1.0 wt.% NS/epoxy (i) 3.0 wt.% NS/epoxy

Figure 5.4: Cross-sectional SEM image of samples: (a)-(i)

5.2.3 Transmission electron microscopy (TEM)

Transmission electron microscopy (TEM) photograph of as-received raw CNT, GNP, and NS nanoparticles was shown in Figs. 5.5(a)- 5.5(c), respectively. The TEM graphs at high resolution allow one to observe the nanoparticles virtually. The observation was used to characterize the microstructures of three different nanoparticles.

As shown in Fig. 5.5, it was clear that the three types of nanoparticles could be defined as zero (NS), one (CNT), or two-dimensional (GNP) materials which indicate there are 0, 1, or 2 dimensions are larger than 100 nm, correspondingly. This observation shows strong agreement with the assumption that purposed in the previous study, which part of the project objective was to investigate the reinforcing properties provided by the nanoparticles due to their unique shapes. Cylindrical shape was observed in carbon nanotube (CNT) with a diameter around 20 nm. The graphene nanoplatelets (GNP) were stacked single layers sheets with an extremely small thickness. Furthermore, the homogeneous size distribution of the spherical particles was identified in Nano-silica (NS), with an average diameter of 15 nm.

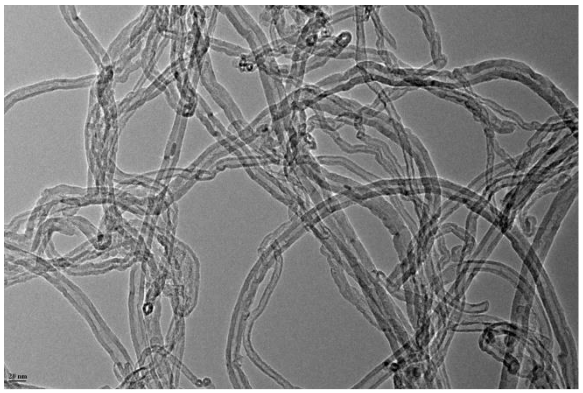

(a)

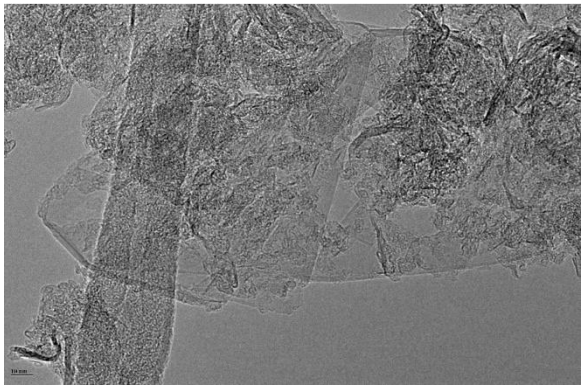

(b)

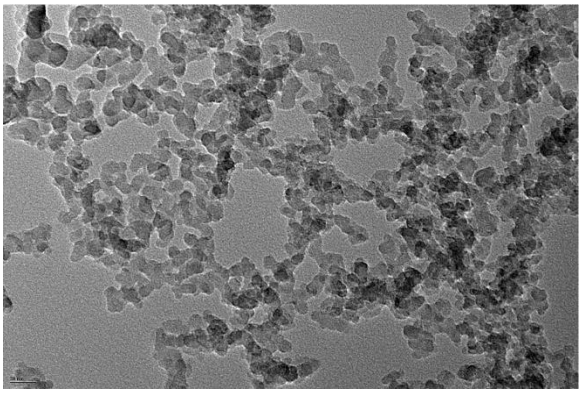

(c)

Figure 5.5: TEM photograph of (a) CNT, (b) GNP, and (c) NS filler

5.2.4 X-ray powder diffraction (XRD)

The XRD results were conducted to demonstrate the degree exfoliation of various fillers [77], as shown in Fig. 5.6. The interlayer spacing of the nanofillers could be calculated based on the diffraction peak angle and wavelength by utilizing Bragg's law Equation [78]:

$$\text{Bragg's equation: } \lambda = 2d \sin\theta \quad (1)$$

where λ = wavelength (1.54056 nm in this study), d = interlayer spacing between atoms, and θ = diffraction angle. As illustrated in Fig. 5.6, both CNT and GNP exhibited a sharp peak at 26.5°, corresponding highly-ordered nanoparticle structure with an interlay spacing of 3.4 nm. However, the intensity of the peak of GNP was much stronger than CNT, indicating the poor exfoliation of graphene sheets in the matrix [79], which is reasonable considering the shape difference between these two nanoparticles. The sharp peaks indicating the GNP sheets are crystalline solids (see Figure 5.7).

For the Nano-silica samples, a broad peak was appeared 19.5°, indicating the assigned SiO_2 particles were distributed with an interlayer spacing of 4.5 nm. The broad shaped peak confirmed that the amorphous nature of the Nano-silica (see Figure 5.7) [50].

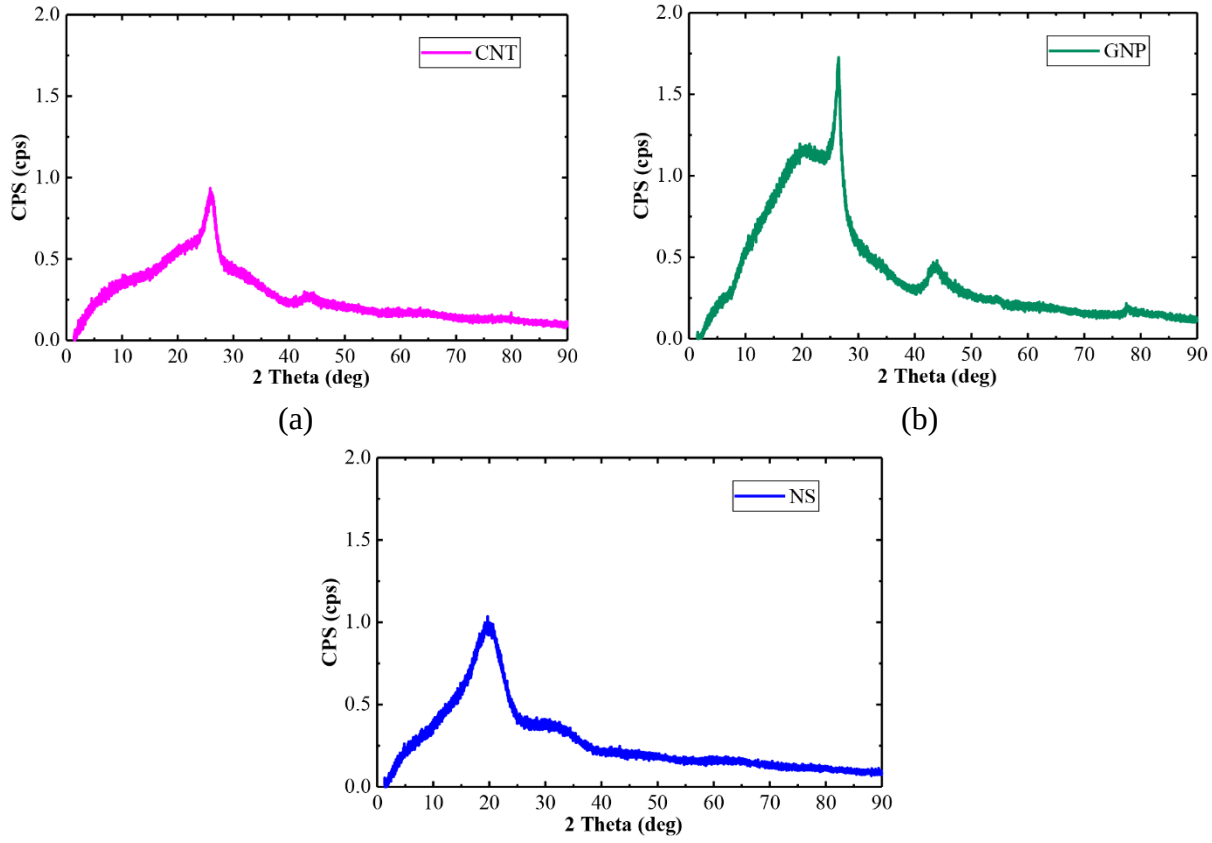

Figure 5.6: X-ray powder diffraction (XRD) curves of (a) CNT, (b) GNP, and (c) NS filler

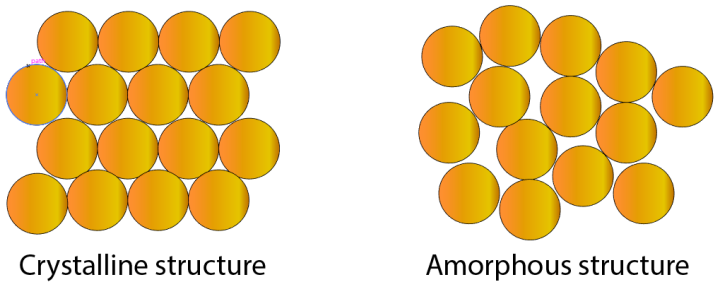

Figure 5.7: Schematic of crystalline and amorphous structures

5.3 PERFORMANCE OF SINGLE FILLER REINFORCED NANOCOMPOSITES

5.3.1 Corrosion resistance

(a) Neat epoxy

The results of the neat epoxy group were employed as a reference for all the nanofiller coatings, as typical degradation process was observed in the samples during the Salt fog test. A typical degradation process of a coating film should be observed from both impedance and phase angle curve in the Bode plots. As the exposure time elapsed, the following changes could be observed in a typical degradation process of a protective coating film:

a) A decrease of impedance value at the low-frequency region (0.01 Hz)
b) The minimum region of phase angle plot shifted toward the high-frequency region

The observations of the neat epoxy group during the exposure could well fit the suggestion above:

I. In the impedance curve, the Zmod value was continuously decreased with the increase of exposure hours. As illustrated in Fig. 5.8, the impedance value has dropped.

II. The frequency value for the minimum phase angle has shifted 0.01 Hz to 100 Hz.

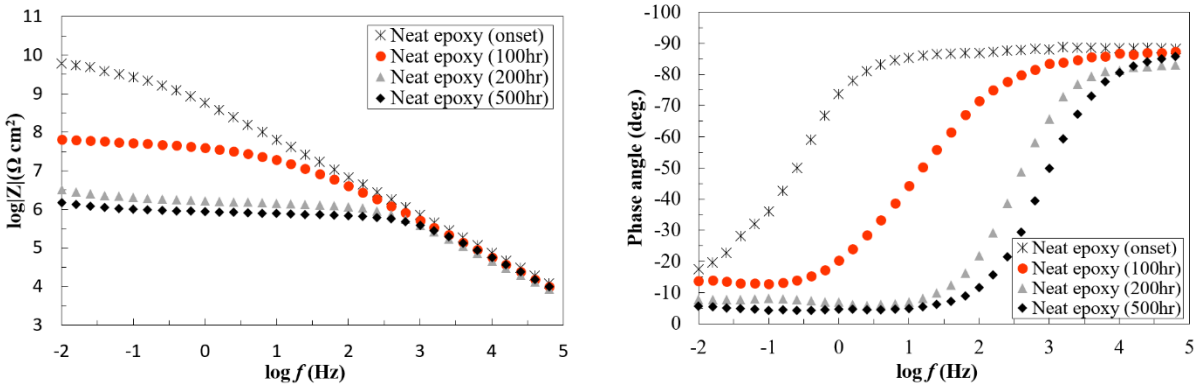

(a) (b)

Figure 5.8: Impedance curve (a) and phase angle curve (b) of the neat epoxy group

Subsequently, the electrical equivalent circuit (EEC) model could be determined by interpreting the impedance and phase curves. The EEC model could also be used to demonstrate the

degradation process of the neat epoxy coating, which was illustrated in Figure 11. At the fresh stage, model B with Warburg impedance element (W) was introduced to fit the EIS data. It appeared that there were diffusion paths for the electrolyte to reach the coating-substrate interface and initiated coating degradation. After 500 hours of exposure, model C was suitable for the neat epoxy sample due to the accumulated corrosion products at the coating-substrate interface.

Observation indicated neat epoxy could potentially generate micro-pores, which allow electrolyte to penetrate through the film and reach coating-metal interface, eventually leading to a reduction in barrier performance, particularly in long-term performance, as confirmed elsewhere [27, 28]. The suggestion was confirmed by employing SEM images of the abraded coating surfaces; the observation, illustrated in Fig. 5.9(a), indicated that neat epoxy coating is a porous layer with air entrapped in the voids [69]. On the contrary, a clear benefit of reducing the porosity of epoxy resin was observed in the nanofiller/epoxy coating; hence, the micro-pores and voids were filled with nano filler and led a significant enhancement in barrier properties to prevent penetration of corrosive materials (see Fig. 5.9(b)).

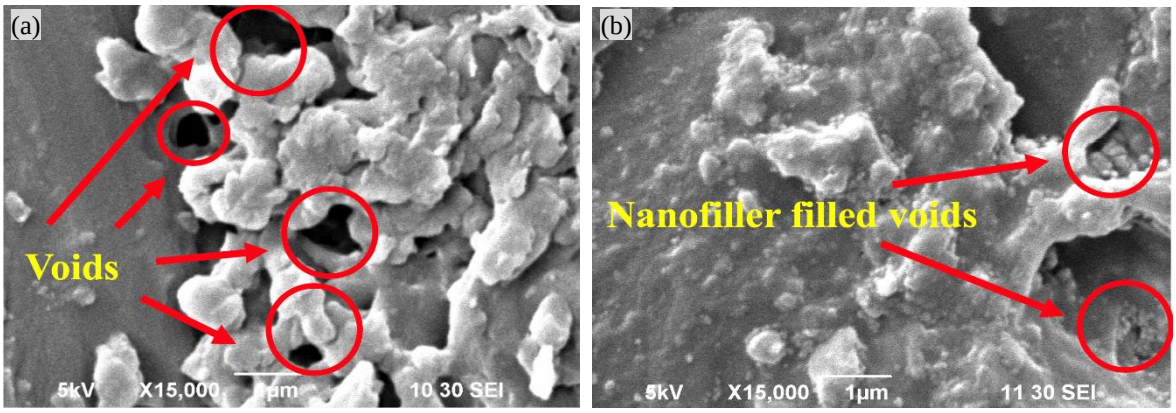

Figure 5.9: SEM image of the abraded surface for (a) neat epoxy surface with voids, (b) NS/epoxy with filled voids

(b) CNT/epoxy nanocomposites

Before exposure: Fig. 5.10 has shown the Bode plots for the coatings that incorporated with CNT. Compared with neat epoxy, a reduction of impedance value was observed at the lower frequency region of impedance plots, and it is observed that the values were gradually decreased with higher content of CNT in the composites. The electrical resistance of the coatings was reduced by the high conductive network formed by CNT, and also reduced the polymer interfacial layer thickness for the hopping of electrons [24], [80]. In the phase angle plot, with the breakpoint frequency at -45° shifted to the high-frequency region, indicating a remarkable drop of capacitance in the coating matrix compared with the neat epoxy system. At this stage, the model B with Warburg element was adequately used to analyze the impedance data for all CNT/epoxy coatings.

After exposure: As the exposure time elapsed, for 1.0%, 1.5%, and 3.0%C-Epoxy groups, both of the impedance value at the lowest frequency in the Bode plot has increased after exposure. This phenomenon was attributed to the corrosion product layer formed by corrosion reactions. As the exposure time elapsed, the accumulated corrosion products formed a thin film on the substrate

surface. Slight decreases of impedance modulus were observed for the coating with low content of CNT (0.1 and 0.5 wt.%). All the CNT/epoxy groups reached to stage IV (model C) at 100 hours exposure due to the accumulated corrosion products at the coating-substrate interface.

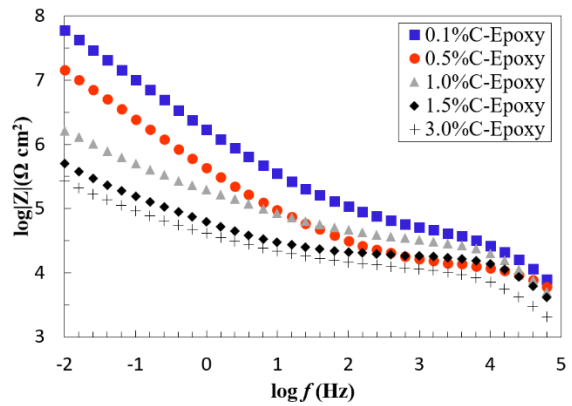

(a)

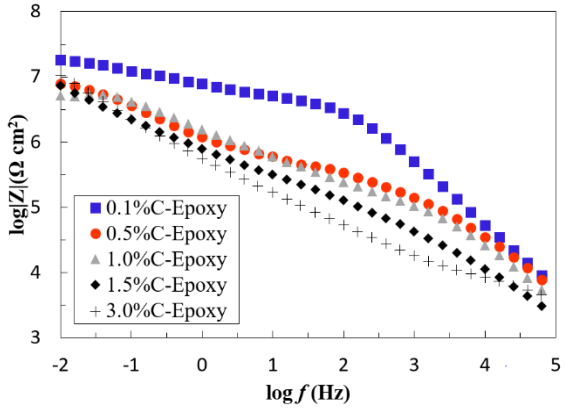

(b)

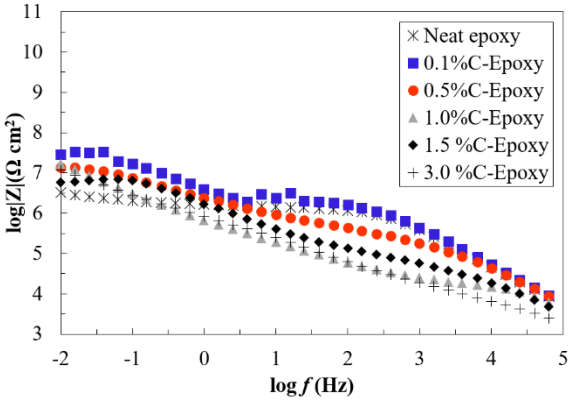

(c)

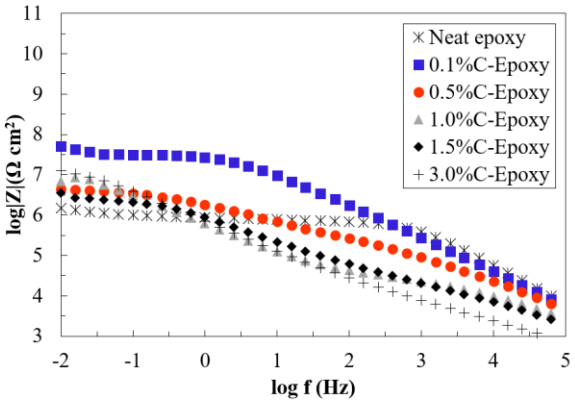

(d)

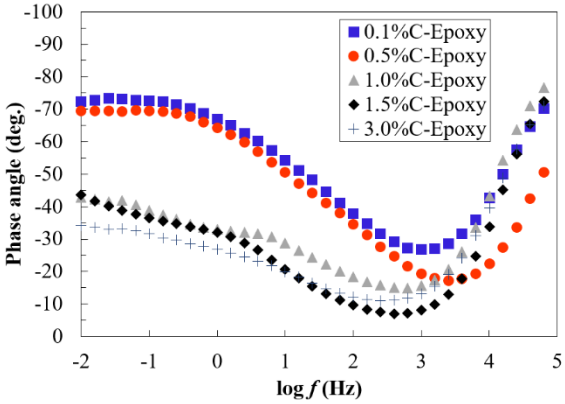

(e)

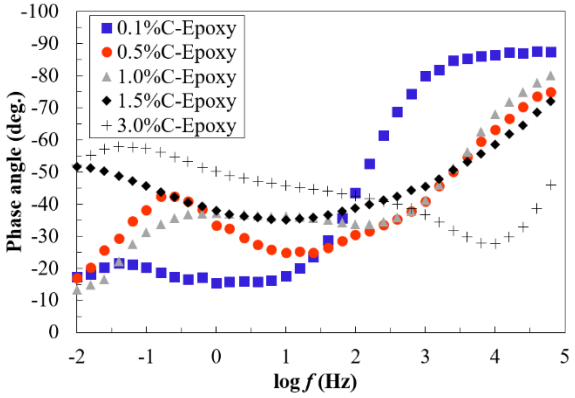

(f)

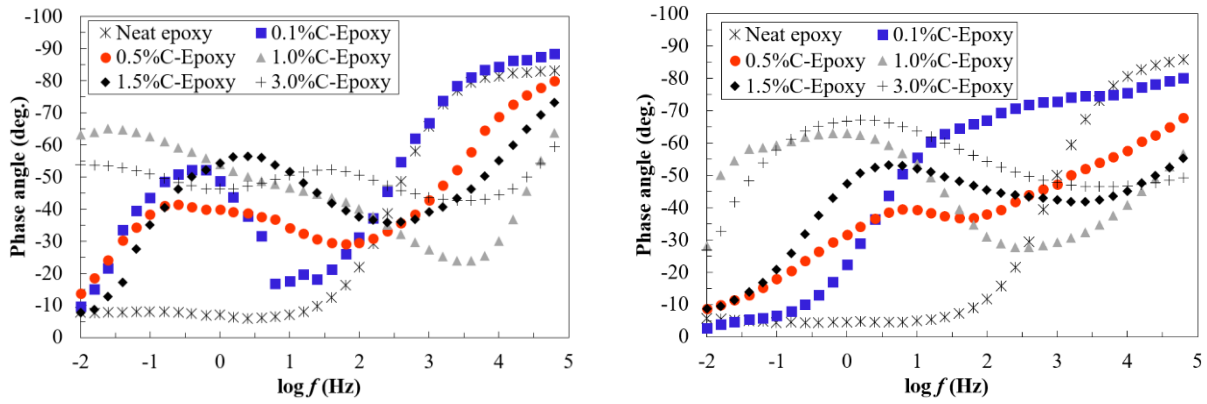

(g) (h)

Figure 5.10: Impedance curve and phase angle curve of the CNT/epoxy before exposure (a)(e), and after 100 hours (b)(f), 200 hours (c)(g), and 500 hours (d)(h).

(c) GNP/epoxy nanocomposites

Before exposure: On the other hand, the anticorrosion properties of the epoxy coating can be considerably improved by the addition of low content of GNP. The 0.1, 0.5, and 1.0 wt.% GNP/epoxy groups exhibit higher impedance modulus compared with the neat epoxy sample. The coating resistance of 0.1%G-Epoxy is much higher than the 0.5%G-Epoxy and 1.0%G-Epoxy. Degradation of the corrosion resistance could be observed with a higher concentration of graphene, which the Zmod value started to decrease in the graphene/epoxy composite with 1.5 wt.% of graphene. This observation indicated that the GNP/epoxy coatings offered the enhanced resistance to corrosion. As there was no electrode reach the coating-substrate interface, model A was fitted well with groups 0.1% to 1.0%G-Epoxy.

Moreover, model B with the Warburg element was used to fit the EIS data for the neat epoxy, 1.5%G-Epoxy, and 3.0%G-Epoxy samples. It appeared that there were diffusion paths for the electrolyte to reach the coating-substrate interface and initiated coating degradation. Particularly, the group 3.0%G-Epoxy, illustrated in the inserted plot in Fig. 5.11, exhibited the lowest impedance values in the low-frequency region of the Bode plot. As a result, the 3.0%G-Epoxy has the weakest corrosion resistance and cannot provide effective corrosion protection as a coating.

After exposure: As clearly illustrated in Fig. 5.11, the durability tests further confirmed that using graphene nanoplatelets as nanofillers to modify the polymeric coatings significantly enhanced their long-term barrier performance. Among all the GNP/epoxy coatings, the group 0.1, 0.5 and 1.0%G-epoxy exhibited the best performance in terms of significant improvements of durability. With a slight decrease in the impendence modulus at 0.01 Hz, suggesting that the coating film with 0.1 to 1.0 wt.% GNP content still provided an effective barrier for the substrate after the 100-hour exposure. However, the phase angle at low frequency has reduced, presenting the penetration of electrode media into the coating film. Model B was well fitted for the 0.1 to 1.0%G-Epoxy groups at 100 hours and changes to model B with Warburg elements at 500 hours.

Similar to the short performance, the higher graphene contents had little contribution to the corrosion resistance mainly due to the graphene agglomeration. Fig. 5.11 showed that the 1.5%,

and 3.0%G-Epoxy groups, exhibited the inferior long-term performance, identical to the neat epoxy ones, and results were well fitted with model C at 500 hours.

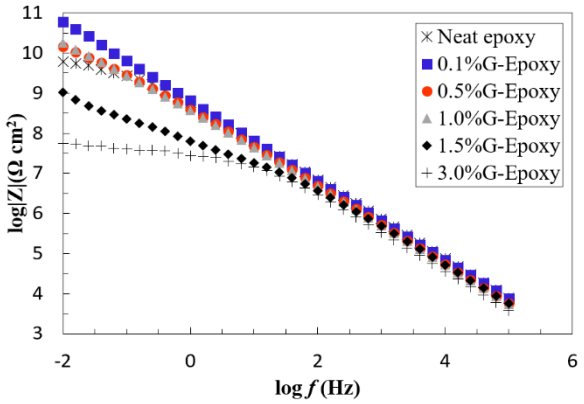

(a)

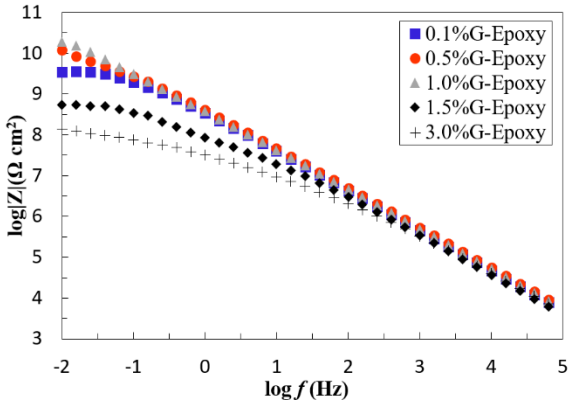

(b)

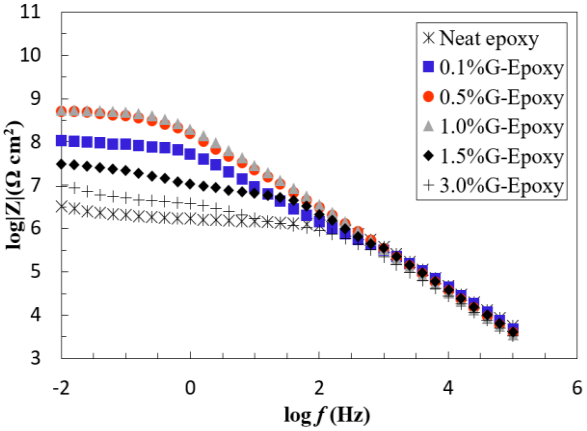

(c)

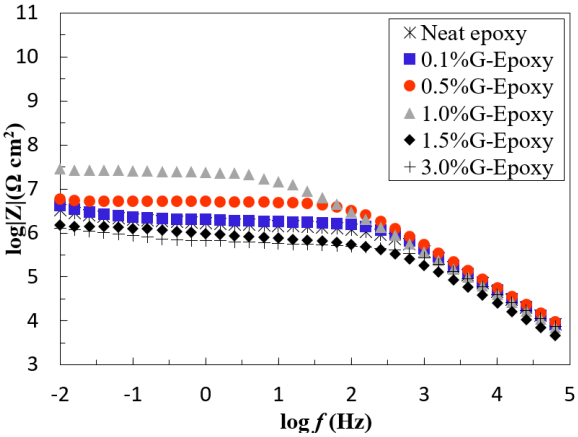

(d)

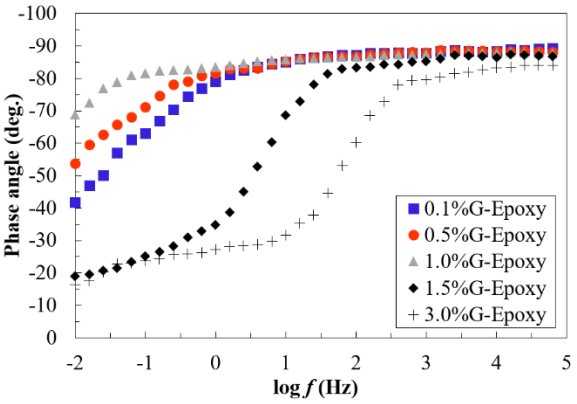

(e)

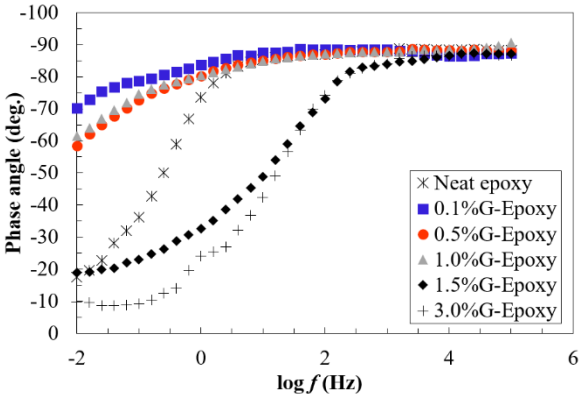

(f)

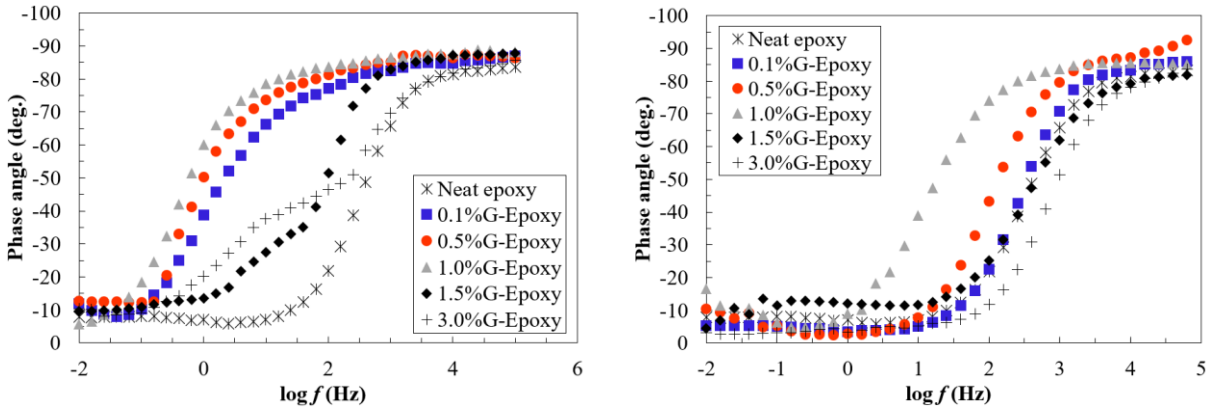

(g) (h)

Figure 5.11: Impedance curve and phase angle curve of the GNP/epoxy before exposure (a)(e), and after 100 hours (b)(f), 200 hours (c)(g), and 500 hours (d)(h).

(d) NS/epoxy nanocomposites

Before exposure: All prepared NS/epoxy groups, illustrated in Fig. 5.12, demonstrated high impedance value at the low-frequency region (0.01Hz), which reflected a better protective property of the coatings. Also, the phase angles reached up mostly approached 90° in a wide frequency region, indicating the coating behaved as an intact layer for corrosion protection [81]. At this stage, model A was well fitted for sample 0.5% to 1.0%S-Epoxy, as the incorporation of NS into epoxy resin could act as barriers fillers to prevent penetration of electrodes, result in a remarkable enhancement in corrosion protection performance [50].

However, for the 0.1%, 1.5% and 3.0% NS/epoxy system, the decreased impedance value (at 0.01Hz) in the Bode plot was observed. This observation suggested that 0.1 wt.% NS particles were not providing strong enhancement compared with 0.5% and 1.0 wt.% NS. Also, similar to GNP/epoxy system, material degradation could be obtained while higher content of NS particles was added, possibly caused by the severe agglomeration of nanoparticles. At this stage, the electrochemical behavior of the 0.1%, 1.5%, and 3.0%S-Epoxy could be presented with model B with the Warburg element, as shown in Fig. 5.12.

After exposure: Results in Fig. 5.12 showed a remarkable drop in the impedance value in Bode plot for most of the NS/epoxy groups, besides the 0.5%S-Epoxy. Compared with the results in the short term, which excellent corrosion protection was obtained in all tested groups, it can be understood that the NS/epoxy coating suffer delamination of corrosion protection during the exposure. Similar to the neat epoxy group, EIS results indicating the corrosive media have penetrated the coating films and initiated the corrosion process with the metal substrate. However, in contrary, the 0.5%S-Epoxy system with 0.5 wt.% of NS revealed a remarkable enhancement in corrosion protection performance. At the stage, the 0.5%S-Epoxy coating remained. This observation indicates the 0.5 wt.% NS has effective enhance the barrier property of epoxy, which filled the pores and diffusion pathways in the polymeric matrix, and the coating maintained in stage one which could be presented by model A from 100 to 200 hours, and then changed to model B with Warburg elements at 500 hours. Besides the 0.5%S-Epoxy, model B with Warburg elements was used to describe the corrosion stage of other NS/epoxy samples from 100 to 200 hours and changed to model C at 500 hours.

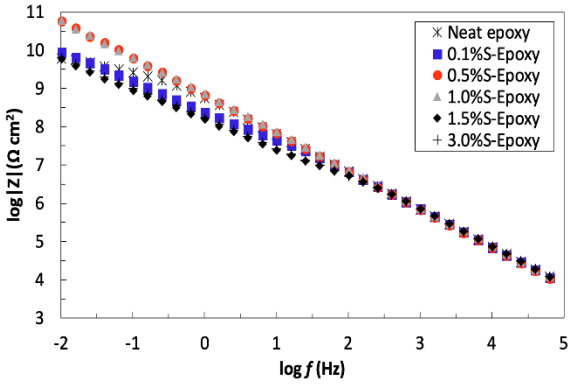
Neat epoxy
0.1%S-Epoxy
0.5%S-Epoxy
1.0%S-Epoxy
1.5%S-Epoxy
3.0%S-Epoxy
log|Z|(Ω cm²)
log f (Hz)

(a)

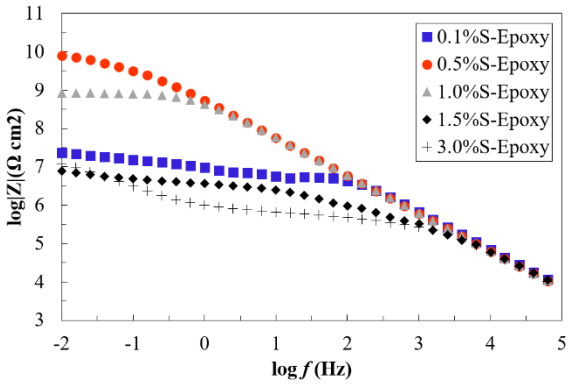
0.1%S-Epoxy
0.5%S-Epoxy
1.0%S-Epoxy
1.5%S-Epoxy
3.0%S-Epoxy
log|Z|(Ω cm2)
log f (Hz)

(b)

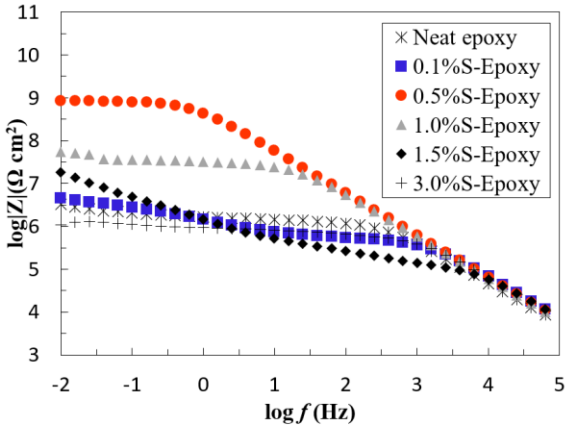
Neat epoxy
0.1%S-Epoxy
0.5%S-Epoxy
1.0%S-Epoxy
1.5%S-Epoxy
3.0%S-Epoxy
log|Z|(Ω cm²)
log f (Hz)

(c)

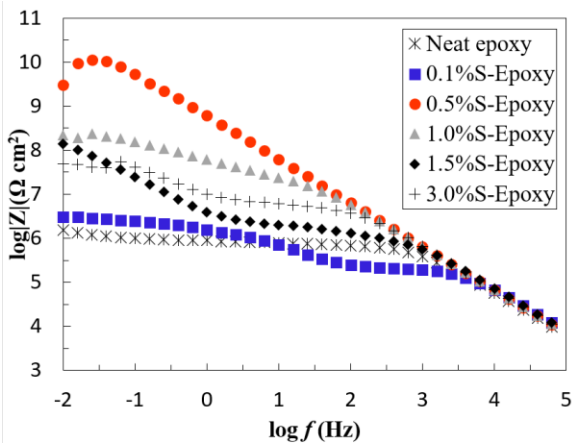
Neat epoxy
0.1%S-Epoxy
0.5%S-Epoxy
1.0%S-Epoxy
1.5%S-Epoxy
3.0%S-Epoxy
log|Z|(Ω cm²)
log f (Hz)

(d)

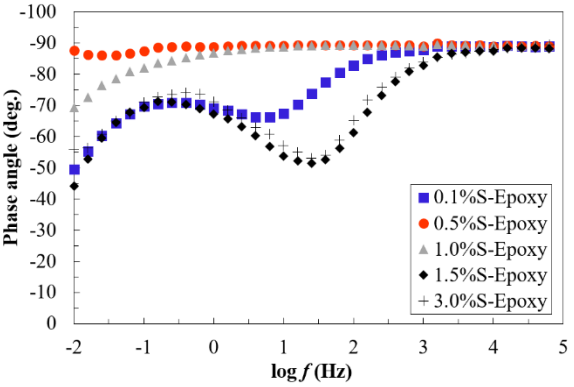
0.1%S-Epoxy
0.5%S-Epoxy
1.0%S-Epoxy
1.5%S-Epoxy
3.0%S-Epoxy
Phase angle (deg.)
log f (Hz)

(e)

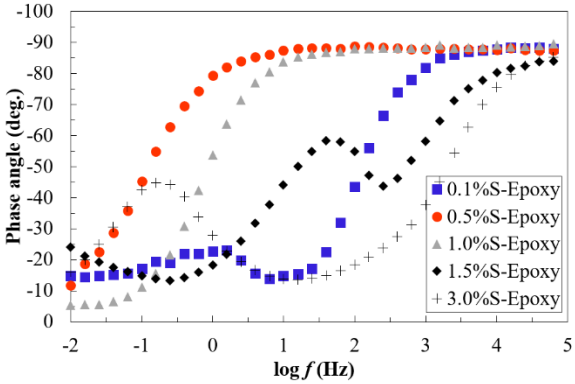
0.1%S-Epoxy
0.5%S-Epoxy
1.0%S-Epoxy
1.5%S-Epoxy
3.0%S-Epoxy
Phase angle (deg.)
log f (Hz)

(f)

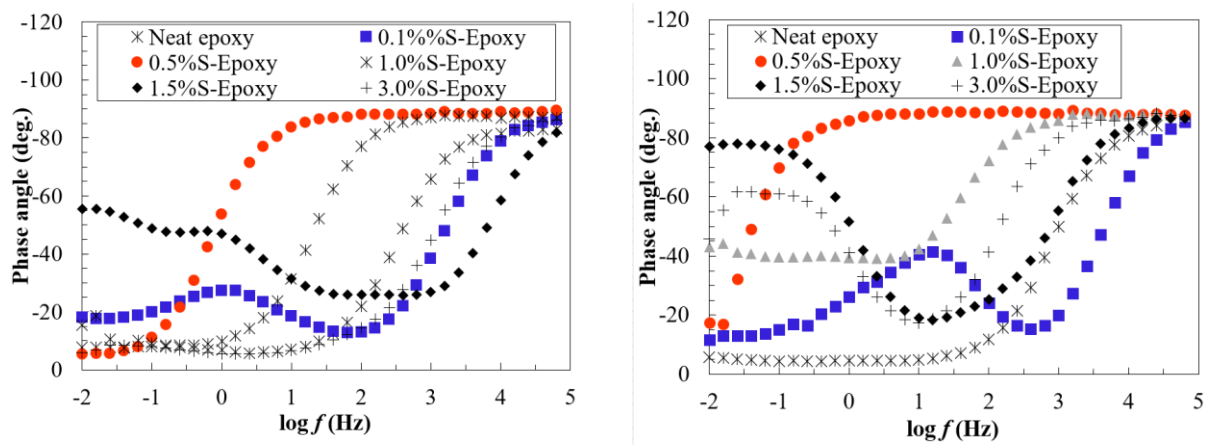

Figure 5.12: Impedance curve and phase angle curve of the NS/epoxy before exposure (a)(e), and after 100 hours (b)(f), 200 hours (c)(g), and 500 hours (d)(h).

In addition, the corrosion stage for each nanocomposite at different stage are presented in Table 5.1, which clearly that most of the nanocomposite reached to Model C after 500-hour exposure. However, the GNP and NS reinforced nanocomposite showed improved corrosion resistance while small amount of nanoparticles were added.

Table 5.1: Coating performance over time using equivalent circuit models

Label	Type of nanofillers	Nanofillers content (wt.%)	Corrosion stage under accelerated environmental stresses		
			Onset	100-hr	500-hr
Neat epoxy	/	/	Model B with W	Stage III	Stage IV
0.1% C-Epoxy	CNT	0.1	Stage III	Stage IV	Stage IV
0.5% C-Epoxy	CNT	0.5	Stage III	Stage IV	Stage IV
1.0% C-Epoxy	CNT	1.0	Stage III	Stage IV	Stage IV
1.5% C-Epoxy	CNT	1.5	Stage III	Stage IV	Stage IV
3.0% C-Epoxy	CNT	3.0	Stage III	Stage IV	Stage IV
0.1% G-Epoxy	GNP	0.1	Stage I	Stage II	Stage III
0.5% G-Epoxy	GNP	0.5	Stage I	Stage II	Stage III
1.0% G-Epoxy	GNP	1.0	Stage I	Stage II	Stage III
1.5% G-Epoxy	GNP	1.5	Stage III	Stage III	Stage IV
3.0% G-Epoxy	GNP	3.0	Stage III	Stage III	Stage IV
0.1% S-Epoxy	NS	0.1	Stage III	Stage III	Stage IV
0.5% S-Epoxy	NS	0.5	Stage I	Stage II	Stage III
1.0% S-Epoxy	NS	1.0	Stage I	Stage III	Stage III
1.5% S-Epoxy	NS	1.5	Stage III	Stage III	Stage IV
3.0% S-Epoxy	NS	3.0	Stage III	Stage III	Stage IV

5.3.2 Abrasion resistance

The results of the abrasion test for the nano-silica/epoxy groups were presented in Fig. 5.13. The abrasion resistance of the epoxy was significantly increased by the reinforcement of nano-silica. The lowest wear index value was observed in group 3.0% NS-Epoxy, which indicates maximum reinforcement was produced by the 3 wt. % of nano-silica. Also, the tendency of the curve shows

that the wear index was continuously decreased by increasing the concentration of nano silica from 0.1 to 3 wt. % and no degradation was observed in the test range. A comparison of abrasion resistance reinforcement between nano silica, CNT and GNP were performed in Fig. 5.13. The silica-epoxy groups exhibit higher abrasion resistance compared with graphene/epoxy groups in all the tested concentrations. Lowest wear index was still obtained in 1.0 and 1.5 CNT groups from the previous experiments. However, material degradation was observed in the high concentration of CNT/epoxy and graphene/epoxy groups. On the other hand, the wear index value of the nano-silica/epoxy groups was continuously decreased when the filler concentration was increased, which indicates the possibility of higher abrasion resistance could be observed with a higher concentration of nano-silica.

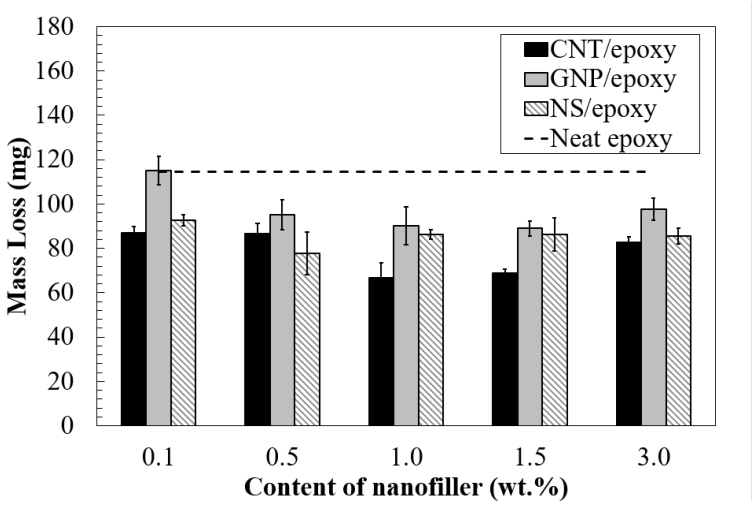

Figure 5.13: Abrasion resistance of single filler nanocomposite coatings

Fig. 5.14 presented the wear surfaces of the pure epoxy and nanocomposites; thus, A rougher surface was observed on the surface of pure epoxy resin, with a considerable proportion of micro-cracks and fractures (Fig. 5.14(a)), suggesting that the pure epoxy coating was subjected to plastic deformation and it has low wear resistance. On the other hand, as illustrated in Figure. 5.14(b)-(d), improved performance was observed in nanofiller composites based on the surface profiles. Generally, a reduction in the amount and size of micro-cracks was found in all the nanofiller / epoxy system, indicating enhanced abrasion resistance.

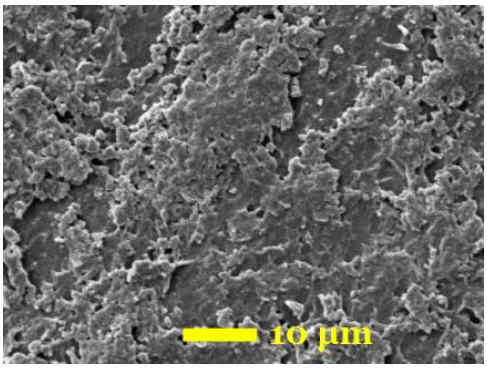

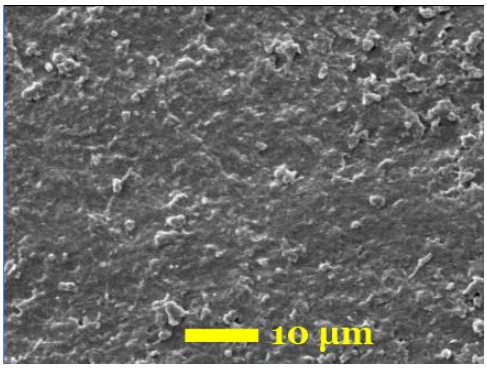

(a) Neat epoxy

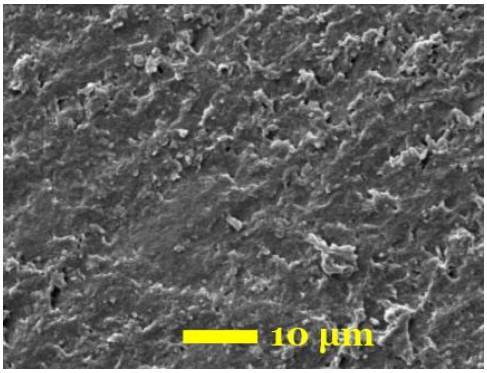

(b) 1.0 wt.% CNT/epoxy

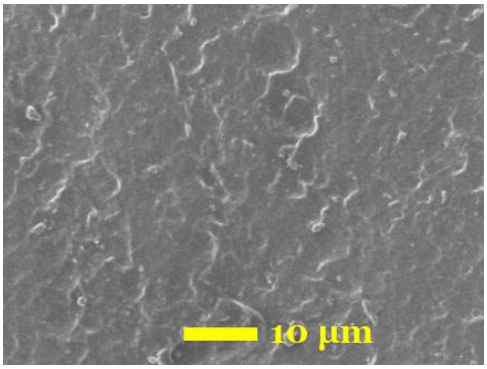

(c) 1.0 wt.% GNP/epoxy

(d) 1.0 wt.% NS/epoxy

Figure 5.14: SEM image of abraded surfaces

5.3.3 Coupon tension test

The tensile property of varied nanofiller reinforced epoxy was determined by the dogbone tensile test, following ASTM D638. The Nanocomposites can be characterized by measuring maximum tensile stress, strain at failure, and Young's modulus in this test. The tensile tests of CNT, GNP, and NS groups were performed in this work.

Fig. 5.15 displayed the tensile strength of the tested nanocomposites at varied concentrations, and a similar tendency was observed as shown in Young's modulus curves. The results indicated the CNT had the highest reinforcement in the tensile strength, which could be contributed by the higher bonding strength between CNT and epoxy resin. CNT provided more effective way to enhance the coating strength, as compared to other two nanoparticles. A gradual increase of the tensile strength was observed in CNT groups as increased in the particle content, and the maximum tensile strength reached up to 38.0 MPa at 1.0 wt.% of CNT, with a 55% increase as compared to that of pure epoxy groups (i.e., 24.0 MPa). The tensile strength exhibited a reduction at higher concentration of CNT at 1.5 wt. % or more due to particle agglomeration. Differently, the highest strength value at the GNP/epoxy groups were found at content rate of 0.1 wt.%, with a 40.0 % improvement. The maximum tensile strength of NS/epoxy groups occurred in 0.5, 1.0, and 1.5 wt.% groups, which increased by 33.0 % as compared to that of the epoxy group. Material degradation was found at higher concentration (3.0 wt.%) in all the three types of nanoparticle reinforced composites.

Fig. 5.16 showed the recorded results of Young's modulus for different nanocomposites. Clearly, carbon nanotube responded for the highest reinforcement to stiffness of composite coatings, and similar trend was observed from their tensile strength. The Young's modulus of the 1.0 % wt. C-Epoxy group reached the maximum of 1350.0 MPa, in an increase of 35.0% as compared to that of the pure epoxy. Young's modulus of GNP/epoxy or NS/epoxy groups had no apparent increase in most cases, indicating that neither Graphene nor nano silica had less contribution to improve coating stiffness. With increase of nanoparticle content over 1.5 wt.% or more, particle agglomeration was responsible for decreasing of Young's modules.

As clearly shown in Fig. 5.17, the trend for ultimate strain was different to those of tensile strength or Young's modulus. NS provided the highest enhancement to coating strain. The ultimate strain

in 1.5 % NS/epoxy group was 3.3 %, by 46.3% as compared to strain of 2.4 % in pure epoxy. Similar observations were found in CNT and GNP groups. Both composites exhibited a slight increase in ultimate strain with increase of particle content, particularly at 1.0 wt. % or more.

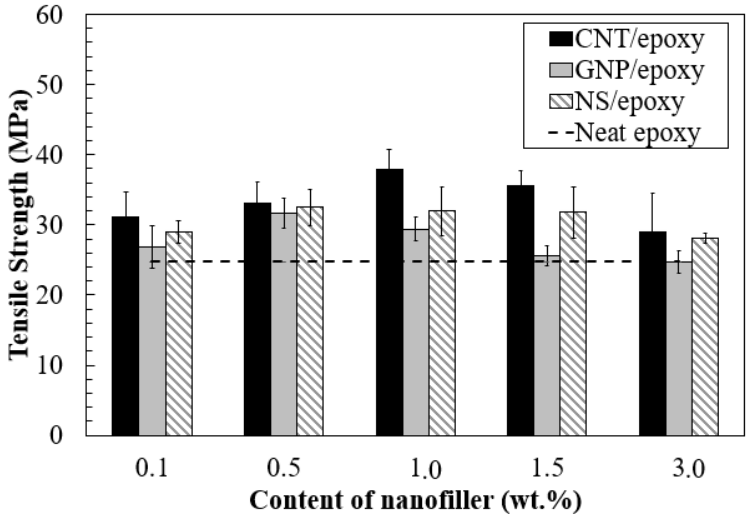

Figure 5.15: Tensile stress of nanofiller reinforced epoxy composites

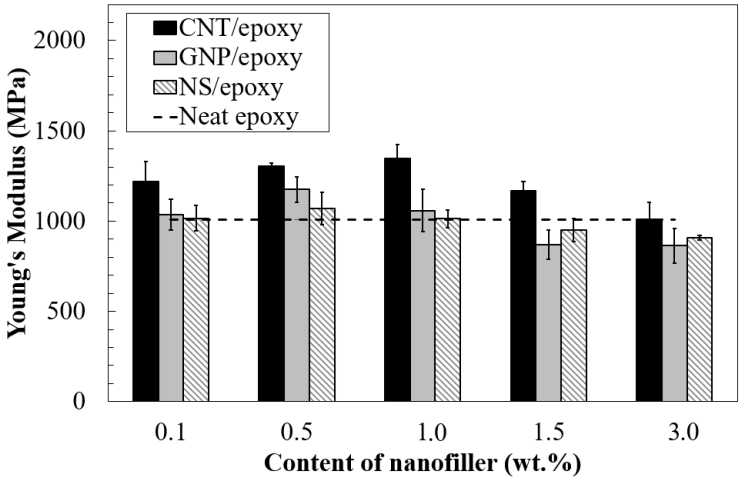

Figure 5.16: Young's modulus of nanofiller reinforced epoxy composites

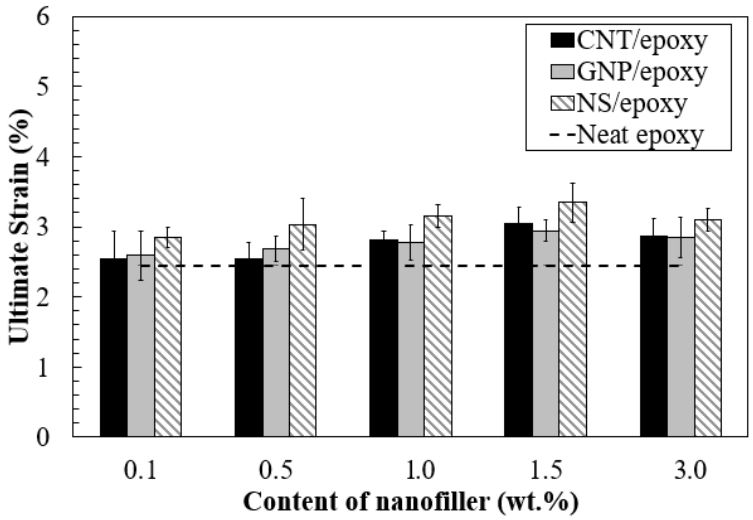

Figure 5.17: Strain at the failure of nanofiller reinforced epoxy composites

Fractured surfaces of specimens after tensile test were observed by microscopy and their microstructure were illustrated by SEM images, as shown in Figs. 5.18(a)-(d). A relatively smooth surface was observed in the pure epoxy sample, as shown in Fig. 5.18(a), which suggesting that the pure epoxy has typical brittle fracture behavior, and this was related to the low impact resistance and fracture toughness of the unreinforced composite material. As presented in Figs. 5.18(b)-(d), fracture surfaces of all nanocomposites were significantly rougher than pure epoxy materials. Especially for composites that containing silica nanopowders, as shown in Fig. 5.18(d), which has higher surface roughness and more compacted cracking cleavages, suggesting the samples has higher energy absorption and better resistance to fracture. These observations show a good agreement with the obtained tensile properties from NS/epoxy groups, as the nanocomposites have higher failure strain. Similar observations were found in CNT and GNP groups, which responded for good representative of strong adhesion between epoxy and well-dispersed nanofillers in the polymer matrix.

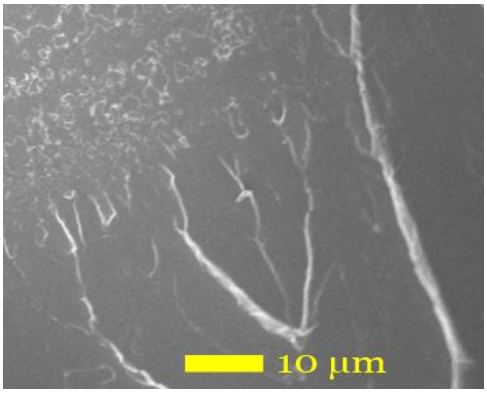

(a) Neat epoxy

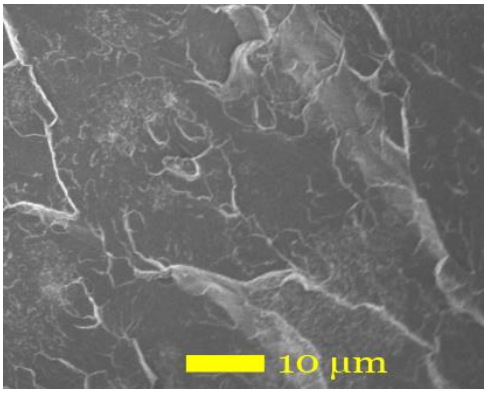

(b) 1.0 wt.% CNT/epoxy

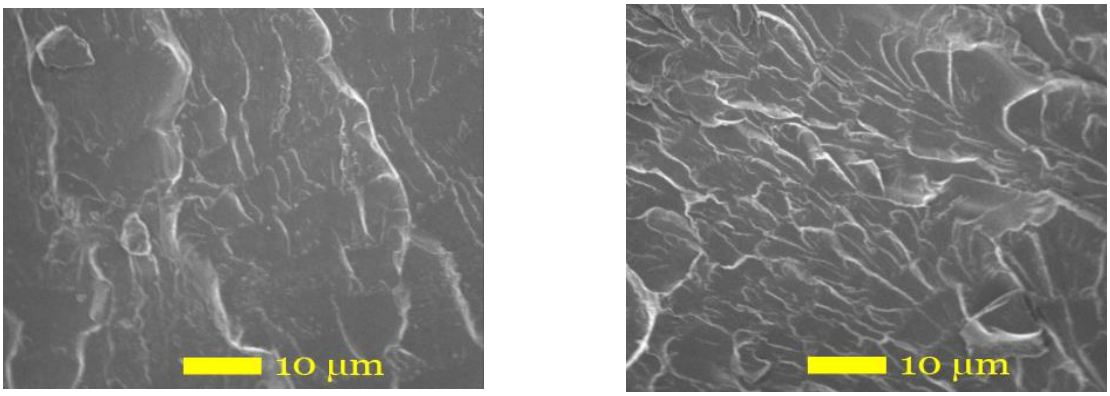

(c) 1.0 wt.% GNP/epoxy (d) 1.0 wt.% NS/epoxy

Figure 5.18: SEM images of fractured surface of the nanocomposites

5.3.4 Water contact angle

From the previous work, the contact angle of water for pure epoxy is around 51 degrees. The contact angle of water was significantly decreased when nano silica was added into the composites. Fig. 5.19 shows an example of water contact test for a sample of SE nanocomposites which the contact angle was decreased to 16 degrees. This result indicates that incorporating nano silica will not improve the hydrophobicity of the surface, possibly because SiO_2 nanoparticles are hydrophilic.

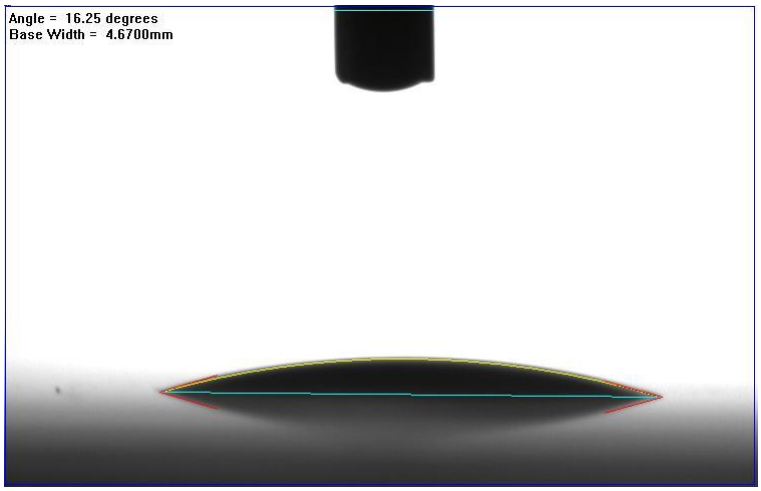

Figure 5.19: Water contact angle of 1% NS-Epoxy specimen

The surface roughness of the nanocomposite coatings was measured by Atomic force microscopy on the nanoscale. The obtained height changes can be used to sketch a 3-D image of the tested samples. A 3-D image example of neat epoxy and nanocomposites with each type of nanofiller was illustrated in Figs. 5.20(a)-(d), respectively. The surface roughness can also be calculated with these height change values.

Clearly, the overall of surface roughness had their characteristics, and the surface roughness of epoxy resin was dramatically decreased with the addition of the nanoparticles. The Ra value of pure epoxy is 29 nm, and it was decreased to less than 5 nm for most of the tested groups. These

results indicate that a significant decrease in surface roughness can be obtained by adding a small amount of nanofillers (0.1 wt.%). NS/epoxy groups exhibit the largest reduction in surface roughness which the Ra values are less than 3 nm at all tested concentrations.

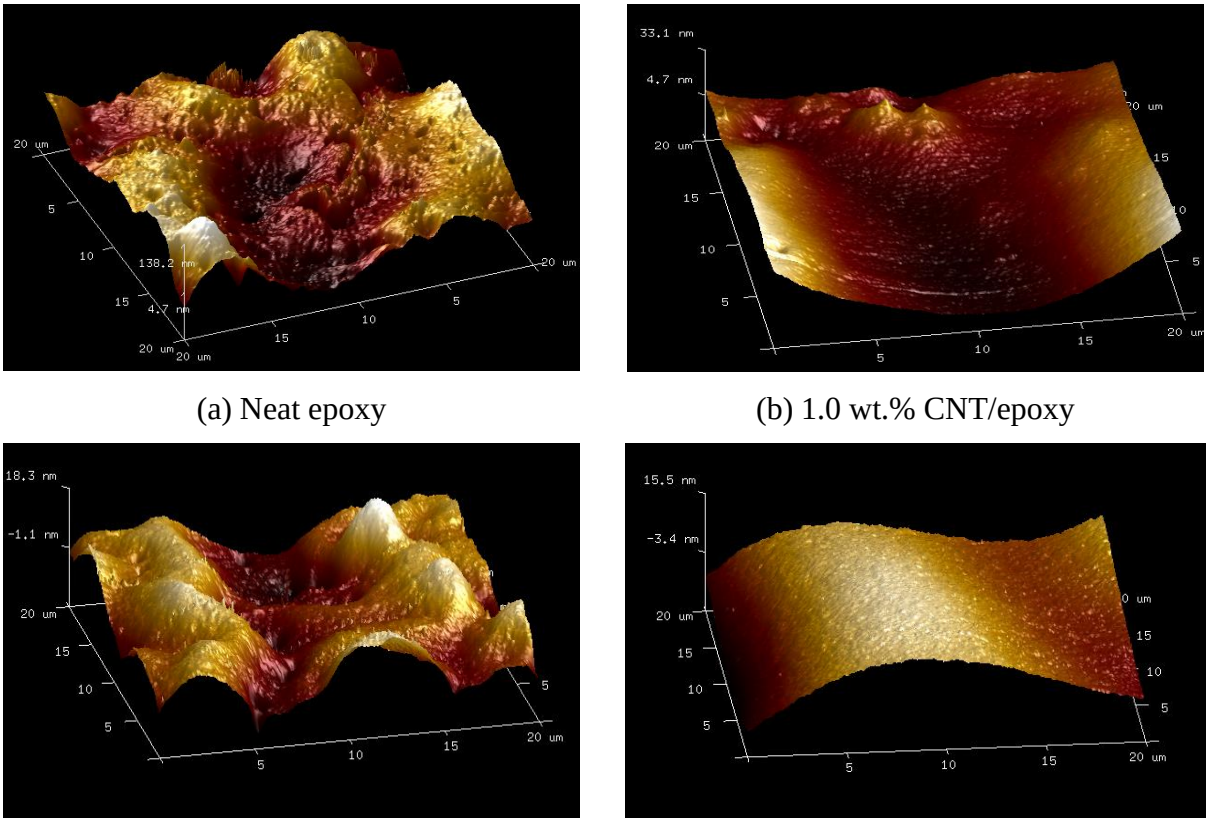

(a) Neat epoxy (b) 1.0 wt.% CNT/epoxy

(c) 1.0 wt.% GNP/epoxy (d) 1.0 wt.% NS/epoxy

Figure 5.20: AFM image of specimen surfaces

5.3.5 Adhesion to substrate

The pull-off strength (adhesion) was measured by following ASTM D4541 to evaluate the tensile bond strength of a Nano-reinforced epoxy with various CNT and graphene concentration. The tensile bond strength over the nanofiller concentration was shown in Fig. 5.21. The test results were also evaluated by the ANOVA method with a 99% confidence level. A similar tendency was obtained in CE groups, the adhesive strength had an increase due to the presence of CNT and reached the maximum at a critical CNT concentration, and material degradation was observed. The adhesion was improved in all CNT & epoxy groups with a maximum increase of 44% at 1 wt.% of CNT. It can be clearly observed that the adhesion generally decreases by incorporating NS into the epoxy adhesive. The results show that the tensile bond strength was decreased along with the increased concentration of NS in the composites and the maximum reduction was 43% at 3 wt. % of NS. Compared with NS and CNT, no significant changes of the adhesion were observed in the epoxy group with the addition of GNP. Slightly decreases were obtained when the concentration of GNP is larger than 0.5 wt. % and the adhesion have been reduced by 12% when the concentration of graphene is 1 wt.%.

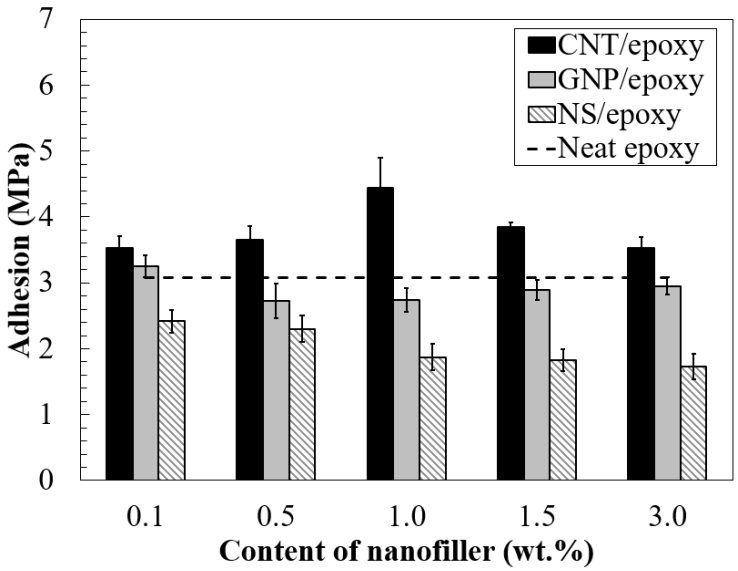

Figure 5.21: Pull off the strength of nanofiller/epoxy composites

The failure mode of the adhesive strength test is shown in Fig. 5. 22. It was clear that the coating completely peeled off the substrate in the neat epoxy, GNP/epoxy and NS/epoxy groups, suggesting the failure mode was adhesive failure. However, CNT/epoxy group showed cohesive failure, and it was attributed by the stronger adhesion of the coatings to the steel substrate, this observation showed good agreement with the corrosion protection performance of CNT/epoxy group in the previous discussion. A SEM image of the bottom surface of CNT/epoxy coating was presented in Fig. 5.23, it could be observed that the CNTs were exposed to the surface, which suggesting that they were providing mechanical interlocking between coating and substrate and improved the adhesion strength [82].

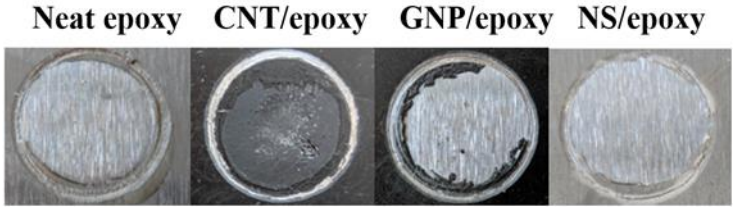

Figure 5.22: Failure mode of pull off test for nanofiller/epoxy composites

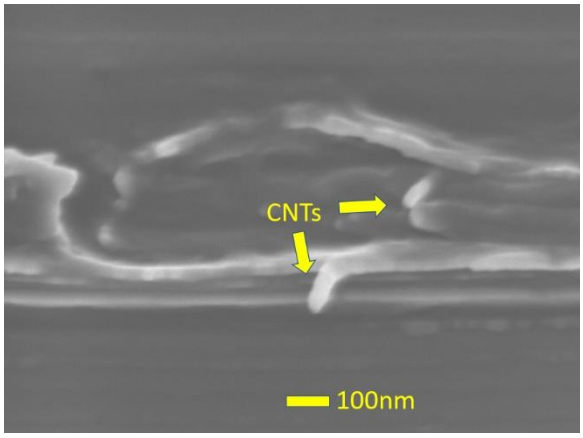

Figure 5.23: SEM image of bottom surface photograph of CNT/epoxy coating

5.4 SUMMARY

The electrical properties of epoxy-based nanocomposites with differently shaped nanofillers were evaluated in this study. Incorporation of carbon nanotubes, graphene nanoplatelets, and nanosilica into epoxy resin was employed to study their potentials as high-performance coatings to protect metallic structures. The nano-reinforced epoxy coating systems were prepared with the varied contents of nanofillers, ranging from 0.1 to 3.0 wt.%. The following major findings were summarized based on experimental results:

(a) Microstructural characterization indicated that the CNT and NS particles had the highest and lowest tendency to form agglomerates, respectively, and GNP is in between.
(b) Incorporating graphene or nanosilica in the polymer matrix significantly enhanced corrosion barrier performance in both short-term and long-term corrosive exposure.
(c) A remarkable drop of impendence modulus was observed in all tested CNT-epoxy composites at the fresh stage, but the composites exhibited a slow-down corrosion degradation rate in the long-term due to their high adhesion to the substrate.
(d) The incorporation of both GNP and NS in the epoxy reduced the water uptake. Increased water uptake was observed in CNT-epoxy composites, which responded to severe agglomeration and increased porosity in the coating system.
(e) The results of the experiments suggested that the 0.5-1.5 wt.% of nanofillers provided the most significant improvement in electrochemical properties.

CHAPTER 6. HYBRID NANOFILLER REINFORCED COMPOSITE COATINGS

**Note: the information in this Chapter has patent protection in the United States.*

6.1 BACKGROUND

Due to the limitations of using single nanofiller material, researchers have utilized the hybrid nanofiller materials to explore the synergistic effect of the nanofillers, thus, developing multifunctional coatings based on hybrid nanofiller composites [35], [83], [84]. Based on their studies' results, the hybrid filler system could form a more robust nanoparticle network with a better dispersion state and superior improvements compared with the polymer with a single filler. In this section, three types of hybrid nanofillers were examined, which included CNT/NS, GNP/NS, and CNT/GNP. The hybrid filler concentration was fixed at 1.0 wt.%, as the single filler nanocomposites with this weight content generally showed great overall improvement compared with others. Meanwhile, the nanofillers were mixed with a ratio of 25:75, 50:50, and 75:25 in order to comprehensively examine the "hybrid effect" of the binary nanofiller reinforcements.

6.2 PERFORMANCE OF HYBRID FILLER REINFORCED NANOCOMPOSITES

6.2.1 Corrosion resistance

(a) GNP/NS epoxy nanocomposites

Before exposure: The EIS results of epoxy with GNP/NS binary nanofillers were illustrated in Fig. 6.1. Compared with the neat epoxy, all GS-Epoxy groups exhibited high impedance value at the low-frequency region, suggesting that the excellent barrier performance of the protective coatings. Moreover, the phase angle remained close to 90 degrees in all the tested frequency, which reflected that the coating film behaved as an intact layer to protect the substrates. Overall, model A was suitable for all the GS-Epoxy groups at the fresh stage.

After exposure: Results indicated that the 1%GS-Epoxy (25:75) has weaker corrosion protection, compared with 1%GS-Epoxy (50:50) and 1%GS-Epoxy (75:25) samples. Remarkable drop of impedance value and phase angle shift were observed at 100 hours for the 1%GS-Epoxy (25:75) samples, which the overall performance was suitable for model B. On the other hand, the 1%GS-Epoxy (50:50) and 1%GS-Epoxy (75:25) samples maintained excellent corrosion protection properties at 100 hours, which model A was still well fitted for the EIS results.

After 500 hours of exposure, the 1%GS-Epoxy (50:50) has shown its extraordinary anti-corrosion performance. It is clear to observe that the impedance has been recovered during the immersion, as the impedance value was slightly decreased at 200 hours but recovered back at 500 hours. This observation suggested that the recovery is related to the NS/GNP nanofiller with a ratio of 50:50 since it was not observed in the neat epoxy coating. In summary, the 1%GS-Epoxy (50:50) sample remained in model A during the whole exposure, while the 1%GS-Epoxy (25:75) and 1%GS-Epoxy (75:25) were in model B with Warburg elements.

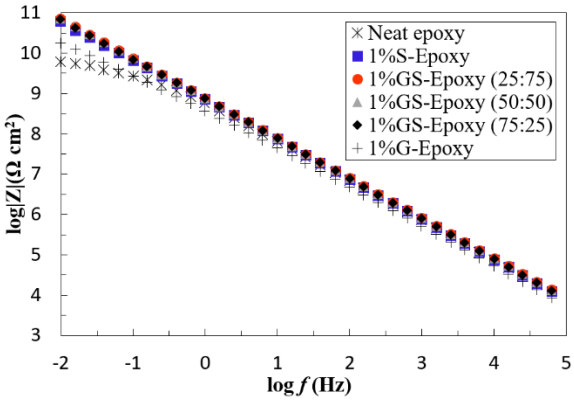
Neat epoxy
1%S-Epoxy
1%GS-Epoxy (25:75)
1%GS-Epoxy (50:50)
1%GS-Epoxy (75:25)
1%G-Epoxy
log|Z|(Ω cm²)
log f (Hz)

(a)

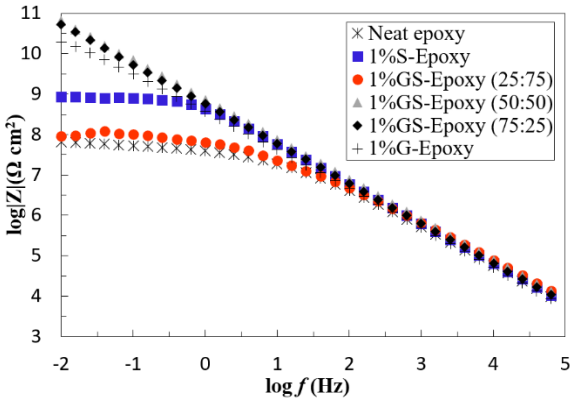
Neat epoxy
1%S-Epoxy
1%GS-Epoxy (25:75)
1%GS-Epoxy (50:50)
1%GS-Epoxy (75:25)
1%G-Epoxy
log|Z|(Ω cm²)
log f (Hz)

(b)

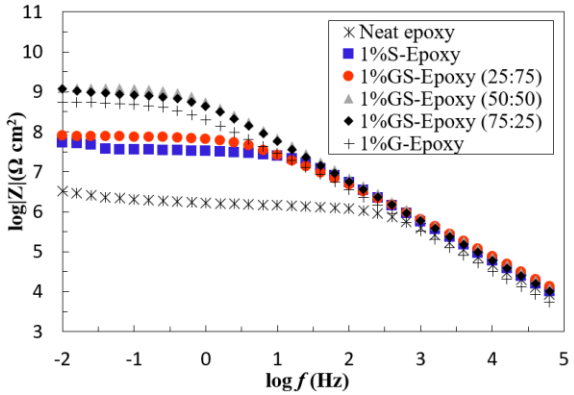
Neat epoxy
1%S-Epoxy
1%GS-Epoxy (25:75)
1%GS-Epoxy (50:50)
1%GS-Epoxy (75:25)
1%G-Epoxy
log|Z|(Ω cm²)
log f (Hz)

(c)

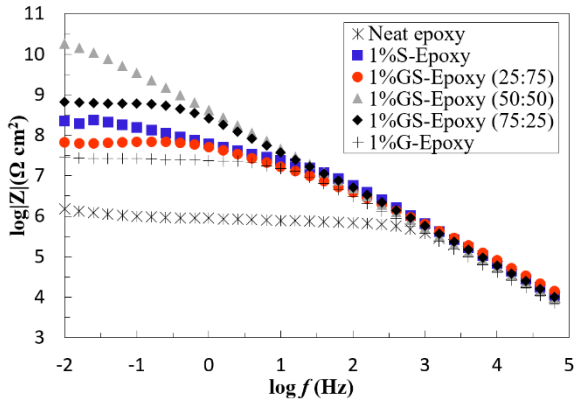
Neat epoxy
1%S-Epoxy
1%GS-Epoxy (25:75)
1%GS-Epoxy (50:50)
1%GS-Epoxy (75:25)
1%G-Epoxy
log|Z|(Ω cm²)
log f (Hz)

(d)

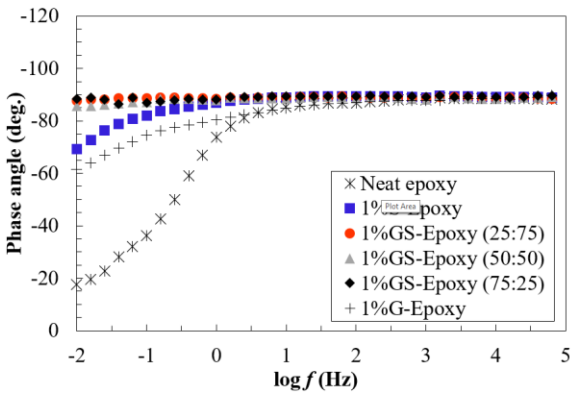
Neat epoxy
1%GS-Epoxy (25:75)
1%GS-Epoxy (50:50)
1%GS-Epoxy (75:25)
1%G-Epoxy
Phase angle (deg.)
log f (Hz)

(e)

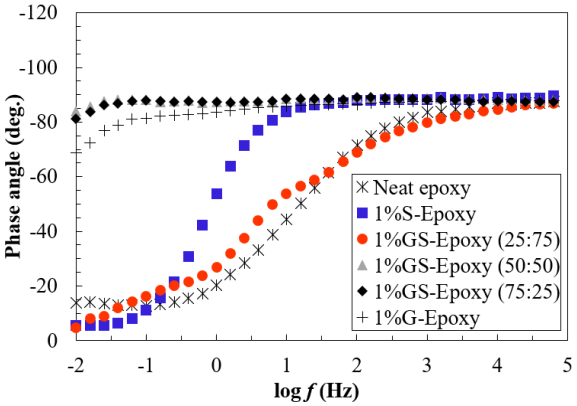
Neat epoxy
1%S-Epoxy
1%GS-Epoxy (25:75)
1%GS-Epoxy (50:50)
1%GS-Epoxy (75:25)
1%G-Epoxy
Phase angle (deg.)
log f (Hz)

(f)

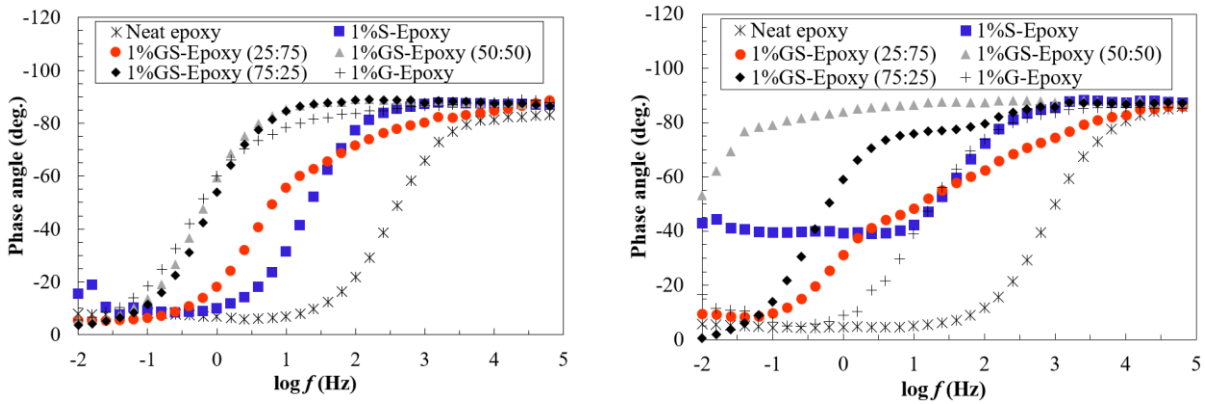

Figure 6.1: Impedance curve and phase angle curve of the GNP/NS epoxy before exposure (a)(e), and after 100 hours (b)(f), 200 hours (c)(g), and 500 hours (d)(h).

(b)CNT/NS epoxy nanocomposites

Before exposure: At fresh state, the CS-Epoxy exhibited a reduction of impedance along with the increase in the amount of CNT in the composites, which is not surprising as CNT has excellent conductibility, as shown in Fig. 6.2. Highest impedance value was observed in the 1%CS-Epoxy (25:75), with a slope of -1 and phase angles maintained around in 90 degrees. The overall performance indicated that the 1%CS-Epoxy (25:75) behaved as an intact coating which is in stage I (model A). Meanwhile, the other groups were in stage III, indicating there was the electrochemical reaction in the coating-substrate interface.

After exposure: The long-term performance of the CS-Epoxy confirmed the corrosion protection behavior in the short-term test. The impedance value of the 1%CS-Epoxy (25:75) was decreased in the 100 hours test, but recovered back after 200 hours, then slightly dropped in the 500 hours test. The corrosion phase was in stage III at 500 hours. Interestingly, the impedance recovery was observed in the CS-Epoxy group. We suggested that this phenomenon might be related with the NS in the composite as the impedance recovery has been observed in other composites with NS as well, for example: the 1%GS-epoxy (50:50) and 0.5%S-Epoxy.

On the other hand, the impedance value of the 1%CS-Epoxy (50:50) and 1%CS-Epoxy (75:25) was continuously decreased during the whole test, and the corrosion phase was in stage IV (model C) at 500 hours, revealing severe damage was occurred due to the corrosion attack.

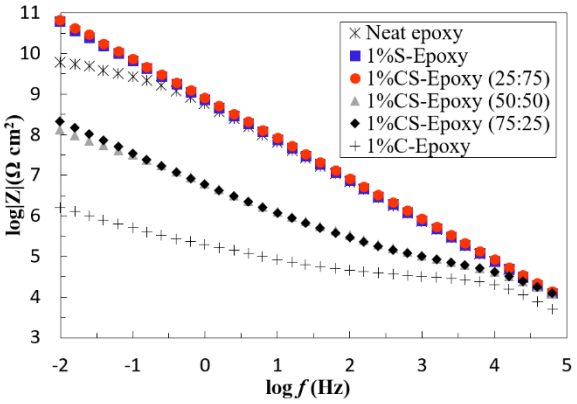
Neat epoxy
1%S-Epoxy
1%CS-Epoxy (25:75)
1%CS-Epoxy (50:50)
1%CS-Epoxy (75:25)
1%C-Epoxy
log|Z|/(Ω cm²)
log f (Hz)

(a)

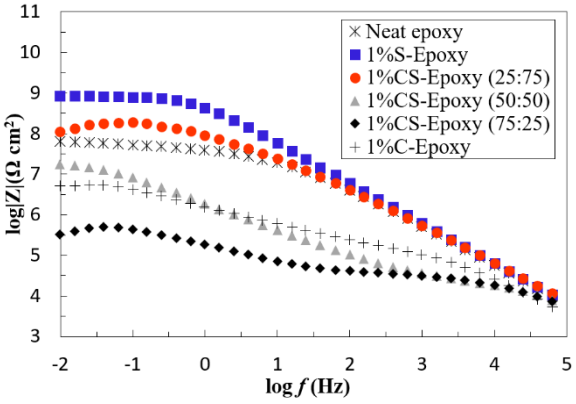
Neat epoxy
1%S-Epoxy
1%CS-Epoxy (25:75)
1%CS-Epoxy (50:50)
1%CS-Epoxy (75:25)
1%C-Epoxy
log|Z|/(Ω cm²)
log f (Hz)

(b)

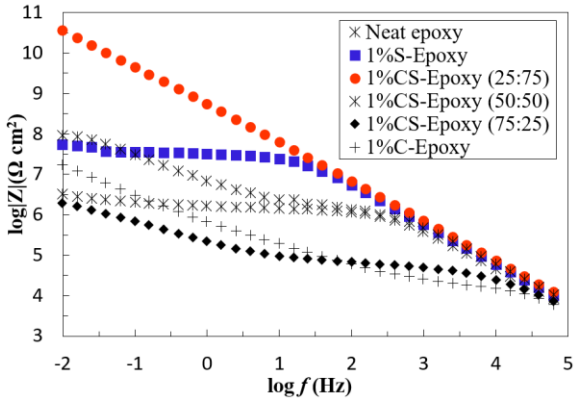
Neat epoxy
1%S-Epoxy
1%CS-Epoxy (25:75)
1%CS-Epoxy (50:50)
1%CS-Epoxy (75:25)
1%C-Epoxy
log|Z|/(Ω cm²)
log f (Hz)

(c)

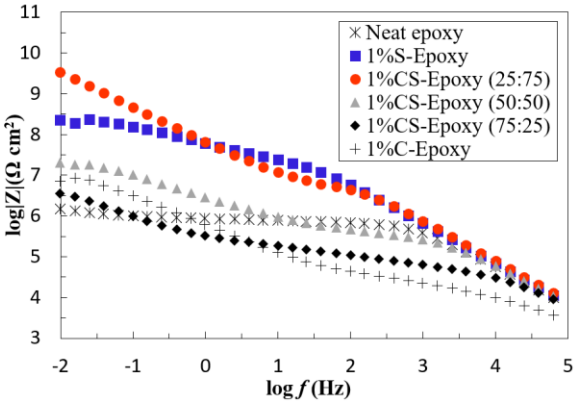
Neat epoxy
1%S-Epoxy
1%CS-Epoxy (25:75)
1%CS-Epoxy (50:50)
1%CS-Epoxy (75:25)
1%C-Epoxy
log|Z|/(Ω cm²)
log f (Hz)

(d)

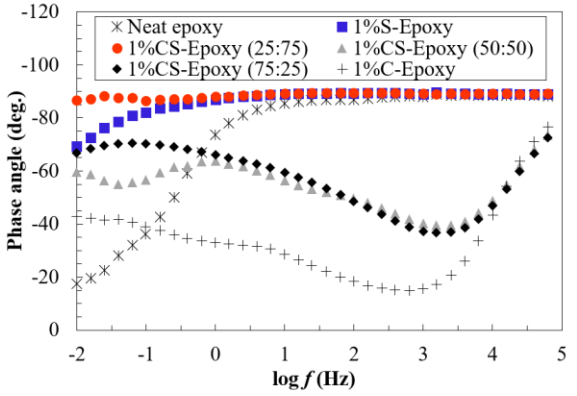
Neat epoxy
1%S-Epoxy
1%CS-Epoxy (25:75)
1%CS-Epoxy (50:50)
1%CS-Epoxy (75:25)
1%C-Epoxy
Phase angle (deg.)
log f (Hz)

(e)

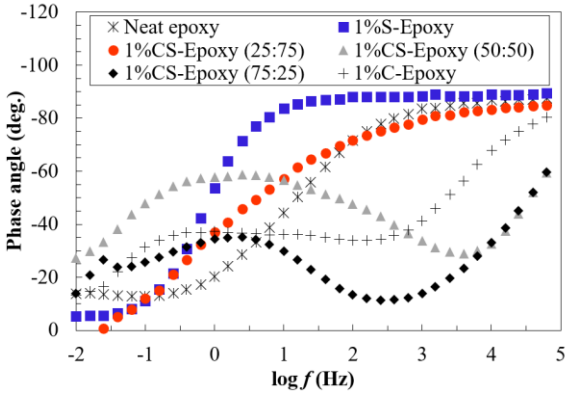
Neat epoxy
1%S-Epoxy
1%CS-Epoxy (25:75)
1%CS-Epoxy (50:50)
1%CS-Epoxy (75:25)
1%C-Epoxy
Phase angle (deg.)
log f (Hz)

(f)

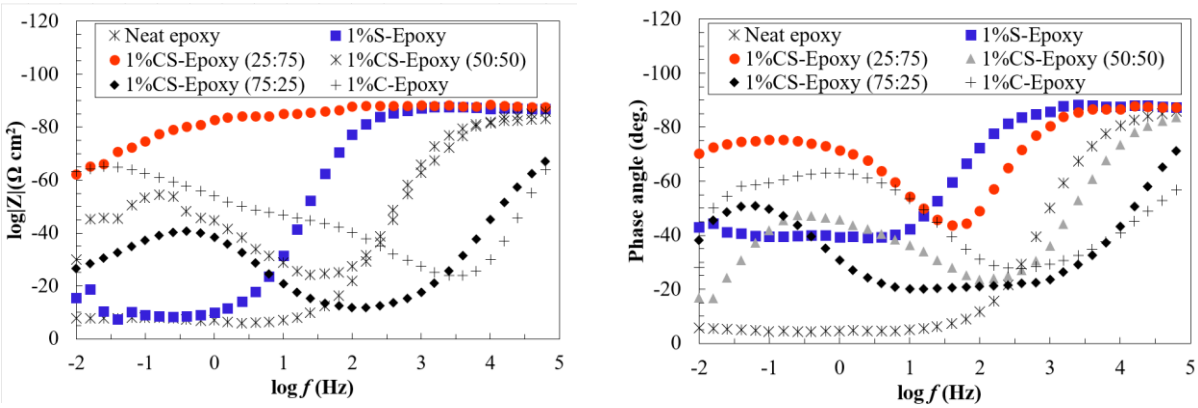

(g) (h)

Figure 6.2: Impedance curve and phase angle curve of the CNT/NS epoxy before exposure (a)(e), and after 100 hours (b)(f), 200 hours (c)(g), and 500 hours (d)(h).

(c) CNT/GNP epoxy nanocomposites

Before exposure: For the coatings that were containing CNT/GNP binary nanofillers as shown in Fig. 6.3, low impedance value was observed in all tested samples, which should be attributed to the high conductive network consisting of CNT and GNP. At this stage, all the test CG-Epoxy samples were in stage III (model B with Warburg element)

After exposure: Compared with the short-term performance, similarity of long-term performance was observed in the CG-Epoxy coatings, as the lower impedance value observed in the samples containing a higher content of CNT. The overall results suggested that the combination of CNT and GNP has weaker anti-corrosion properties in both short-term and long-term performance. The corrosion phase of all the tested CG-Epoxy samples reached stage IV (model C) at 500 hours.

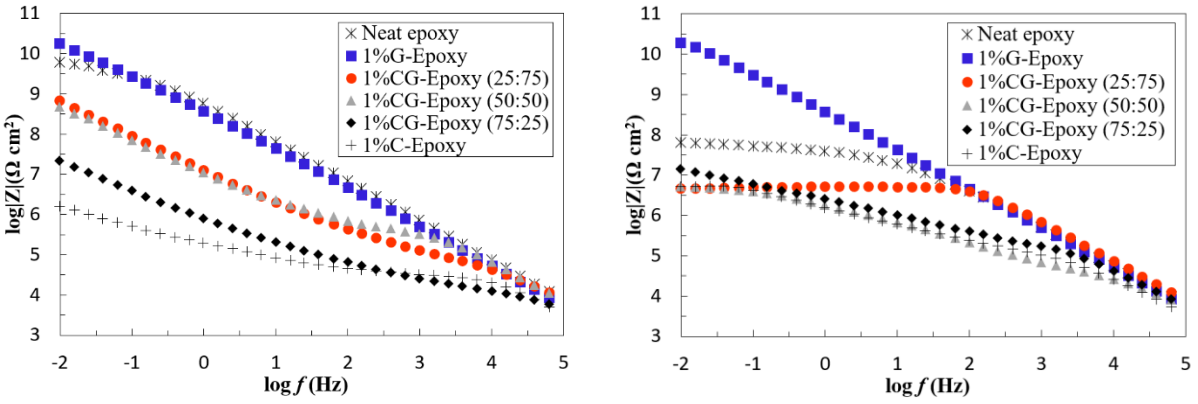

(a) (b)

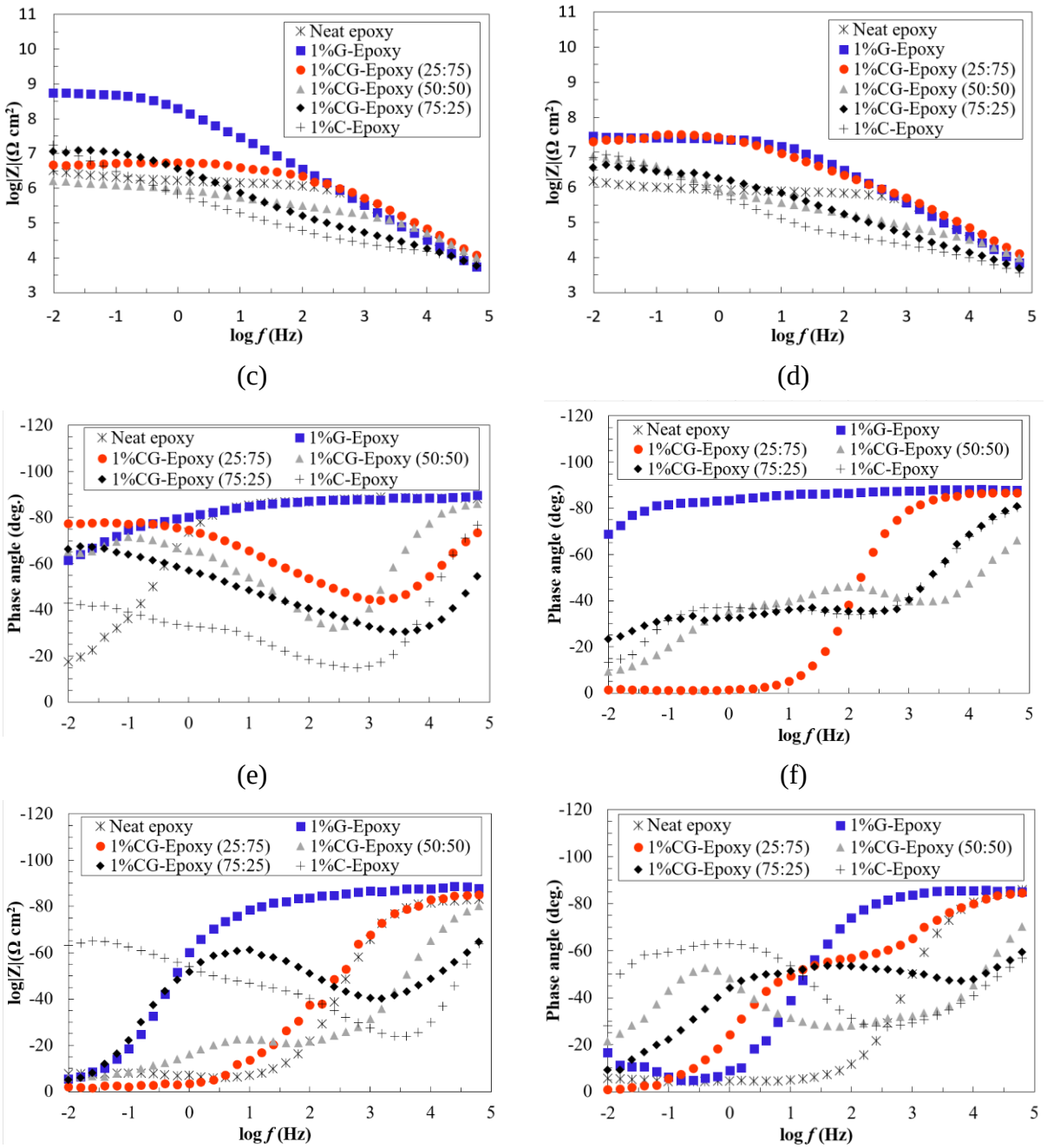

Figure 6.3: Impedance curve and phase angle curve of the CNT/GNP epoxy before exposure (a)(e), and after 100 hours (b)(f), 200 hours (c)(g), and 500 hours (d)(h).

6.2.2 Abrasion resistance

Figure 6.4 shows the wear index values of the nanofiller reinforced epoxy that obtained from abrasion test. A comparison of abrasion resistance reinforcement was performed between single nanofiller, hybrid nanofiller. Generally, for each combination of the hybrid nanofiller, the lowest wear index values were observed in the mixture that with a mix ratio of 0.5:0.5, indicating the maximum reinforcement was produced. The wear index values become higher at 0.25:0.75 and

0.75:0.25 groups which are generally higher than the single filler group (besides CG-Epoxy 25). Material degradation were observed in CS-Epoxy25, GS-EPoxy75. The wear index values are 0.1181 and 0.1270 for CS-Epoxy 25, GS-Epoxy 75 correspondingly, which are higher than neat epoxy (0.1135).

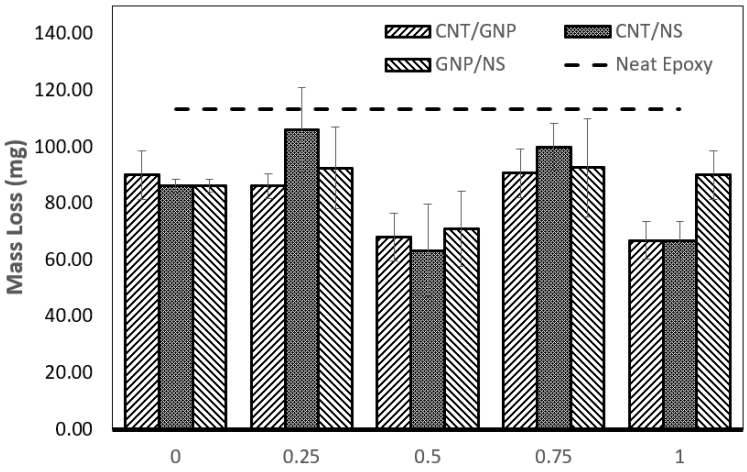

Figure 6.4: Wear index of hybrid nanofiller composites

6.2.3 Coupon tension test

The tensile properties of hybrid nanofiller reinforced epoxy is presented in Figures 6.5-6.7, and the results include maximum tensile stress, strain at failure, and Young's modulus which was obtained by the dogbone tensile test (ASTM D638). To evaluate the influence of varied mix ratios in the hybrid nanofillers, Figures 6.5-6.7 are used to demonstrate the maximum tensile stress vs. mix ratio, strain at failure vs. mix ratio, and Young's modulus vs. mix ratio, respectively.

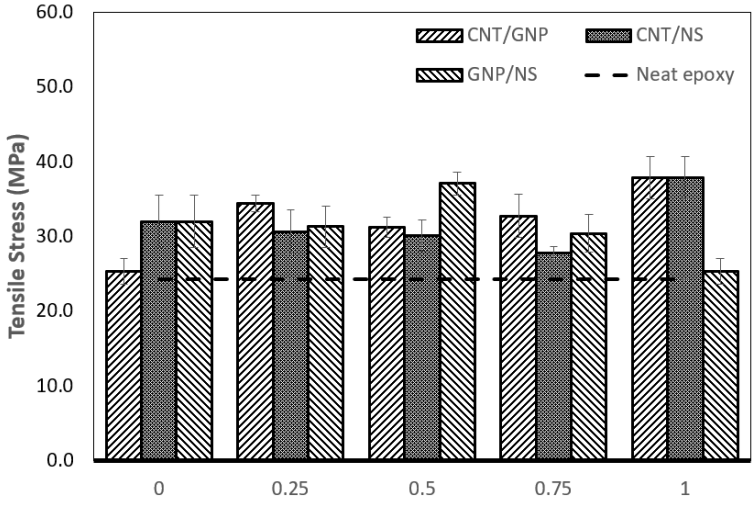

Figure 6.5: Max tensile stress of hybrid nanofiller composites

The variation of the max tensile stress of the CNT/GNP, CNT/NS and GNP/NS groups is shown in Figure 6.5. The highest tensile stress was observed in 1 wt. % of CNT with a value of 40.24 MPa. Dissimilar tendencies were observed in these three curves. In the CNT/GNP groups, the tensile stress was increased along with the higher mix ratio of CNT in the hybrid nanofiller.

Besides the pure CNT group, the CG-Epoxy 25 exhibits the highest max tensile stress value (34MPa) in the CG-Epoxy groups. However, the incorporation of the hybrid CNT/NS filler leads to a deduction of the max tensile stress compared with single filler reinforced epoxy. The tensile stress decreased to 27.77 MPa in CS-Epoxy 75 group, and the higher stresses were obtained in NS and CNT groups. Compare with CG-Epoxy and CS-Epoxy groups; the max tensile stress was obtained in the GS-Epoxy 50 group which is 36.66 MPa. The result indicates that the combination of GNP and NS in a ratio of 0.5:0.5 forms a more robust nanoparticles network.

Furthermore, the results of failure strain are presented in Fig. 6.6. Unlike the tensile stress curve, the highest failure strain was obtained in the hybrid nanofiller reinforced composite (CS-Epoxy 25) which a failure strain of 7.45% was observed. The strain was decreased in CSE1-50 group (5.84%) and then a higher strain was observed in the CS-Epoxy 75 group (6.47%). In CG-Epoxy groups, significant improvements of the failure strain were observed in all tested hybrid nanofiller composites. However, lower strain values were obtained in GS-Epoxy groups, which means the presence of GNP leads to decrease the flexibility of the NS composites.

The Young's modulus curves were shown in Fig. 6.7, and the highest value was still observed in 1% CNT groups. However, in the GS-Epoxy groups, a strong reinforcement was obtained in GS-Epoxy 50 group, Young's modulus reaches 643.17 MPa which has increased 28% and 26% comparing with SE and GE groups, correspondingly.

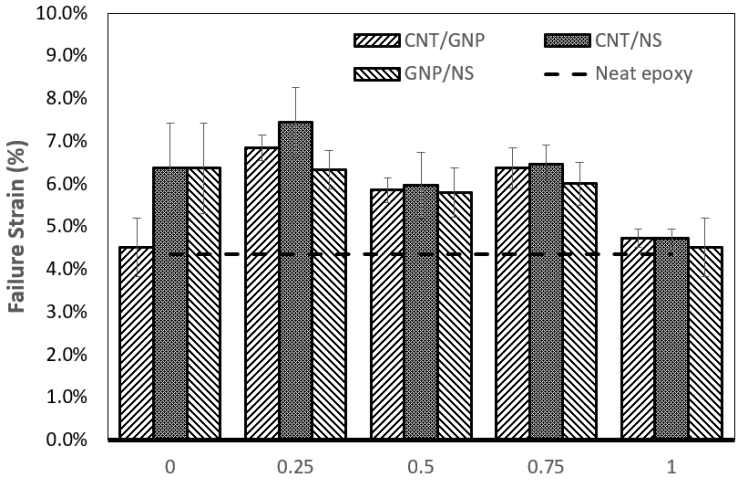

Figure 6.6: Strain at the failure of hybrid nanofiller composites

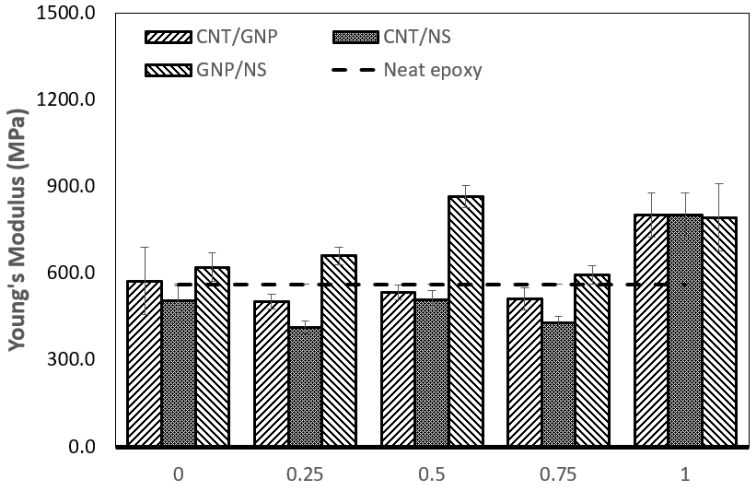

Figure 6.7: Young's modulus of hybrid nanofiller composites

6.2.4 Water contact angle

Compare with the last report, similar results of the contact angles tests were obtained. It is easy to observe that the contact angle was still dramatically decreased in the hybrid nanofillers reinforced epoxy with varied mix ratios. Generally, as shown in Fig. 6.8, the water contact angle was less than 10 degrees, indicating the surface became extremely hydrophilic when the hybrid nanofiller were added to the epoxy resin.

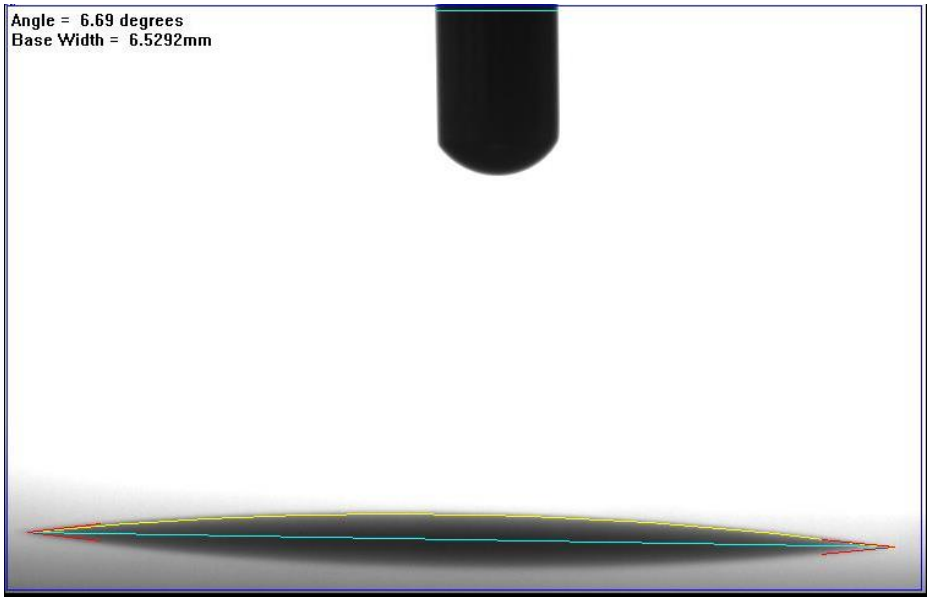

Figure 6.8: Water contact angle of CNT/Epoxy 25

6.3 SUMMARY

6.3.1 Selection of Nanofiller Reinforcement for Pipeline Applications

For simplicity, five types of nanocomposite coatings that exhibited excellent anti-corrosion performance were selected, with the impedance value and EEC model. The selected coatings were presented in Table 6.1, and they were ranked by considering the impedance values and the EEC model after exposure. It was clear to observe that the 1%GS-Epoxy (50:50) and 0.1%GS-Epoxy

groups have similar Zmod value and EEC model before and after exposure. However, we suggested that, compared with the 1%GS-Epoxy (50:50) groups, the 0.1%GS-Epoxy has weaker corrosion protection properties as the impedance value was significantly dropped at 100 hours. Excellent anti-corrosion performance was also observed in the 5.0%GS-Epoxy, 0.5%S-Epoxy, and 1.0%CS-Epoxy group, followed by the 1.0%GS-Epoxy (50:50) and 0.1%GS-Epoxy groups.

Table 6.1: Selected nanofiller reinforced coatings with excellent anti-corrosion performance

Group	Log Zmod		Corrosion stage	
	Onset	500 hr	Onset	500 hr
1%GS-Epoxy (50:50)	10.86	10.26	Stage I	Stage I
0.1%GS-Epoxy	10.40	10.47	Stage I	Stage I
5.0%GS-Epoxy	10.42	9.58	Stage I	Stage II
0.5%S-Epoxy	10.44	9.48	Stage I	Stage III
1%CS-Epoxy (25:75)	10.83	9.53	Stage III	Stage III

The specimens containing 0.1 and 1.0 wt.% of GNP/NS hybrid filler have shown their excellent anti-corrosion performance. In addition, the mechanical and tribological behavior of the developed nanocomposite coatings was evaluated by contact angle, pull-off strength, abrasion resistance, and dogbone tensile test. The results showed greater improvement was observed on abrasion resistance, mechanical strength for the specimen with 1.0 wt.% GNP/NS hybrid filler. To sum up, the 1.0 wt.% GNP/NS hybrid filler system was selected to reinforce the polymeric coatings, and the detailed characterizations of the nanofillers were presented in the following section.

6.3.2 Characterization of the Selected GNP/NS Hybrid Composite Coatings

In order to understand the synergetic effect of the selected GNP/NS hybrid nanofiller system, several characterization techniques were employed, and the observations were presented below.

(a) Particle size distribution

On the purpose to study the synergistic effect of hybrid nanofillers, particle size distributions of GNP, NS, and the hybrid filler at 1 wt.% were illustrated in Figure 6.9. The results exhibited a narrow size distribution of NS particles, as most of the particles were around 60-300 nm. Due to the NS particles were purchased commercially with a size 10-20 nm, so the results confirmed that the NS particles were further stacked up after dispersion. It was clear that the GNP particles were distributed in the range of 50 to 1000 nm, particles larger than 500 nm probably were attributed to the agglomeration of the particles.

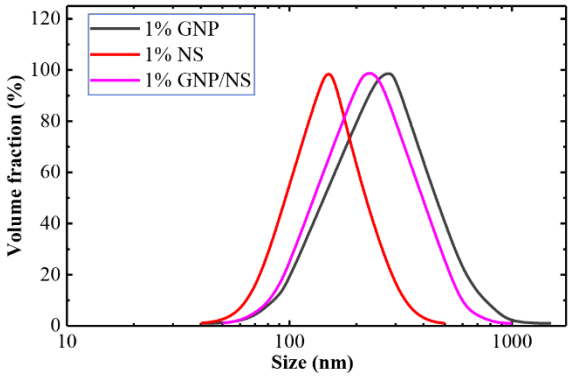

Figure 6.9: The particle size distribution of GNP/NS hybrid filler

As observed that the size distribution of the GNP/NS hybrid fillers was narrower than GNP particles, and also the average size was much smaller than the GNP particles. These observations indicated that the dispersion level was significantly improved in the hybrid filler system, as the formation of nanofiller aggregates were mitigated.

(b) Transmission electron microscopy (TEM)

Figure 6.10 presented the TEM micrograph of the morphology of the GNP/NS hybrid nanofillers. The images confirmed that the Nano-silica particles have uniformly hanged on the surface of the graphene nanoplatelets. Apparently, the Nano-silica particles were attached to the GNP during the dispersion procedure, which contains high-speed dispersion and ultrasonication. Overall, a unique three-dimensional structure was developed in the hybrid nanofillers by combining GNP and NS [85]. Based on the experimental results in the previous study, these hybrid particles have provided a stronger reinforcement compared with both single fillers (GNP and NS) when dispersed it into the epoxy resin as nanofillers.

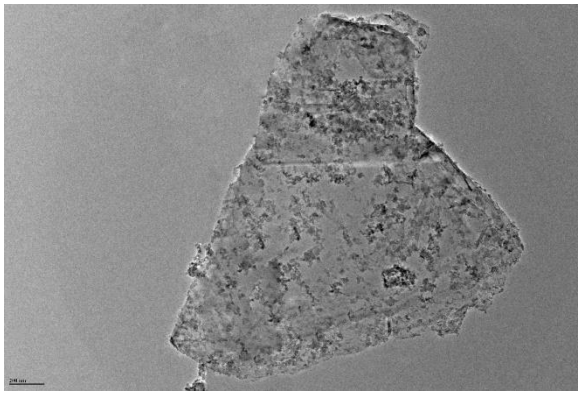

Figure 6.10: TEM photograph of GNP/NS hybrid filler

(c) X-ray powder diffraction (XRD)

Apart from that, Figure 6.11 presented the XRD patterns of GNP/NS hybrid fillers, and the results were compared with GNP and NS single fillers. It was clear that the hybrid filler showed two weak diffraction peaks at 26.5° and 19.5°. Based on the results before, the first peak was originated from the NS and the second one was from GNP sheets, indicating the NS and GNP particles were well mixed in the matrix.

However, note that the intensity of both peaks was weakened compared with singles fillers, especially the peaks that assigned to GNP, indicating proper intercalation and an increased degree exfoliation of GNP sheets in the matrix. The result also indicated that the nanoparticles were dispersed better in the hybrid filler system compared with the single fillers. The improved exfoliation state in the hybrid system suggested that the presence of NS particles destroyed the agglomerate of GNP sheets during the dispersion procedure, and after that, the covered NS on the GNP sheets has prevented them restacking together [64], [77], [79], [85].

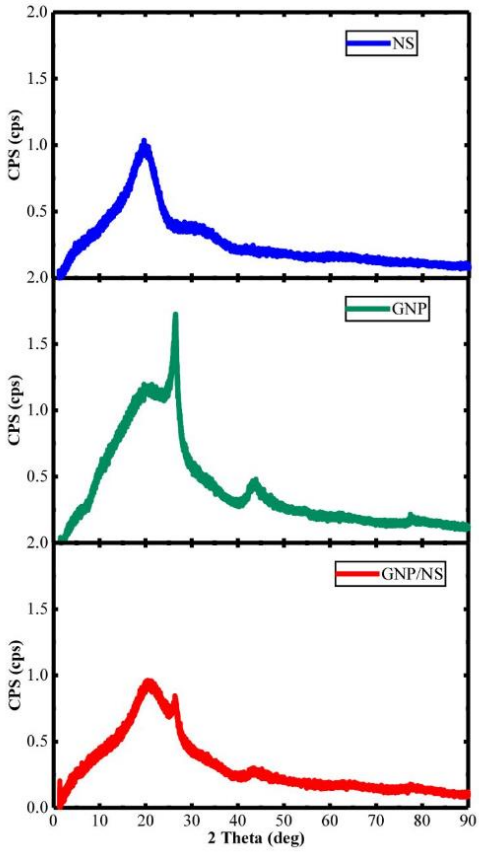

Figure 6.11: X-ray powder diffraction (XRD) curves of GNP/NS hybrid filler

CHAPTER 7. ENHANCEMENT OF SELECTED NANOCOMPOSITE COATINGS FOR PIPELINE APPLICATIONS

**Note: the information in this Chapter has patent protection in the United States.*

7.1 BACKGROUND

In this section, Polydimethylsiloxane (PDMS) was introduced to modified epoxy resin, as the intercalation of PDMS and epoxy revealed will result in a hydrophobic surface, which leads to an increase in contact angle. Different weight contents of PDMS were used, and the modified resins have incorporated with 1.0 wt.% GNP/NS hybrid filler. These combinations allow us to discover the synergistic effect between the modified resin and selected nanofiller reinforcement; thus, the coating with the best overall performance was selected for further study.

7.2 CHARACTERIZATION OF OPTIMIZED NANOCOMPOSITES

7.2.1 Corrosion behavior

All prepared PDMS modified epoxy coating with 1% GNP/NS demonstrated high impedance value at the low-frequency region, and the phase angle was around 90 degrees in both high and low-frequency region. The impedance and phase curves for the tested groups were very close to the 1%GS-Epoxy group, as shown in Fig. 7.1. The results reflected an excellent protective property of the coatings, which indicated that the coating was not degraded by the incorporation of PDMS.

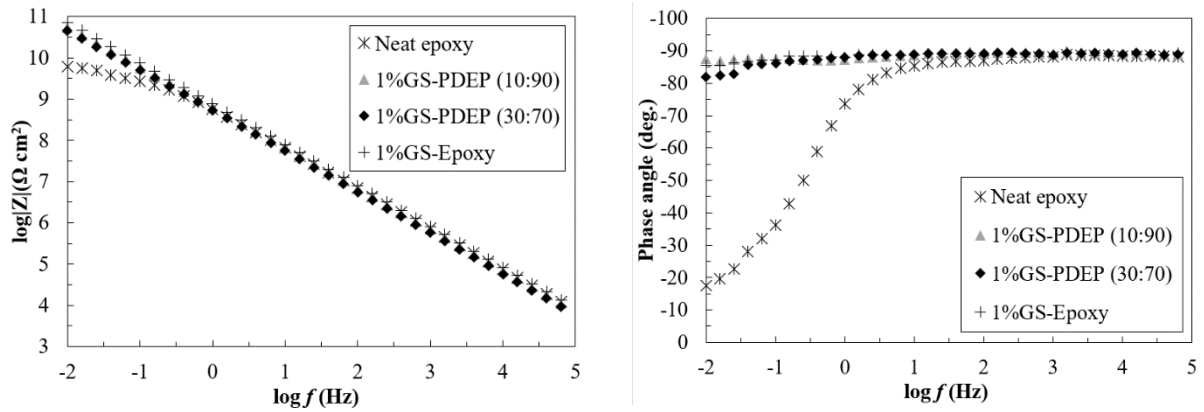

(a) (b)

Figure 7.1: Impedance curve (a) and phase angle curve (b) of the 1%GS-PDEP at the fresh stage

7.2.2 Abrasion Resistance

The abrasion resistance of PDMS modified epoxy was illustrated in Figure 7.2, which the red dashed line shown the mass loss of the neat epoxy coating. Compared with 1%GS-Epoxy coating, it was clear that the mass loss of the 1%GS-PDEP (10:90) group was slightly higher, but it worth to mention that the mass loss was still lower than the neat epoxy group. On the other hand, stronger improvement of abrasion resistance was obtained in the 1%GS-PDEP (30:70) group, and the mass loss was around 48 mg during the test. The results showed that the 1%GS-PDEP (30:70) group has better abrasion resistance than 1%C-Epoxy group, which has the lowest mass loss in the previous study.

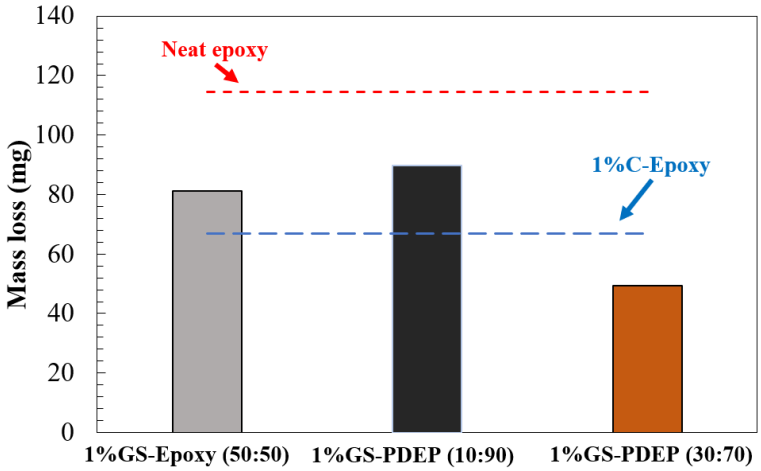

Figure 7.2: Abrasion resistance of the 1%GS-PDEP samples

7.2.3 Contact Angle Test

The results from the contact angle test confirmed that the incorporation of PDMS would significantly increase the water repellency of the epoxy composites. The contact angle has increased from 26 degrees (1%GS-Epoxy) to around 110 degrees by incorporating the PDMS modified epoxy. Moreover, the contact angle increased to around 120 degrees after abrasion. Figure 7.3 and Table 7.1 presented the contact angle of each composite before and after abrasion, and it was clear that the PDMS modified epoxy resin has superior water repellency with great durability.

Table 7.1: The contact angle for composites with PDMS modified epoxy

Group	Contact Angle (°)	
	before	after
Neat epoxy	51	50
1%GS-Epoxy (50:50)	26	95
1%GS-PDEP (10:90)	106	119
1%GS-PDEP (30:70)	109	115

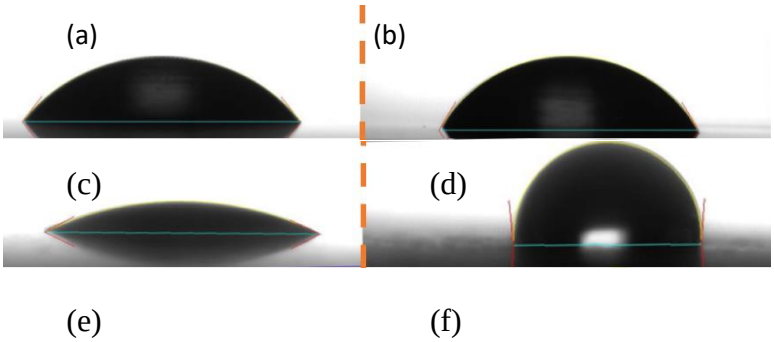

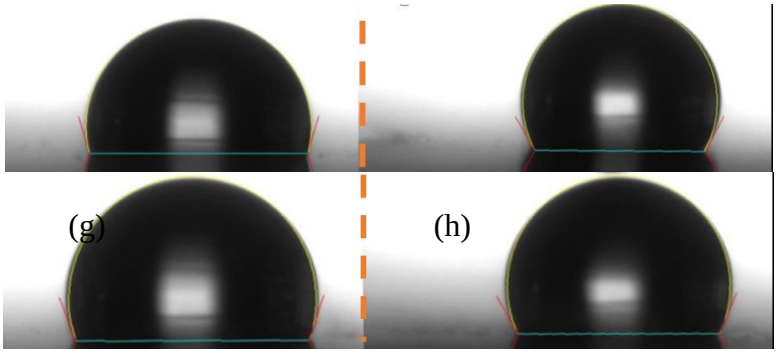

Figure 7.3: Contact angle before and after abrasion for the neat epoxy (a)(b), 1%GS-Epoxy (50:50) (c)(d), 1%GS-PDEP (10:90) (e)(f), and 1%GS-PD/EP (30:70) (g)(h) samples

7.2.4 Coupon Tensile Test

Figure 7.4 presented the analysis of tensile properties for the developed 1%GS-PDEP coatings, which was determined by the coupon tensile test. The maximum tensile stress, strain at failure, and Young's modulus were illustrated in Figures 7.4(a)-7.4(c), correspondingly. Neat epoxy and 1%GS-epoxy were used as references.

In Figure 7.4(a), a significant increase of tensile stress could be observed in 1%GS-PDEP (10:90) group, which increased 75% by compared with neat epoxy. This indicated the incorporation of PDMS reinforced the tensile properties as the strength was even higher compared with 1%GS-Epoxy group. However, the stress exhibits a degradation at higher concentration of PDMS. The stress decreased to 23.2 MPa, which was slightly lower than the neat epoxy (24.7 MPa).

Furthermore, a similar tendency was observed in both strain and Young's modulus for the tested samples, which were presented in Figures 7.4(b)-7.4(c), respectively. Apparently, the highest reinforcement was obtained in 1%GS-PDEP (10:90) composites, which has an excellent improvement in both tensile strain and Young's modulus. However, Young's modulus of 1%GS-PDEP (30:70) was decreased by the incorporation of 30 wt.% PDMS in epoxy resin. The overall results indicated that the modification of epoxy by 10 wt.% of PDMS could significantly improve the tensile properties of neat epoxy without compromising the effect of hybrid fillers.

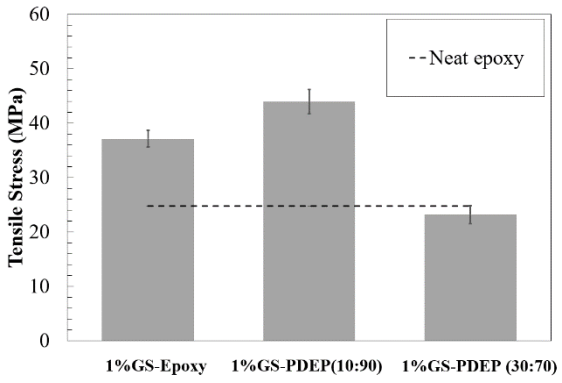

(a)

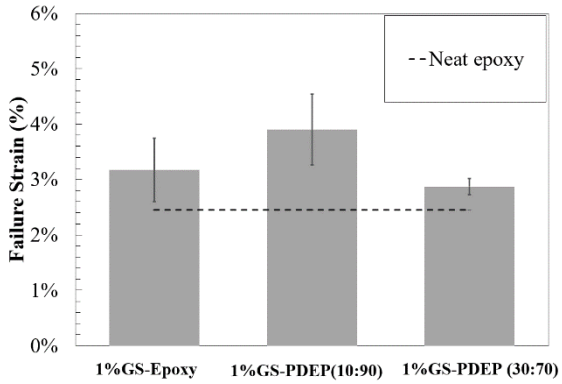

(b)

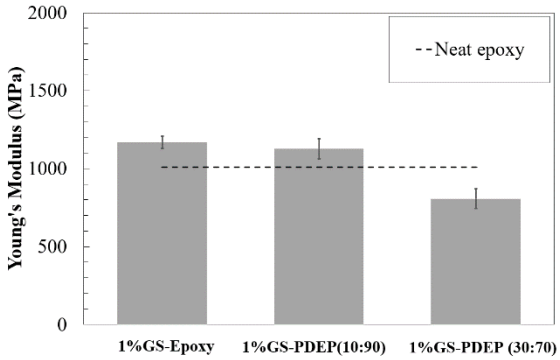

(c)

Figure 7.4: Tensile properties of 1%GS-PDEP coatings, (a) tensile strength, (b) strain at failure, and (c)Young's modulus

7.3 DURABILITY AND RELIABILITY UNDER SALT FOG EXPOSURE (B117)

7.3.1 Corrosion barrier performance during salt fog test

The long-term performance of the 1%GS-PDEP coatings showed a good agreement with the EIS results in the previous study. All the tested samples have been exposed in salt spray test (ASTM B117) for 500 hours, and EIS measurement was performed in 0, 100, 200, and 500 hours after exposure. The test results from neat epoxy have been used as a reference, which was illustrated in Figures 7.5(a) and 7.5(b). The performance before exposure was discussed in the previous report, which both 1%GS-PDEP coatings have excellent barrier properties compared with neat epoxy.

Moreover, as clearly illustrated in Figs. 7.5(c)-7.5(f), the durability tests further confirmed that the 1%GS-PDEP coatings significantly enhanced the long-term barrier performance. The Zmod values for both 1%GS-PDEP coatings maintained higher than 10^9 in the test range, while the Zmod value has decreased to 10^6 for neat epoxy at 500 hours. The phase angle at low and middle-frequency region showed a good agreement with the results in Zmod curves. In the low-frequency region, the phase angle of the neat epoxy group has dropped very closed to 0 degrees even after 100 hours. On the other hand, the value of phase angle in the low frequency maintained much higher in1%GS-PDEP coatings.

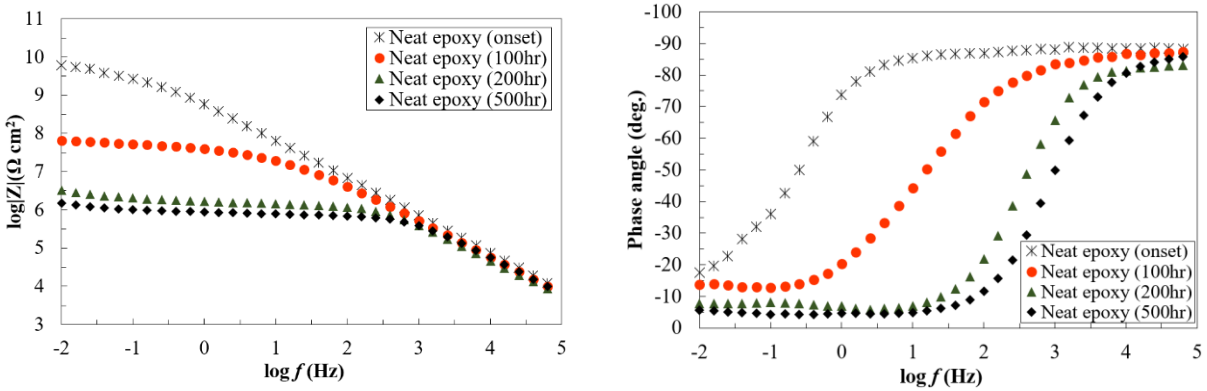

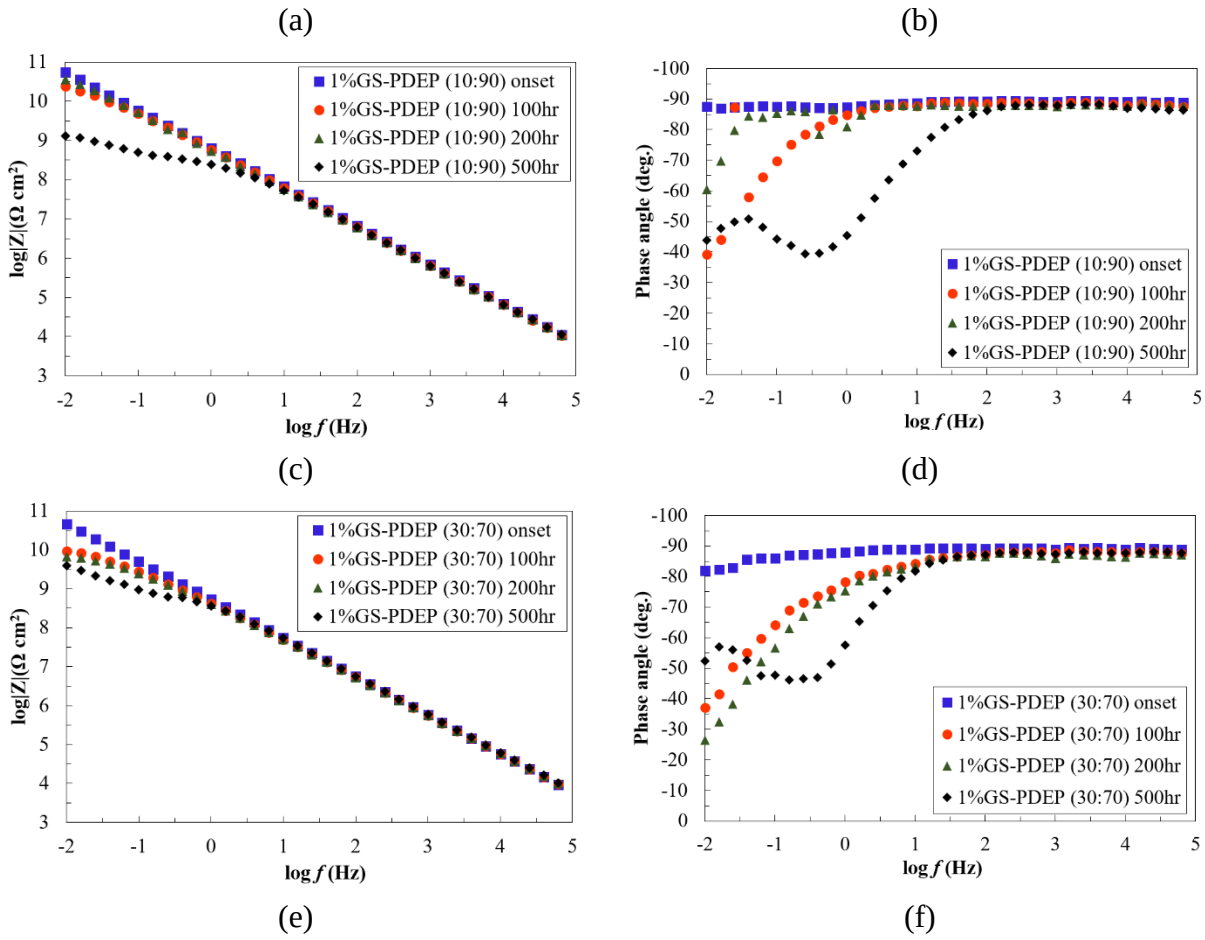

Figure 7.5: Bode curves of (a), (b) the neat epoxy, (c), (d)1%GS-PDEP (10:90), and (e), (f) 1%GS-PDEP (30:70) coatings after 500 hours exposure

7.3.2 Hydrophobicity during salt fog test: contact angle

On the purpose of studying the effect on hydrophobicity during the coating damage process, the contact angle for the coatings was measured at 0, 100, 200, and 500 hours as well, as listed in Table 7.2. The image of the water droplet on the panels was presented in Fig. 7.6, which includes both 1%GS-PDEP (10:90) and 1%GS-PDEP (30:70) groups. The results suggested that both coatings have robust water repellency as the durability allow them to maintain a high water contact angle after the salt spray test. From the previous study, PDMS modified epoxy with hybrid filler has shown its robustness after abrasion test as well, which shown a good agreement with the results in this report. The integration of the results in this and previous study indicated that the developed 1%GS-PDEP coating systems have superior water repellency with great durability.

Table 7.2: The contact angle for GS-PDEP coatings

Group	Contact angle (°)			
	Onset	100hr B117	200hr B117	500hr B117
1%GS-PDEP (10:90)	107	104	107	97
1%GS-PDEP (30:70)	109	111	114	105

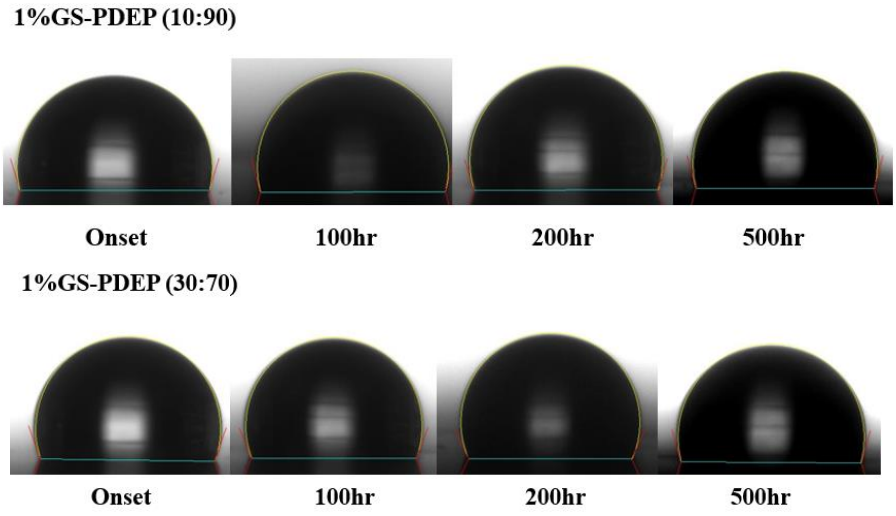

Figure 7.6: The water contact angle of the 1%GS-PDEP coatings after exposure

7.4 SUMMARY

In this chapter, GNP-NS loaded PDMS-epoxy nanocomposite was successfully synthesized via a facile solvent-free fabrication method, and the comprehensive investigation confirmed that the developed hybrid nanocomposite coatings offered robust water-repellent, anti-corrosion properties, with specific conclusions as follows:

- The developed coating has a dramatic improvement in anti-corrosion performance, and the coating displayed long-term resistance after exposed to accelerated weathering environments. Such a robust multifunctional corrosion protection coating with remarkable durable hydrophobicity is viable as alternatives for current coatings, thus enriching the categories of structural materials for metallic structures.
- The increased contact angle suggested that the coating has excellent hydrophobicity. Moreover, the surface was robust enough as the hydrophobicity has remained even after mechanically damaged or exposed to an accelerated weathering environment.
- The results of the coupon tensile test confirmed that the inclusion of GNP-NS nanofiller in the polymer resin improved the critical mechanical properties for engineering applications, such as strength, strain, and Young's modulus.

CHAPTER 8. ROBUST, HIGH-PERFORMANCE MULTIFUNCTIONAL COATINGS FOR PIPELINE APPLICATIONS

**Note: the information in this Chapter has patent protection in the United States.*

8.1 BACKGROUND

The proposed high-performance multifunctional coating was schematically shown in Figure 8.1. Experimental results revealed that the incorporation of GNP/NS hybrid nanofiller led to a dramatic improvement on both corrosion resistant, mechanical strength, abrasion resistance, and durability (as shown in previous chapters). The only drawback of the GNP/NS nanofiller was the decreased water repellency; however, this challenge was solved by the superamphiphobic layer and modified polymer.

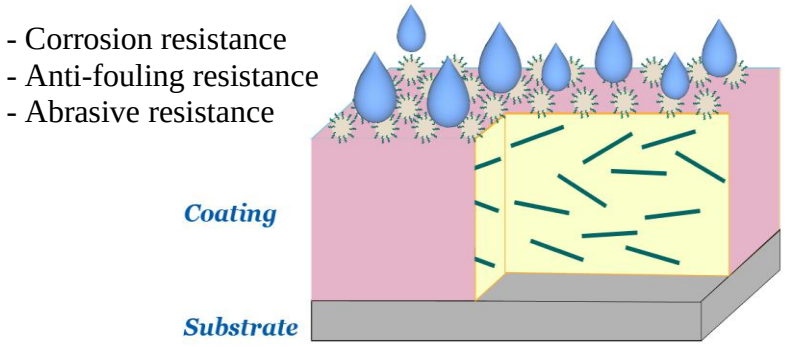

Figure 8.1: Proposed high-performance multifunctional coating

8.2 NEW COMPOSITE COATINGS WITH SUPERAMPHIPHOBIC SURFACE

8.2.1 Corrosion Barrier Performance

The initial corrosion barrier performance of the new high-performance coating was measured by EIS test, and the results were presented in Fig. 8.2. Clearly, the Bode plots reflected excellent corrosion protective property of the developed coating, as high impedance value at the low-frequency region, and phase angle was around 90 degrees in both high and low-frequency region. At this stage, the EIS data was also well fitted to the model A electrical equivalent circuit (EEC), indicating the coating behaved as an intact protective layer for the substrate.

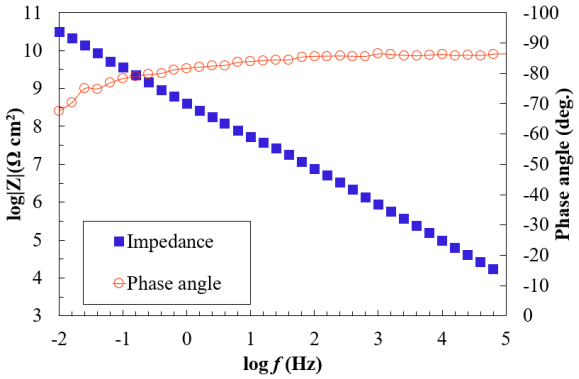

Figure 8.2: Impedance curve and phase angle curve of the proposed high-performance multifunctional coating

8.2.2 Contact Angle Test

To investigate the water and oil repellency of the developed coating, the contact angle of both water and organic liquid to the coating surface was determined. The contact angle of the neat epoxy was 51 degrees, and dramatic improvement was observed in the new high-performance coating. Due to the uniformly distributed fluorinated nanoparticles on the top surface, the coating has excellent superamphiphobic property; hence, the contact angle of water and hexadecane was increased to around 160 and 145 degrees, respectively.

8.2.3 Water Droplet Ascending and Descending from the Coating Surface

As mentioned earlier, water adhesion of the contact surface is also a major factor contributing to the water repellency of coatings. Figure 8.3(a)-(b) showed a series of images taken during water droplet ascending and descending the surface of neat epoxy, and the high-performance coating, respectively. For the neat epoxy, it was found the water droplet was completely detached from the tip with a low contact angle, hence, indicating the neat epoxy was hydrophilic and has low water repellency. Excellent water repellency was observed in the high-performance, as it was found that the water droplet was easily detached from the surface and suspending on the tip, as presented in Figure 8.3(b). To sum up, the developed coating has an excellent superhydrophobic surface and improved water repellency, which allowed water easily to roll off the coating surface.

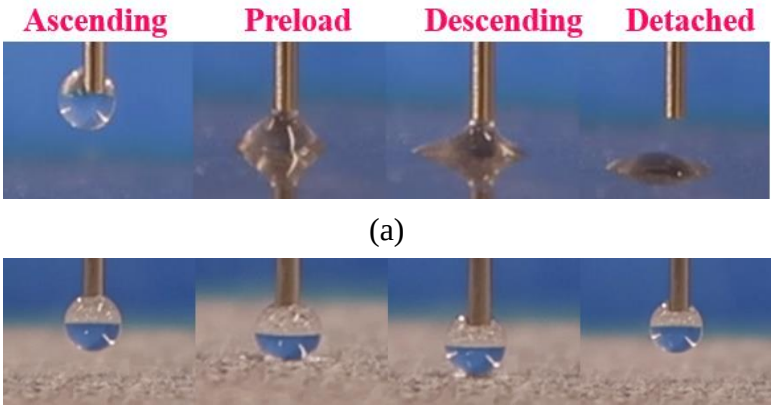

(a)

(b)

Figure 8.3: Water droplet ascending and descending of (a) neat epoxy, (b) high-performance coating

8.3 LONG-TERM DURABILITY OF NEW HIGH-PERFORMANCE COATINGS

8.3.1 Durability and Reliability Under Salt Fog Exposure

The impedance and phase angle plots for the proposed coatings were illustrated in Figs. 8.4(a) – (b), no degradation on corrosion resistance of the coating was observed during the entire 2000 hours exposure time. The coating behaved as an intact protective film as a straight line was observed in impedance curve and the phase angle was around -90 degrees in over a wide frequency region. As expected, the results confirmed the proposed coating has extraordinary anti-corrosion performance and durability; hence, the coating remained in model A after 2000 hours of exposure. For the developed coating, the impedance value was over 10^{10} Ω/cm^2 after different exposure periods; meanwhile, the neat epoxy has lower impedance value at the fresh stage and gradually decreased during the exposure time (Fig. 8.4(c)). On the other hand, the EIS test was not able to be performed on the neat epoxy sample after 1500 hours, as the coating was significantly damaged (as shown in Fig. 8.4(d)). The results further confirmed that the proposed coating has extraordinary anti-corrosion performance and durability; hence, the coating behaved as an intact protective layer and remained in model A after 2000 hours of exposure.

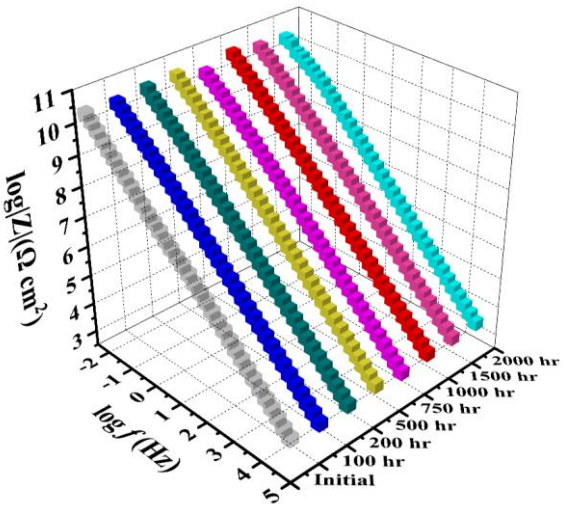

(a)

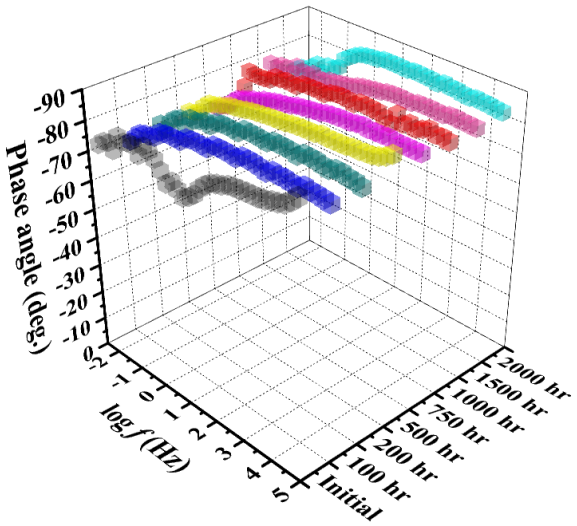

(b)

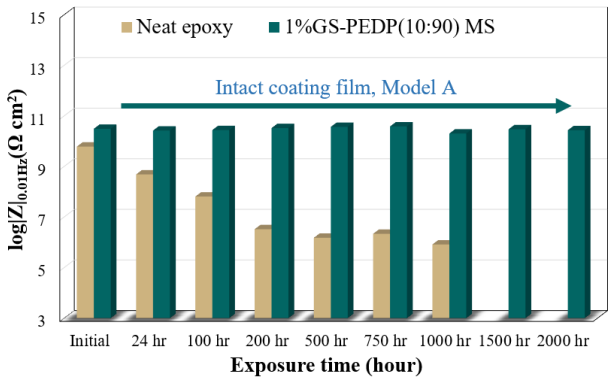

(c)

(d)

Figure 8.4: (a) Impedance curve, (b) phase angle curve and (c) Zmod values of the proposed high-performance multifunctional coating after salt spray exposure

8.3.2 Hydrophobicity during salt fog test

(a) Contact angle test (after exposure)

The application of hydrophobic surface was often limited by its poor durability. In order to investigate the robustness of the developed coating, both water and oil droplet contact angles were measured after the exposure, Fig. 8.5 showed the contact angle of the high-performance coating via exposure time, and the results strongly suggested the coating film was robust enough to maintain the superhydrophobic properties under the accelerated corrosive environment. A water contact angle (CA) value around 145 degrees was obtained in both 100, and 200 hours; meanwhile, similar results were also observed with oil droplet (hexadecane), indicating the superior repellency of the developed coating was survived during after exposing to the severe environment.

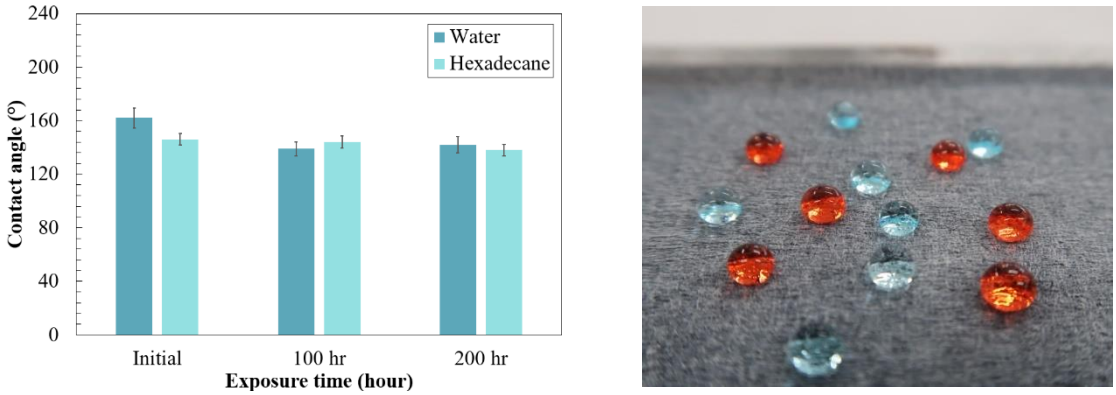

Figure 8.5: Water and oil contact angle of high-performance coating after salt spray exposure

(b) Water droplet adhesion from the coating surface (after exposure)

The results from the water adhesion showed a strong agreement with the contact angle test. As the exposure time elapsed, no significant increased on water adhesion was observed, indicating the surface remained undamaged under the severe environment. It was found that the water droplets rolled off to the side during the preload process, and completely detached from the coating surface after when descending from samples (see Figure 93).

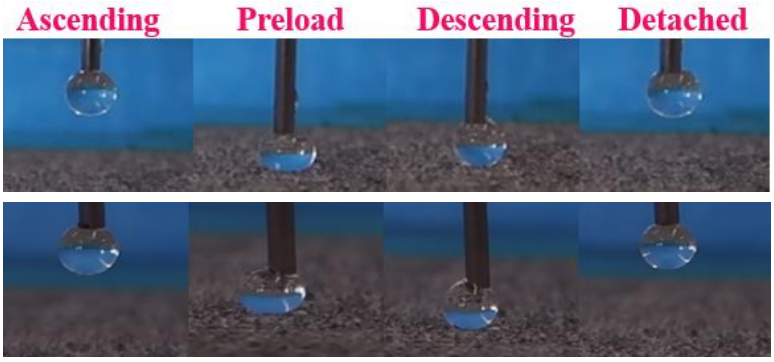

Figure 8.6: Water droplet Ascending and descending on high-performance coating after (a) 100 hours and (b) 200 hours salt fog spray

8.3.3 Simulated field reliability test

(** Field test was not able to be performed due to COVID-19 situation. As such, utilizing the simulated field test was designed as an alternative approach as presented below. Future field test could be performed with a follow-on project when funding is available*)

Fig. 8.11 illustrated the plan view of a liquid flow instrument for a modified long-term test. The test instrument includes four parts: a fluid reservoir, a pump, a valve, and a channel to simulated pipeline flows. The channel was designed to test three coated panels at one time, and the panels are removable, so EIS test can be performed to evaluate the corrosion resistance after they were exposed to the water flow.

Figure 8.7: Simulated long-term field test of the developed coatings

To investigate the corrosion performance of the developed coatings under dynamic liquid flow, EIS measurements were performed after the flow test. Three types of coating were evaluated, which included the neat epoxy, one hybrid filler reinforced coating, and one high-performance coating. The EIS test was conducted before, 100, 200, and 500 hours after exposure to the liquid flow. For the proposed coating coating, the exposed duration was extended to 1000 hours. As illustrated in Fig. 8.8, the results showed the neat epoxy has good corrosion under liquid flow condition, but a significant degradation was observed after the test, with both impedance and phase angle were decreased in the Bode plots.

On the other hand, improved corrosion resistance was observed in both hybrid coating and the high-performance coatings. By comparing the results from these two coatings, it was worth to mention that a slight degradation was observed in the hybrid coatings; however, the high-performance coatings remained undamaged during the test. They showed excellent durability as the impedance values remain unchanged after the test, which showed a good agreement with the evaluation of long-term performance in the previous chapter.

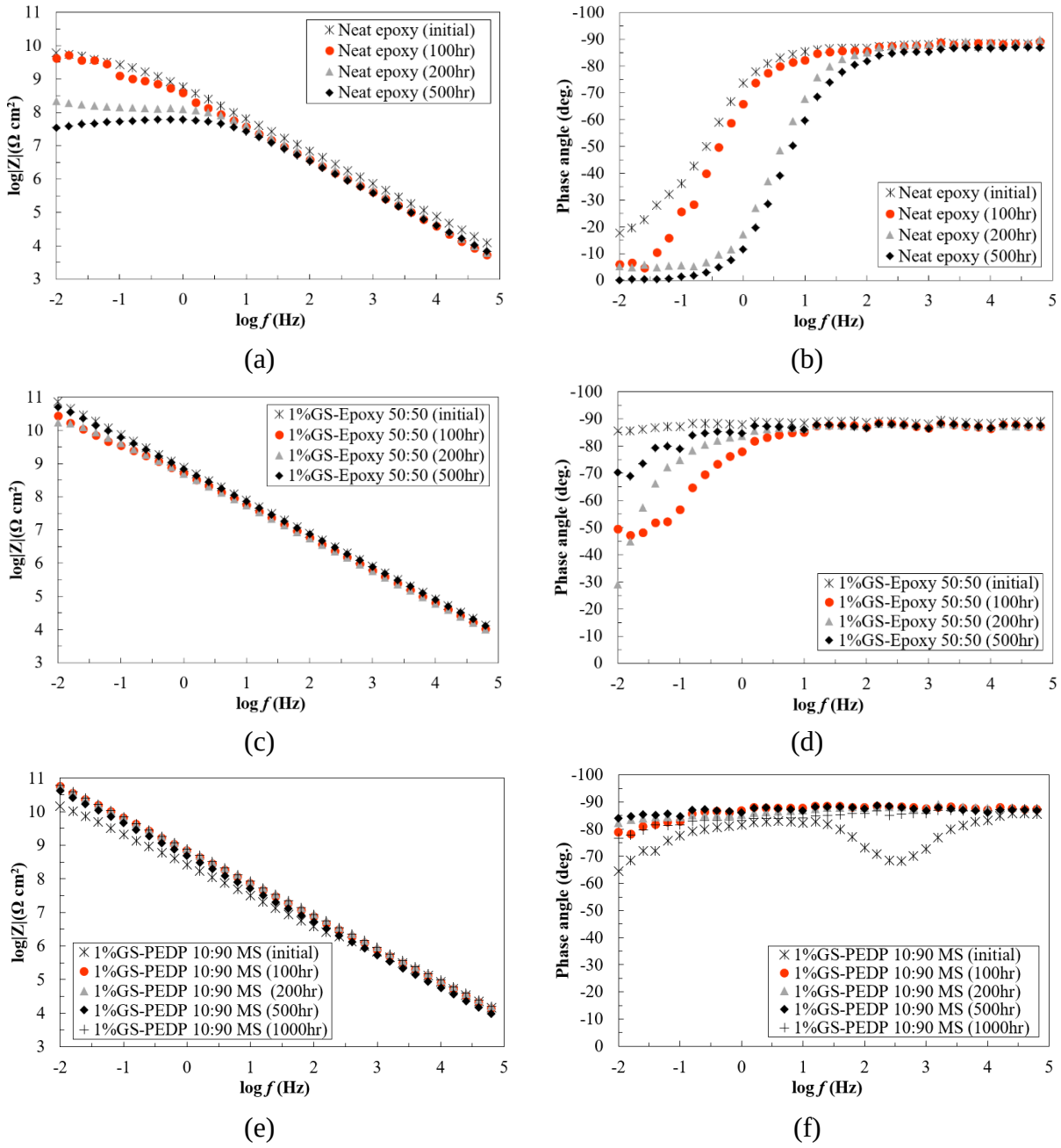

Figure 8.8: Impedance curve and phase angle curve of the (a) (b) neat epoxy, (c) (d) hybrid coating, (e) (f) the high-performance coating

8.4 SUMMARY

This chapter presented the study to the fabrication and performance of the proposed high-performance multifunctional coating. Both short-term and long-term experiments evaluated the overall performance of the proposed multifunctional coating; thus, the following superior properties were observed:

- The developed coating has excellent corrosion resistance as a high impedance value was observed in EIS results.

- By comparing with the neat epoxy, a significant improvement in mechanical properties was obtained in the proposed coating, as the tensile strength has increased by 75%, while an improvement of around 60% was observed in tensile strain.
- The new high-performance coating exhibited high anti-fouling capacity, with the contact angle of water and hexadecane to 160 and 145 degrees, respectively.
- The results obtained during the accelerated corrosion test revealed the proposed coating was durable, as its excellent corrosion resistance and hydrophobicity remained undamaged after exposure.

CHAPTER 9. UNVEILING FAILURE MECHANISM OF COATINGS VID. DEFECT ANALYSIS

9.1 BACKGROUND

Voids are considered as one of the major defects in the nanocomposites, so the voids analysis of nanocomposite coating film was performed by Micro-CT scanning. The 3-D images obtained by Micro-CT were used to investigate the defects in the specimens, while the cross-sectional images were provided along the X-axis, Y-axis, and Z-axis. It is worth to mention that each nanocomposite could have different types of defects in the specimen.

9.2 VOID CHARACTERIZATION

The 3-D images obtained from the Micro-CT scan for the neat epoxy sample were presented in Figure 9.1. Based on the observation, the neat epoxy has a low volume of voids, as most of the scanned areas were perfect layers. Low volume of voids in the coating film leads to a high barrier performance and good mechanical properties, which was confirmed by our previous study, and that is why epoxy is one of the most commonly used protective coating in oil and gas industry. However, a large void could be found in the coating layer, which was possibly created during the application process, as the epoxy resin has relatively high viscosity.

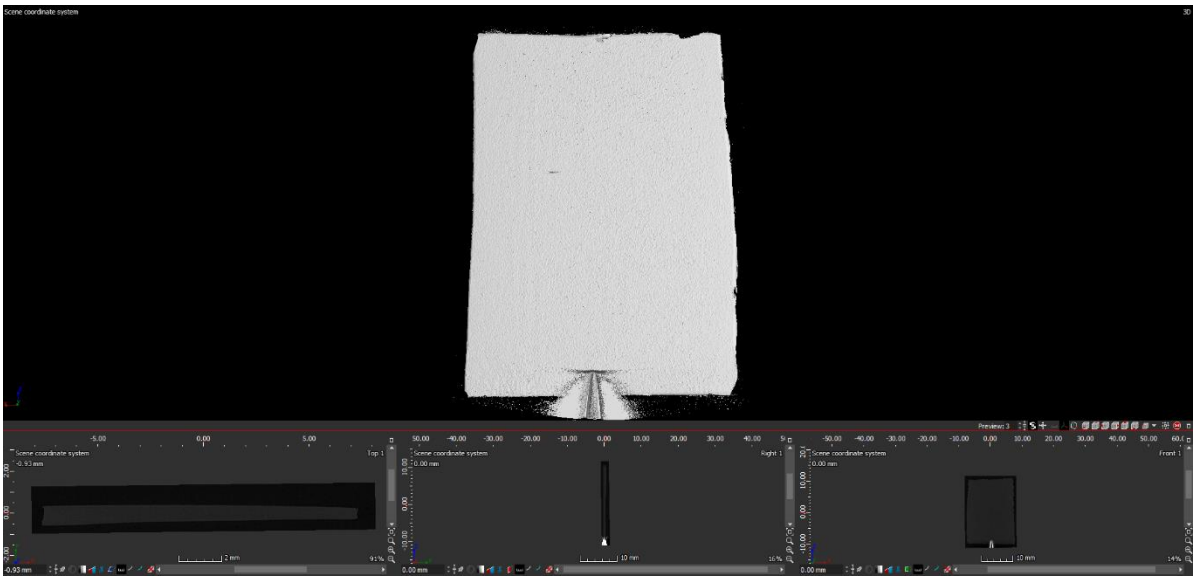

Figure 9.1: Software interface for Micro-CT scan

A defect analysis was performed in the section, and the discussion was based on the obtained results from the Micro-CT scan. For each type of nanocomposite, the void fraction, number of voids per mm^3, and size of void were summarized.

9.3 CORRELATION STUDY BETWEEN DEFECT ANALYSIS AND COATING PERFORMANCE

This section presented the correlation study of the defect analysis (section above) and the coating performance (previous studies), and the discussion has well-explained the nanofiller reinforcement in the polymeric coatings.

In general, the addition of nanofiller could provide nanofiller reinforcement; meanwhile, the nanofiller can also has positive or negative impacts on defects in the matrix. The perfect case is that the nanofiller could provide both improved properties and reduced defects. Another case is the presence of nanofiller would create more defects in the matrix; and improved performance could be obtained in the nanocomposite as long as the nanofiller reinforcement is stronger than the degradation that contributed by the defects. Otherwise, once the material degradation is beyond the nanofiller reinforcement, the overall performance of the nanocomposite could be weaker than the unreinforced group.

9.3.1 Neat epoxy associated with pitting corrosion

As mentioned earlier, the neat epoxy has a low void fraction; however, the size of the void was large (Figure 9.2). Generally, this type of coating will have pitting corrosion in the area containing the large voids, which significantly shortens the service life of the coating. The results from our previous studies showed a firm agreement with the assumption above, and large spots with pitting corrosion were observed after salt spray exposure (Figure 9.2(b)).

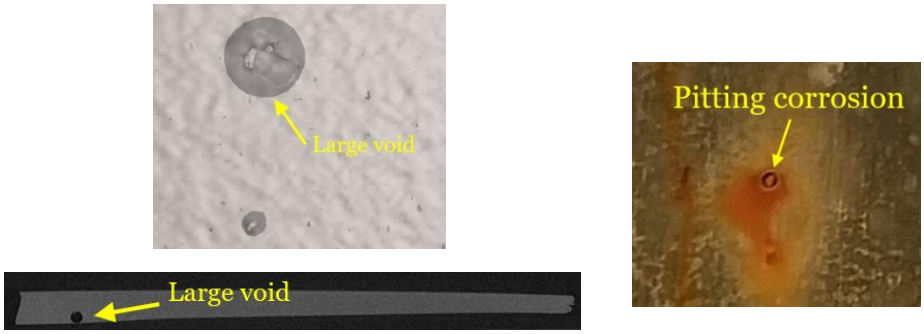

(a) (b)

Figure 9.2: Defects and pitting corrosion in the neat epoxy coating

9.3.2 Single filler/epoxy reinforcement

The tensile properties and void size were selected to as representatives to explain the relations between the defects in the matrix and the performance of nanocomposites. It is well known that the presence of CNT will increase the tensile properties of nanocomposites.

Based on the observation, the 1.0 wt.% content of nanofiller behaved as a critical point in the defect analysis, which surprisingly showed a perfect agreement with the coating performance from previous works. In general, significant increased void size results in a higher severity level of defects and reduce the coating performance. Figure 9.3 was used as an example, in which the tensile strength and void size of CNT/epoxy were presented. It is easy to be observed that the 1.0 wt.% of CNT has the greatest improvement on the tensile strength of nanocomposite; at this point, the addition of CNTs has provided reinforcement by its excellent mechanical properties and also

by reducing the defects. The size of the voids increased when 1.5 wt.% of CNTs were incorporated into the epoxy, while the degradation of tensile strength was observed in this specimen as well. Specially for 3.0 wt.% CNT/epoxy group, the increased defects have the highest negative impacts on the coating performance, as the lowest tensile strength was observed. It is worth mentioning that even the 3.0 wt.% CNT/epoxy group has tensile strength that more robust than the neat epoxy, which is contributed by the excellent mechanical properties of the CNTs.

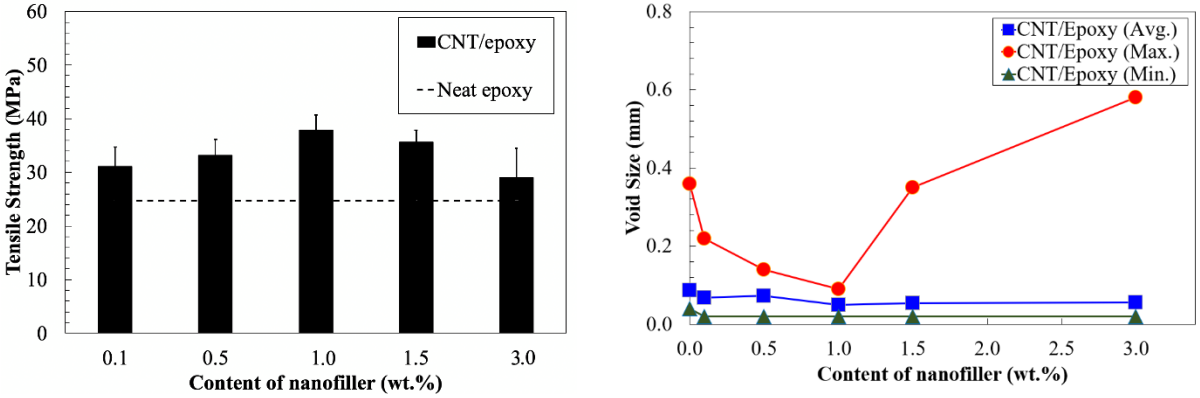

(a) (b)

Figure 9.3: Relation between tensile properties and defect analysis in the CNT/Epoxy nanocomposites

9.3.3 Graphene nanoplatelets reinforcement

Based on the results from previous studies, the addition of GNPs has the highest reinforcement on the corrosion resistance of the nanocomposites. In Figure 9.4, the impedance value, and void fraction in the GNP/epoxy groups were selected as representatives to show the influence of void fraction on coating performance.

Apparently, the incorporation of 0.1 to 1.0 wt.% of GNPs has no significant impacts on the void fraction; in this case, the corrosion resistance of the nanocomposite was improved as the addition of GNPs increased the impermeability of the epoxy. However, as the void fraction was increased when higher content of GNPs was added (1.5 and 3.0 wt.%), the coating performance was degraded even the GNPs can improve the corrosion resistance.

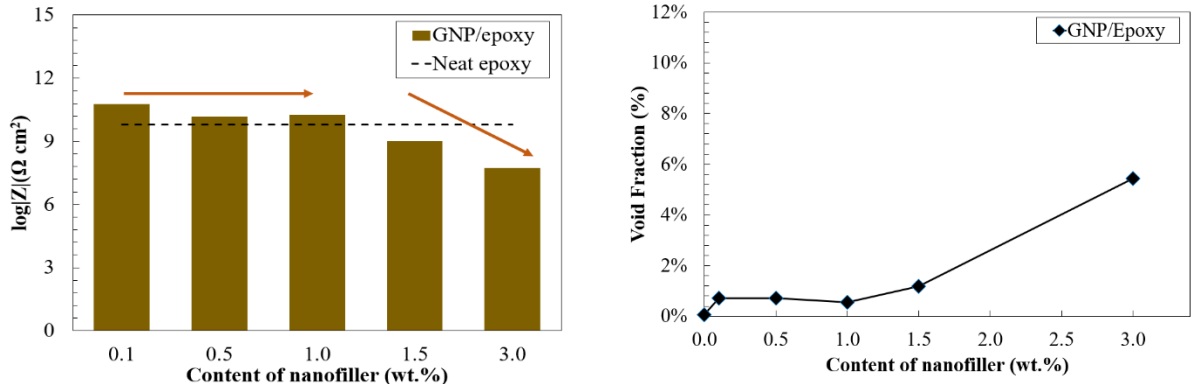

(a) (b)

Figure 9.4: Relation between corrosion resistance and defect analysis in the GNP/Epoxy nanocomposites

9.3.4 Nano silica reinforcement

Nano silica powders have the greatest influence on reducing the defects in the polymeric matrix, as they can significantly reduce both the void fraction and the size of voids. Apparently, fewer defects in the coating lead to improved coating performance; in this case, improved abrasion resistance of the NS/epoxy was observed. Meanwhile, unlike the CNTs and GNPS, the higher amount of NS has not increased the void size and fraction; this leads to on significant degradation on the coating performance, as confirmed by the abrasion resistance (see Figure 9.5).

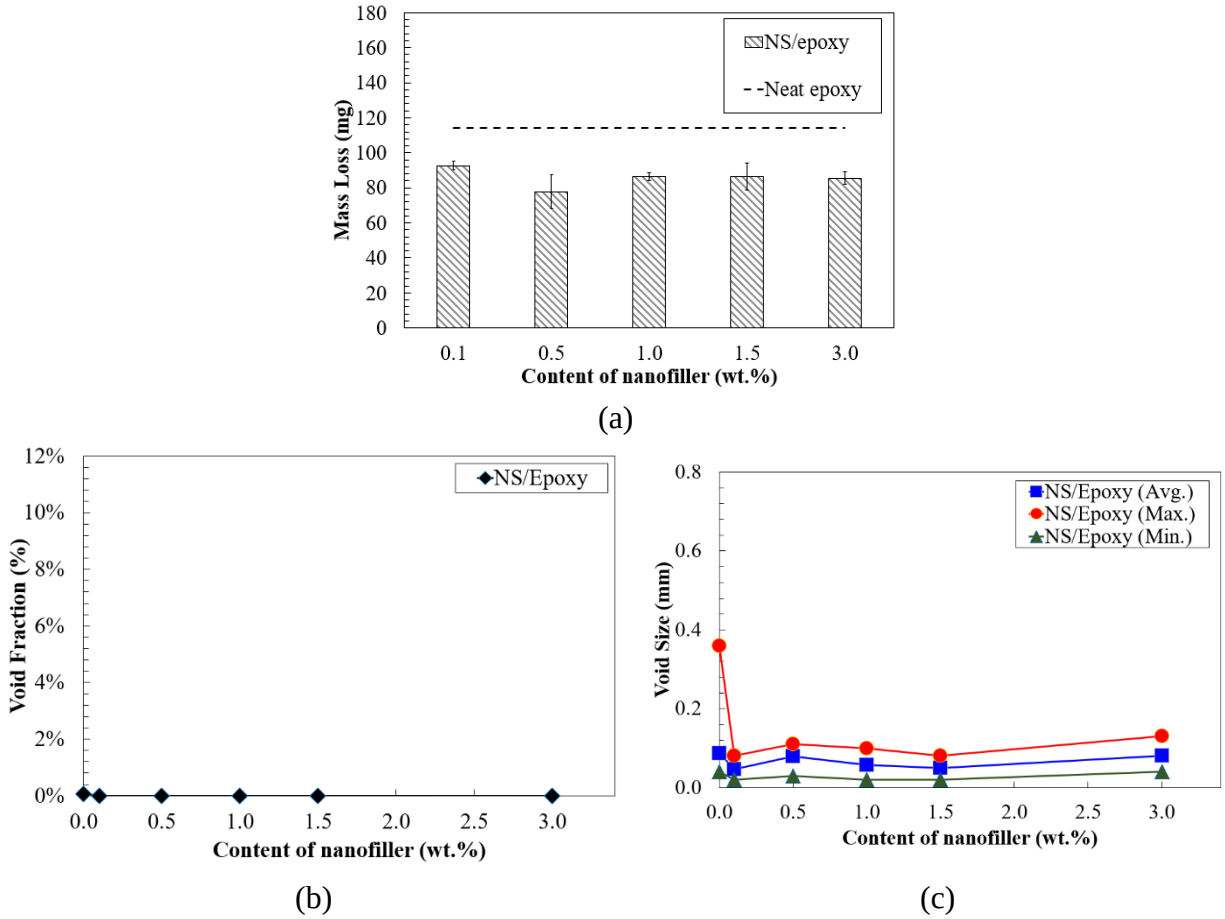

Figure 9.5: Relation between abrasion resistance and defect analysis in the NS/Epoxy nanocomposites

9.4 SUMMARY

This chapter addressed the failure mechanism of coating through defect analysis. Correlation study between defect analysis and coating performance reveals the neat epoxy has low void content, but the large-sized void in the matrix resulted in pitting corrosion and weak spots for mechanical damage tolerance.

The presence of nanofillers create more defects in the matrix, and improved performance could be obtained in the nanocomposite as long as the nanofiller reinforcement is stronger than the

degradation that contributed by the defects. At this stage, the nanofillers are providing some reinforcement for the composites.

Once the material degradation is beyond the nanofiller reinforcement, the overall performance of the nanocomposite could be weaker than the unreinforced group. At this stage, the addition of nanofiller has considerably reduced the performance of the composite.

CHAPTER 10. EXPLORATION OF COATINGS ON WELDMENT IN PIPELINES

10.1 BACKGROUND

Despite great efforts in protective coatings used for corrosion control, lack of sufficient damage tolerance and corrosion resistance of these existing coatings make weldments the most common contribution to pre-mature malfunction and even structural failure. Nano-modified composites showed great potentials toward high-performance protective coatings for metallic substrates. Therefore, this study investigated the performance of welded joints that are protected by nanocomposite coatings. Threes type of carbon-based nanoparticles, carbon nanotubes, graphene, and fullerene-C60 were selected as one, two, and zero dimensional materials. Results revealed that the nanocomposite coatings had provided excellent protection properties for weld joints. The electrochemical impedance spectroscopy (EIS) results suggested that the addition of graphene and fullerene-C60 led to enhance anti-corrosion performance, while significant improvement in abrasion resistance and mechanical properties were observed in the nanocomposite reinforced by carbon nanotube and fullerene-C60. Viscosity and particle size distribution test were utilized to study the interaction between nanoparticles and epoxy resin.

10.2 EXPERIMENTAL PROGRAM

10.2.1 Materials

The materials and chemicals were obtained from the market and used as received without any treatment. A1018 low-carbon steel rod was used as filler material for weldment, and by using the shielded metal arc welding process, the steel plates were welded together using the butt joint. A bisphenol A (BPA) epoxy resin, EPON^{TM} Resin 828, was used in this study; thus, Epikure 3175 was selected to as the curing agent for epoxy. Both the resin and curing agent were purchased from Hexion Inc. (Columbus, OH, USA). Three types of carbon-based nanoparticles were chosen as nanofillers in this study, including Carbon Nanotubes, Graphene Nanoplatelets, and Fullerene-C60.

10.2.2 Welding Process and Fabrication of Nanocomposite Coatings

The A1018 low-carbon steel rod was welded to the steel plate by utilizing the shielded metal arc welding procedure. The welding process parameters were listed in Table 10.1, and the voltage, current, and travel speed were controlled during the application.

Table 10.1: Parameters for Welding Process

Welding Parameter	Description
Technique	Shielded Metal Arc Welding
Filler material	AISI 1018 Low-Carbon Steel
Voltage	20 V
Current	60 A

Travel speed	0.16 in/sec
Width of weld bead	0.25 in

The nanocomposites were dip-coated to the welded steel plates, and then the samples were dry to 24 hours before any measurements or experiments; and Figure 10.1 showed the appearance of coated weldment specimens. For simplicity, the nanocomposite coatings were labeled by the incorporated carbon-based additives.

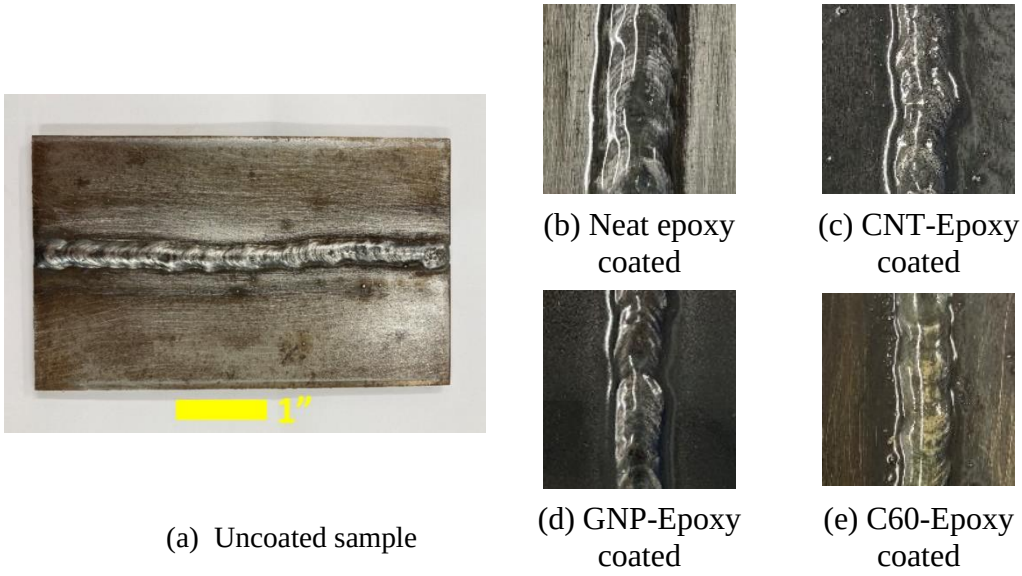

(a) Uncoated sample

(b) Neat epoxy coated

(c) CNT-Epoxy coated

(d) GNP-Epoxy coated

(e) C60-Epoxy coated

Figure 10.1: The appearance of welded joints (a) before, and (b)-(e) after coating by prepared coatings

10.3 CHARACTERIZATION OF THE WELDMENT WITH AND WITHOUT COATING

10.3.1 Corrosion resistance determination

To evaluate the corrosion resistance of the prepared coatings on the welded joints, electrochemical impedance spectroscopy (EIS) test was performed by a Gamry Reference 600 Spectroscopy. The impedance vs. frequency curve from the EIS test was utilized to evaluate the coatings' barrier properties. As presented in Figure 10.2, a plastic tube was used as a container for 3.5% NaCl solution during the test. For the reference electrode, a saturated calomel electrode reference electrode was used; hence, a platinum mesh was used as the counter electrode and the working electrode was worked as a steel panel. During the test, the data was collected over a frequency range of 10mHz to 100kHz through sinusoidal perturbation; the obtained results were transformed into a Bode and Nyquist map.

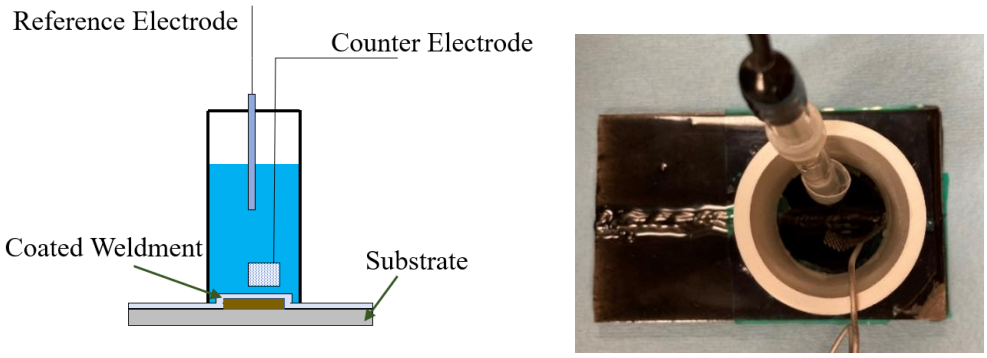

(a) (b)

Figure 10.2: Schematic diagram and (b) specimen for electrochemical impedance spectroscopy (EIS)

The Falling Sand Abrasion test was utilized to evaluate the wear resistance of the nanocomposites that were used to protect welded joints; as presented in Figure 10.3, a standard sand falling tester was used by following ASTM D968. The sand was designed to drop from the funnel to the coated sample by going through a 36" smooth tube. The sand's flow rate was 0.095 to 0.085 liter/second, and thickness loss was measured during the test. The abraded pattern formed an ellipse-shaped area, and the thickness measurement was performed on the welded joint in this study. For each sample, the wear resistance (R_w) was determined by: $R_w = \frac{V}{T_0 - T}$, where V= Volume of sand used, T_o = Averaged thickness before the test, and T = Averaged thickness after the test.

(a) (b)

Figure 10.3: (a) standardized falling abrasive tester and (b) sample after abrasion

10.3.2 Anti-Corrosion Performance of the Coated Weldments

The EIS measurement was utilized to characterize the electrochemical properties of coated steel welds, which can be used to evaluate nanocomposite coatings' effect on the corrosion protection properties for welded joints. The obtained results were plotted into Bode and Nyquist curves; thus, the Bode plots have consisted of impedance and phase angle curves, as shown in Figure 10.4. The arc radius of the Nyquist curve is related to the corrosion resistance, and a larger radius reveals the coating has stronger performance [90]. The impedance value at the low frequency, 0.01Hz,

indicates the coating film's barrier properties, which relates to the effectiveness of coating to isolate the substrate to the corrosive environment [69]. Generally, a coating is expected to have a maximum impedance value greater than 10^6 Ω cm^2 in order to provide corrosion protection to the substrate [91].

Furthermore, the phase angle values reflected the intactness of the protective film layer. Coating layer with a high degree of intactness will have phase angle value approach to 90 ° in most tested frequency ranges [92]. Ideally, the electrolytes cannot penetrate into an intact protective film to initiate corrosion reaction in the coating-substrate interface. The corresponded EIS results for an intact coating should have the following behaviors: 1) the sample should have a high impedance value, 2) the impedance curve should be straight with a slope of -1, and 3) the phase angle curve approached to -90° in all the tested frequency range.

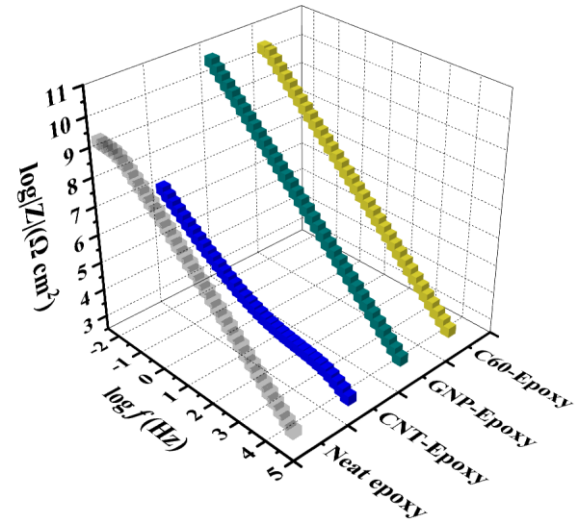

(a) impedance curves

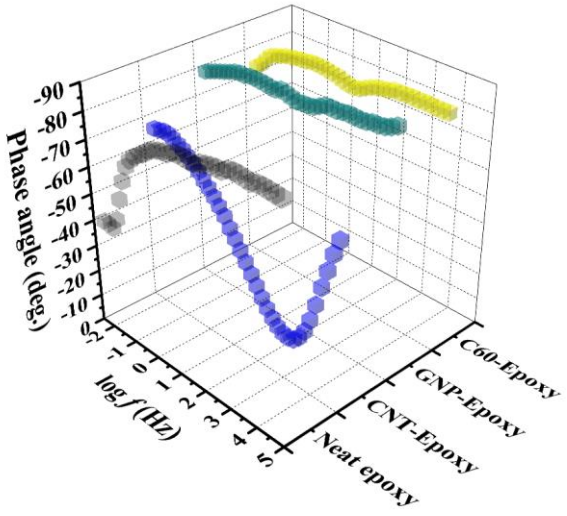

(b) phase angle curves

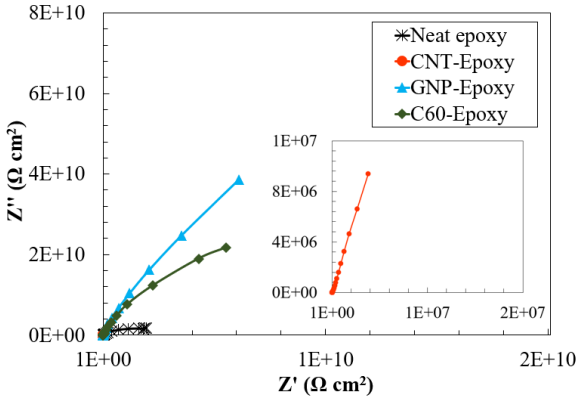

(c) Nyquist plots

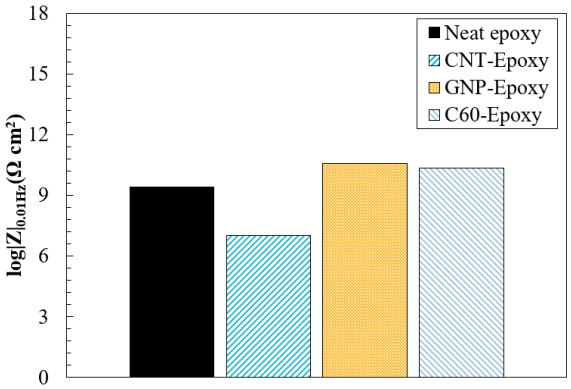

(d) impedance value at 0.01 Hz

Figure 10.4: EIS results for the coated weldments

Based on the observation in Figure 10.4, the incorporation of CNTs in the epoxy matrix exhibited a decreased barrier performance. Compared with the neat epoxy, the impedance curve for CNT-Epoxy exhibited a reduced value in most tested frequency ranges. The value at 0.01Hz decreased

from 10^9 to 10^7 Ω cm^2, as shown in Figure 10.4(b). Also, the phase angle curve showed that the value of CNT-Epoxy reduced dramatically. The addition of CNT negatively influences the penetration of the electrode, which is contributed by the highly conductive network constructed by the fibrous shaped CNTS [10, 31]. In addition, the large size agglomeration and the increased void fraction are also responsible for the decreased corrosion resistance, as both of them act as defects to reduce the diffusion pathway in the coating film.

The welded joint protected by GNP-Epoxy and C60-Epoxy showed improved corrosion resistance properties compared with the neat epoxy sample. In both GNP and C60 groups, straight lines with a slope of -1 were observed in the impedance curve, and the phase angle values were approaching -90 degrees (see Figure 10.4). The observations revealed that the addition of GNP and C60 significantly improved the barrier performance of the neat epoxy, while the impedance value increased to 10^{10} Ω cm^2. However, the mechanisms of GNP and C60 reinforcement are dissimilar, while for C60-Epoxy, the improvement was majorly contributed by the reduced void fraction in the matrix, as discussed previously. On the other hand, addition of GNPs increased the void fraction, so the improved barrier performance was majorly contributed by the lamellar shape of the GNP, as the unique nanoplatelets can affectively block corrosive media transfer, leads to an increase in the diffusion pathway [24].

10.3.3 Abrasion Resistance of the Coated Weldments

A falling abrasive test evaluated the wear resistance of the nano-modified coatings, and the results were plotted in Figure 10.5. In Figure 10.5(a), thickness loss via abrasive volume was discussed for each type of nanocomposite coatings, and the neat epoxy was used as a reference. To be clarified, the thickness loss value after the test is inversely proportional to the abrasion resistance for the coatings. As displayed in both Figures 10.5(a) and 10.5(b), the neat epoxy has the highest thickness loss regardless of the volume of abrasive, and the thickness loss reached 49.3μm after 120 liters of sands were dropped, and the wear resistance of neat epoxy was 2.4 L/μm, which presents an acceptable wear resistance. On the contrary, all the nanocomposites have lower thickness loss values; this observation indicated that the incorporation of CNT, GNP, and C60 nanoparticles could enhance the abrasion resistance of composites. Research work showed that a sufficient amount of nanofiller in the composite leads to enhancing the composite's cohesion or strength, and the load transferability when subjecting to abrasion stress [94].

Compared with the CNT-Epoxy system, a slight improvement on wear resistance was observed in the GNP-Epoxy group. The wear resistance for the GNP-Epoxy sample was 3.41 L/μm, indicating a 40% enhancement was obtained by the GNP reinforcement. Surprising results were observed in GNP-Epoxy groups, as the lamellar shaped nanoparticles should have excellent reinforcement due to their high specific surface area; however, researchers pointed out that the GNPs nanosheets are easily stack-up, which results in a structure that is weak to mechanical stress [97].

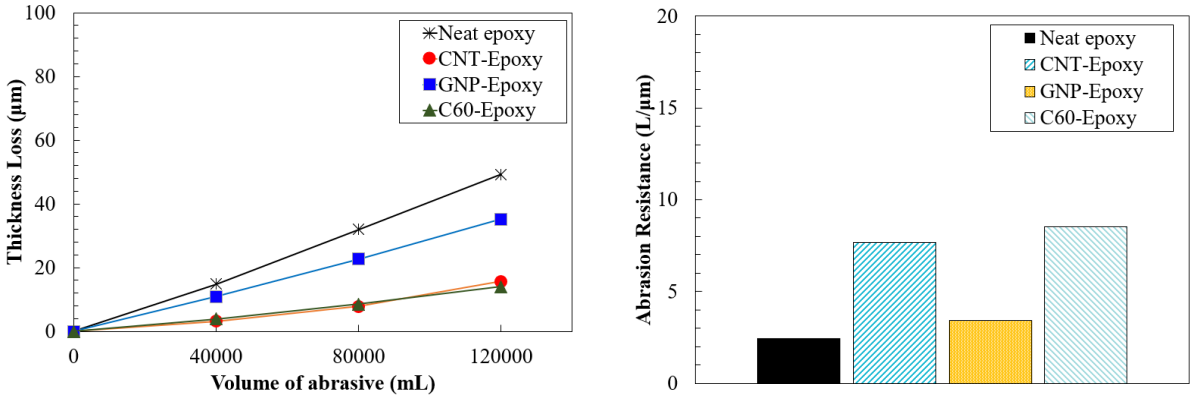

(a) (b)

Figure 10.5: (a) Thickness loss via abrasive's volume, and (b) abrasion resistance of coated weldments

10.4 SUMMARY

In this study, three types of nanofiller-epoxy coatings were used to provide protection properties for steel weldment. Improved corrosion resistance and abrasion resistance were found in the weld joints that were coated with nanocomposite coatings. Meanwhile, an investigation was performed to study the effect of nanoparticle's shape on nanocomposite coatings' performance. The data from the electrochemical impedance spectroscopy (EIS) test indicates that the epoxy coating could not provide sufficient anti-corrosion properties for welded joint, while improved performance was observed in the coatings incorporated with GNP and C60. However, the addition of CNTs has reduced the barrier properties as confirmed by decreased impedance and phase angle values.

Improved wear resistance was observed in the specimen coated with CNT-Epoxy and C60-Epoxy coatings. The falling sand test results indicated that the wear resistance increased 2 and 2.5 times by incorporating CNT and C60 in the epoxy, correspondingly. Meanwhile, the GNP-Epoxy coating showed moderate enhancement, and the thickness loss was reduced by 40% compared with the neat epoxy.

CHAPTER 11. EDUCATION AND OUTREACH ACTIVITIES

11.1 DISSEMINATION OF THE PROJECT

As critical portion of this study, we actively disseminate the research findings in pipeline community through national and international conferences. For instance, as illustrated in Fig. 11.1, Dr. Lin attended the national conference: American Society of Civil Engineers (ASCE) Pipeline 2017 at Phoenix, AZ, August 6-9, where he has chaired one conference session and also presented the group study related to this project. Also, Dr. Lin attended the national conference: **SPIE-Smart Structures + Nondestructive Evaluation**, at Denver, Colorado, March 4-8, 2018, where he presented the group study related to this project. In 2019, Dr. Lin was invited to give a talk, entitled "*Design and Characterization of Functional Nanoengineered Epoxy-Resin Coatings for Pipeline Corrosion Control* ". in the conference, **Coating Trends and Technologies 2019**, at Rosemont, IL, Sept. 10-11, 2019, where he presented the group study on the new coating development and characterization for oil/gas pipeline corrosion control (see Fig. 11.2).

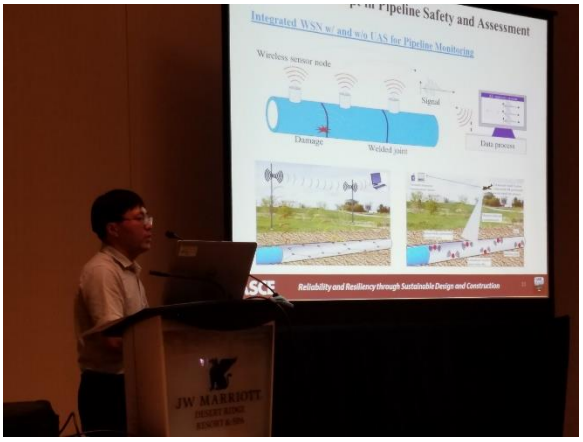

Figure 11.1: ASCE Pipeline conference session chair and presentation at Phonix, US. (Aug., 2017)

Figure 11.2: Dr. Lin gave an invited talk on the national coating conference in Rosemont, IL, on Sept. 10th, 2019

Two graduate students, Matthew Pearson and Xingyu Wang (see Fig. 11.3), participated in the poster session in the ***ND EPSCoR 2018 State Conference*** in Grand Forks, ND, at April 17, 2018 (the poster with acknowledgment to USDOT CAAP support). Since North Dakota has become the

second-leading oil-producing state in the nation and pipeline is used as one major liquid transportation, the study of this project associated with effective corrosion control of pipeline raised much attention from audience in a broader field of public, government, and industry pipeline stakeholders.

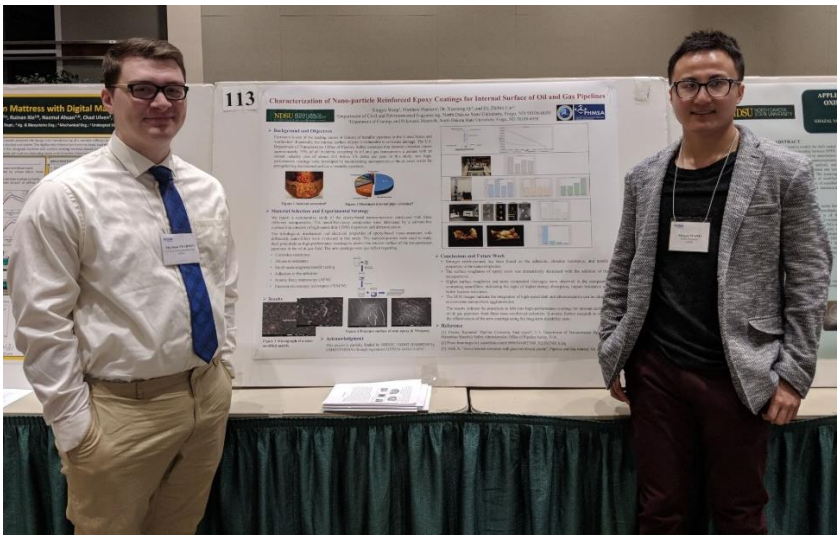

Figure 11.3: MS student Matthew Pearson (left) and PhD student Xingyu Wang (right) attended and presented their US DOT CAAP project in poster session in ND EPSCoR 2018 State Conference in Grand Forks, April 17th, 2018

11.2 OUTRACH ACITIVIES ASSOCIATED WITH THE PROJECT

Dr. Lin has a strong record of participating in outreach programs. Dr. Lin has mentored over eight high school students in the ND Governor's High School program and engaged them in this project for past three years. The summary of the activities is briefly concluded below:

11.2.1 High school student outreach program in 2017

In summer 2017, two high school female students, Joelle Sherlock and Desiree Parsons, from North Dakota Governor's Schools program were invited to have five-week to experience the research in our research group, as shown in Fig. 11.4. They worked with our graduate students for coating processing, including two different epoxy resin and curing agent pairs mixing, and on how to spray on steel plates, and evaluation of coating performance on environmental chamber using basic weight loss. During these weeks, students gained ideas of the corrosion behaviors of metallic materials and conduct experiments in the lab. The outreach was be unique to disseminate our research and foster the next-generation engineers to gain better understanding of the science and material, and could motivate them to pursue this area in their future career.

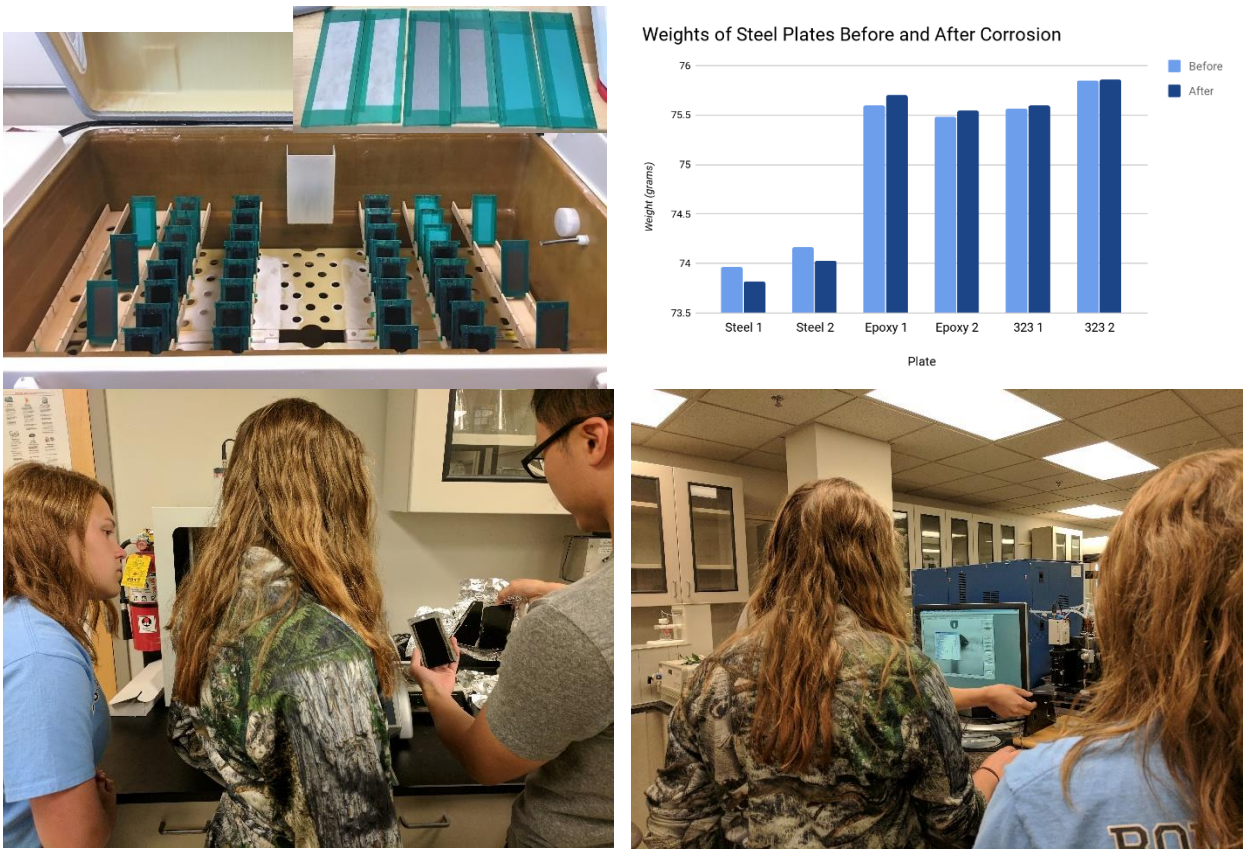

Figure 11.4: High school students participating in our research in 2017

11.2.2 High school student outreach program in 2018

In summer 2018, as illustrated in Figs. 11.5-11.6, four high school students, Josh Gronneberg, Natlie Lemnus, Olivia Svanes and Julia Bauroth from North Dakota Governor's Schools program were recruited in a six-week research in Dr. Lin's group. North Dakota Governor's Schools is a residential program for scholastically motivated North Dakota high school sophomores and juniors. Both lecture and experiment work were conducted for the student to learn the nanoparticle modified coating synthesis, and the corrosion behaviors of metallic materials. Toward the end of the outreach, the high-school students gained better understanding of the science and material through the presentation and poster. They were motivated in STEM career.

Figure 11.5: Four high school students with the graduate student (from left to right: Julia Bauroth, Josh Gronneberg, Xingyu Wang, Olivia Svanes and Natlie Lemnus) in Dr. Lin's research group for preparing coating samples and performing tests

Figure 11.6: High school students presented their work when in Dr. Lin's research group

11.2.2 High school student outreach program in 2019

Continuous efforts in this project were to recruit high-school students each summer to work in the pipeline research and foster their interest in this field. In this summer, Dr. Lin's group recruited two high school students, Isak Harmon and John Goeres, from North Dakota Governor's Schools program (see Fig. 11.7). These two students worked with the graduate students Muhammad Metla, Zi Zhang and Matthew Pearson by participating in the USDOT PHMA to learn the nanoparticle modified coating synthesis, and the corrosion behaviors of metallic materials. This outreach could motivate them to pursue the pipeline safety and corrosion control area in their future career.

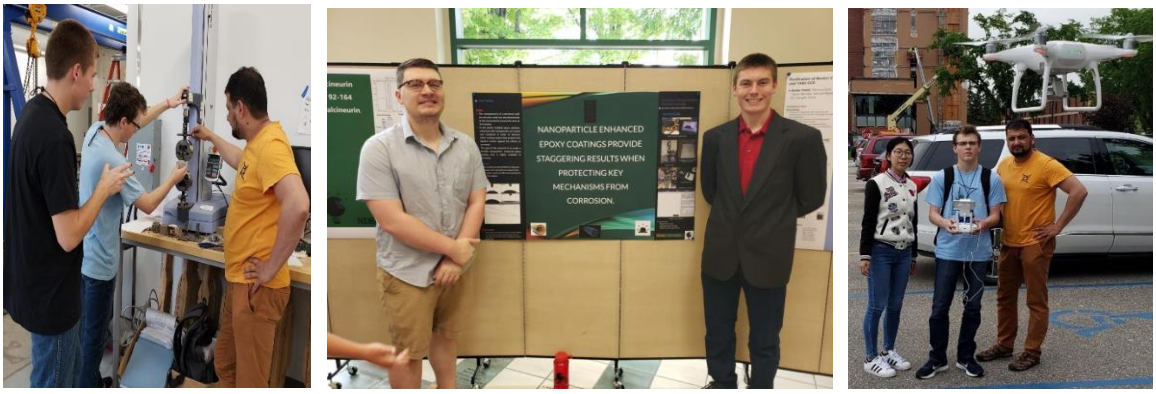

Figure 11.7: Students working at the outreach program: Muhammad Metla, Isak Harmon, John Goeres, Matthew Pearson, and Zi Zhang

CHAPTER 12. CONCLUSIONS

Despite great efforts in polymeric coatings in pipeline industry, premature failures of these coatings often cause pipe corrosion. High-performance composite coatings by incorporation of nanomaterials are recently emerging multifunctional materials. In this project, we provided new insights into developing new high-performance nanocomposite coatings for strengthening the corrosion resistance of metallic pipelines. Three nanoparticles: carbon nanotubes (CNT), graphene nanoplatelets (GNP) and nano-silica (NS), were used as nanofillers for synthesizing epoxy-based nanocomposites. The new nano-modified composite coatings were systematically quantified to understand the link of tribological, mechanical, and electrical properties of the nanocomposites.

For single & hybrid filler nanocomposites, even literature reviews demonstrated that the investigations on these nanofiller/polymer composites, due to widely varied composite designs, different dispersion procedures, and experiment methods, limited and inconsistent conclusions could be made that hindered evaluating the effects of various nanofillers on their tribological, mechanical and electrochemical performance. As a result, without a comparative experiment design and consistent criteria, there was no clear information available to guide scientists and engineers on how to properly select different nanofillers and how to effectively design promising nanocomposites. Especially when specific properties are desired, this report is an opportunity to make a comparison between additives by taking the advantage of experimental results.

By understanding of single and hybrid nanofiller reinforced coatings, we develop the new, robust, high-performance coatings, striving for excellent solution for the internal surface of oil & gas pipelines. According to the experimental study, the new high-performance coating has a significant advantage over existing coatings when tailored to provide multifunctional protection for extended long-term pipeline performance against corrosion fouling-wear issues, which cannot be offered by other systems in the market.

Results revealed that the integration of these reinforcements had improved the coating's overall performance, as the coating consisted of outstanding anti-corrosion performance, wear resistance, mechanical strength, water-repellency property, and damage tolerance. Moreover, the facile fabrication method and simple application procedure exhibited its potential toward large-scale commercialization for metallic infrastructures.

By investigating the performance and micro/nano level characterization, the research offered an opportunity to understand the relationship between the deposition parameters and the coating functionality, the mechanical properties of the coating will be. The research work comparatively evaluates the influence of these nanofillers on nano-reinforcement, primarily, an experimental investigation of the tribological, mechanical and electrochemical properties.

Furthermore, this research work offered an excellent solution for mitigating corrosion and understanding the performance of advanced materials and practical guidelines for their implementation in the durability of civil infrastructure. The proposed study will also overcome the limitations of existing methods and the research findings can significantly benefit civil engineering fabricators, designers, and contractors, States and U.S. department of transportations.

In summary, the highlights of this research work include:

(a) New high-performance nanocomposite coatings exhibited superior anti-corrosion resistance, water-repellency, mechanical and tribological properties, thereby enabling protecting metallic oil/gas pipelines in long term.

(b) A systematic experimental and analytical investigation used for the development and characterization of nano-modified high-performance composite coatings provide scientists and engineers with the opportunity to select different nanofillers and design promising nanocomposites effectively properly.

Reference

[1] V. N. Mochalin and Y. Gogotsi, "Nanodiamond–polymer composites," *Diam. Relat. Mater.*, vol. 58, pp. 161–171, 2015.

[2] X.-L. Xie, Y.-W. Mai, and X.-P. Zhou, "Dispersion and alignment of carbon nanotubes in polymer matrix: a review," *Mater. Sci. Eng. R Rep.*, vol. 49, no. 4, pp. 89–112, 2005.

[3] S. Shadlou, E. Alishahi, and M. Ayatollahi, "Fracture behavior of epoxy nanocomposites reinforced with different carbon nano-reinforcements," *Compos. Struct.*, vol. 95, pp. 577–581, 2013.

[4] J. N. Coleman, U. Khan, W. J. Blau, and Y. K. Gun'ko, "Small but strong: a review of the mechanical properties of carbon nanotube–polymer composites," *Carbon*, vol. 44, no. 9, pp. 1624–1652, 2006.

[5] V. Singh, D. Joung, L. Zhai, S. Das, S. I. Khondaker, and S. Seal, "Graphene based materials: past, present and future," *Prog. Mater. Sci.*, vol. 56, no. 8, pp. 1178–1271, 2011.

[6] S. G. Miller *et al.*, "Characterization of epoxy functionalized graphite nanoparticles and the physical properties of epoxy matrix nanocomposites," *Compos. Sci. Technol.*, vol. 70, no. 7, pp. 1120–1125, 2010.

[7] M. Ayatollahi, E. Alishahi, S. Doagou-R, and S. Shadlou, "Tribological and mechanical properties of low content nanodiamond/epoxy nanocomposites," *Compos. Part B Eng.*, vol. 43, no. 8, pp. 3425–3430, 2012.

[8] A. T. Dideikin, "Applications of Detonation Nanodiamonds," *Detonation Nanodiamonds Sci. Appl.*, p. 239, 2014.

[9] J.-L. Tsai and T.-C. Lu, "Investigating the load transfer efficiency in carbon nanotubes reinforced nanocomposites," *Compos. Struct.*, vol. 90, no. 2, pp. 172–179, 2009.

[10] G. Zhang, J. Karger-Kocsis, and J. Zou, "Synergetic effect of carbon nanofibers and short carbon fibers on the mechanical and fracture properties of epoxy resin," *Carbon*, vol. 48, no. 15, pp. 4289–4300, 2010.

[11] J. R. Potts, D. R. Dreyer, C. W. Bielawski, and R. S. Ruoff, "Graphene-based polymer nanocomposites," *Polymer*, vol. 52, no. 1, pp. 5–25, 2011.

[12] X. Wang, H. Yang, L. Song, Y. Hu, W. Xing, and H. Lu, "Morphology, mechanical and thermal properties of graphene-reinforced poly (butylene succinate) nanocomposites," *Compos. Sci. Technol.*, vol. 72, no. 1, pp. 1–6, 2011.

[13] V. Georgakilas, J. A. Perman, J. Tucek, and R. Zboril, "Broad family of carbon nanoallotropes: classification, chemistry, and applications of fullerenes, carbon dots, nanotubes, graphene, nanodiamonds, and combined superstructures," *Chem. Rev.*, vol. 115, no. 11, pp. 4744–4822, 2015.

[14] J. Slonczewski and P. Weiss, "Band structure of graphite," *Phys. Rev.*, vol. 109, no. 2, p. 272, 1958.

[15] K. S. Novoselov *et al.*, "Electric field effect in atomically thin carbon films," *science*, vol. 306, no. 5696, pp. 666–669, 2004.

[16] A. A. Balandin *et al.*, "Superior thermal conductivity of single-layer graphene," *Nano Lett.*, vol. 8, no. 3, pp. 902–907, 2008.

[17] C. Lee, X. Wei, J. W. Kysar, and J. Hone, "Measurement of the elastic properties and intrinsic strength of monolayer graphene," *science*, vol. 321, no. 5887, pp. 385–388, 2008.

[18] S. Liu, L. Gu, H. Zhao, J. Chen, and H. Yu, "Corrosion resistance of graphene-reinforced waterborne epoxy coatings," *J. Mater. Sci. Technol.*, vol. 32, no. 5, pp. 425–431, 2016.
[19] K.-C. Chang *et al.*, "Room-temperature cured hydrophobic epoxy/graphene composites as corrosion inhibitor for cold-rolled steel," *Carbon*, vol. 66, pp. 144–153, 2014.
[20] Y.-H. Yu, Y.-Y. Lin, C.-H. Lin, C.-C. Chan, and Y.-C. Huang, "High-performance polystyrene/graphene-based nanocomposites with excellent anti-corrosion properties," *Polym. Chem.*, vol. 5, no. 2, pp. 535–550, 2014.
[21] T. Monetta, A. Acquesta, and F. Bellucci, "Graphene/epoxy coating as multifunctional material for aircraft structures," *Aerospace*, vol. 2, no. 3, pp. 423–434, 2015.
[22] M. S. Dresselhaus, A. Jorio, M. Hofmann, G. Dresselhaus, and R. Saito, "Perspectives on carbon nanotubes and graphene Raman spectroscopy," *Nano Lett.*, vol. 10, no. 3, pp. 751–758, 2010.
[23] H. Jeon, J. Park, and M. Shon, "Corrosion protection by epoxy coating containing multi-walled carbon nanotubes," *J. Ind. Eng. Chem.*, vol. 19, no. 3, pp. 849–853, 2013.
[24] F. Zhang *et al.*, "Superhydrophobic carbon nanotubes/epoxy nanocomposite coating by facile one-step spraying," *Surf. Coat. Technol.*, vol. 341, pp. 15–23, 2018.
[25] L.-J. Cui *et al.*, "Effect of functionalization of multi-walled carbon nanotube on the curing behavior and mechanical property of multi-walled carbon nanotube/epoxy composites," *Mater. Des.*, vol. 49, pp. 279–284, 2013.
[26] J. Wernik and S. Meguid, "On the mechanical characterization of carbon nanotube reinforced epoxy adhesives," *Mater. Des.*, vol. 59, pp. 19–32, 2014.
[27] M. Zabet, S. Moradian, Z. Ranjbar, and N. Zanganeh, "Effect of carbon nanotubes on electrical and mechanical properties of multiwalled carbon nanotubes/epoxy coatings," *J. Coat. Technol. Res.*, vol. 13, no. 1, pp. 191–200, 2016.
[28] A. Hernández-Pérez, F. Avilés, A. May-Pat, A. Valadez-González, P. Herrera-Franco, and P. Bartolo-Pérez, "Effective properties of multiwalled carbon nanotube/epoxy composites using two different tubes," *Compos. Sci. Technol.*, vol. 68, no. 6, pp. 1422–1431, 2008.
[29] S. Palraj, M. Selvaraj, K. Maruthan, and G. Rajagopal, "Corrosion and wear resistance behavior of nano-silica epoxy composite coatings," *Prog. Org. Coat.*, vol. 81, pp. 132–139, 2015.
[30] M. Conradi, A. Kocijan, M. Zorko, and I. Verpoest, "Damage resistance and anticorrosion properties of nanosilica-filled epoxy-resin composite coatings," *Prog. Org. Coat.*, vol. 80, pp. 20–26, 2015.
[31] Y. Kang, X. Chen, S. Song, L. Yu, and P. Zhang, "Friction and wear behavior of nanosilica-filled epoxy resin composite coatings," *Appl. Surf. Sci.*, vol. 258, no. 17, pp. 6384–6390, 2012.
[32] M. Conradi, A. Kocijan, D. Kek-Merl, M. Zorko, and I. Verpoest, "Mechanical and anticorrosion properties of nanosilica-filled epoxy-resin composite coatings," *Appl. Surf. Sci.*, vol. 292, pp. 432–437, 2014.
[33] S. Halder, P. Ghosh, M. Goyat, and S. Ray, "Ultrasonic dual mode mixing and its effect on tensile properties of SiO2-epoxy nanocomposite," *J. Adhes. Sci. Technol.*, vol. 27, no. 2, pp. 111–124, 2013.
[34] B. Johnsen, A. Kinloch, R. Mohammed, A. Taylor, and S. Sprenger, "Toughening mechanisms of nanoparticle-modified epoxy polymers," *Polymer*, vol. 48, no. 2, pp. 530–541, 2007.

[35] M. Nuruddin, M. Hosur, R. Gupta, G. Hosur, A. Tcherbi-Narteh, and S. Jeelani, “Cellulose Nanofibers-Graphene Nanoplatelets Hybrids Nanofillers as High-Performance Multifunctional Reinforcements in Epoxy Composites,” *Polym. Polym. Compos.*, vol. 25, no. 4, p. 273, 2017.
[36] L. Yue, G. Pircheraghi, S. A. Monemian, and I. Manas-Zloczower, “Epoxy composites with carbon nanotubes and graphene nanoplatelets–Dispersion and synergy effects,” *Carbon*, vol. 78, pp. 268–278, 2014.
[37] L. Zhai, G. Ling, and Y. Wang, “Effect of nano-Al2O3 on adhesion strength of epoxy adhesive and steel,” *Int. J. Adhes. Adhes.*, vol. 28, no. 1–2, pp. 23–28, 2008.
[38] L. Zhai, G. Ling, J. Li, and Y. Wang, “The effect of nanoparticles on the adhesion of epoxy adhesive,” *Mater. Lett.*, vol. 60, no. 25–26, pp. 3031–3033, 2006.
[39] M. May, H. Wang, and R. Akid, “Effects of the addition of inorganic nanoparticles on the adhesive strength of a hybrid sol–gel epoxy system,” *Int. J. Adhes. Adhes.*, vol. 30, no. 6, pp. 505–512, 2010.
[40] T. Kuilla, S. Bhadra, D. Yao, N. H. Kim, S. Bose, and J. H. Lee, “Recent advances in graphene based polymer composites,” *Prog. Polym. Sci.*, vol. 35, no. 11, pp. 1350–1375, 2010.
[41] W. Zheng, X. Lu, and S.-C. Wong, “Electrical and mechanical properties of expanded graphite-reinforced high-density polyethylene,” *J. Appl. Polym. Sci.*, vol. 91, no. 5, pp. 2781–2788, 2004.
[42] M. A. Aldosari, A. A. Othman, and E. H. Alsharaeh, “Synthesis and characterization of the in situ bulk polymerization of PMMA containing graphene sheets using microwave irradiation,” *Molecules*, vol. 18, no. 3, pp. 3152–3167, 2013.
[43] K. Kalaitzidou, H. Fukushima, and L. T. Drzal, “A new compounding method for exfoliated graphite–polypropylene nanocomposites with enhanced flexural properties and lower percolation threshold,” *Compos. Sci. Technol.*, vol. 67, no. 10, pp. 2045–2051, 2007.
[44] B. Pan, J. Zhao, Y. Zhang, and Y. Zhang, “Wear performance and mechanisms of polyphenylene sulfide/polytetrafluoroethylene wax composite coatings reinforced by graphene,” *J. Macromol. Sci. Part B*, vol. 51, no. 6, pp. 1218–1227, 2012.
[45] I. Neitzel, V. Mochalin, I. Knoke, G. R. Palmese, and Y. Gogotsi, “Mechanical properties of epoxy composites with high contents of nanodiamond,” *Compos. Sci. Technol.*, vol. 71, no. 5, pp. 710–716, 2011.
[46] S. Roy, K. Mitra, C. Desai, R. Petrova, and S. Mitra, “Detonation nanodiamonds and carbon nanotubes as reinforcements in epoxy composites—a comparative study,” *J. Nanotechnol. Eng. Med.*, vol. 4, no. 1, p. 011008, 2013.
[47] J. Liang *et al.*, “Molecular-level dispersion of graphene into poly (vinyl alcohol) and effective reinforcement of their nanocomposites,” *Adv. Funct. Mater.*, vol. 19, no. 14, pp. 2297–2302, 2009.
[48] K.-C. Chang *et al.*, “Room-temperature cured hydrophobic epoxy/graphene composites as corrosion inhibitor for cold-rolled steel,” *Carbon*, vol. 66, pp. 144–153, 2014.
[49] W. Ji *et al.*, “Composite coating with synergistic effect of biomimetic epoxy thermoset morphology and incorporated superhydrophobic silica for corrosion protection,” *Express Polym. Lett.*, vol. 10, no. 11, p. 950, 2016.
[50] S. Ammar *et al.*, “Studies on SiO2-hybrid polymeric nanocomposite coatings with superior corrosion protection and hydrophobicity,” *Surf. Coat. Technol.*, vol. 324, pp. 536–545, 2017.

[51] A. Romo-Uribe, J. A. Arcos-Casarrubias, A. Reyes-Mayer, and R. Guardian-Tapia, “PDMS Nanodomains in DGEBA Epoxy Induce High Flexibility and Toughness,” *Polym.-Plast. Technol. Eng.*, vol. 56, no. 1, pp. 96–107, 2017.
[52] X. Cui *et al.*, “Polydimethylsiloxane-titania nanocomposite coating: Fabrication and corrosion resistance,” *Polymer*, vol. 138, pp. 203–210, 2018.
[53] M. S. Selim *et al.*, “Recent progress in marine foul-release polymeric nanocomposite coatings,” *Prog. Mater. Sci.*, vol. 87, pp. 1–32, 2017.
[54] S. Ammar, K. Ramesh, B. Vengadaesvaran, S. Ramesh, and A. K. Arof, “Amelioration of anticorrosion and hydrophobic properties of epoxy/PDMS composite coatings containing nano ZnO particles,” *Prog. Org. Coat.*, vol. 92, pp. 54–65, 2016.
[55] S. Rath *et al.*, “Coatings of PDMS-modified epoxy via urethane linkage: Segmental correlation length, phase morphology, thermomechanical and surface behavior,” *Prog. Org. Coat.*, vol. 65, no. 3, pp. 366–374, 2009.
[56] H. Wang *et al.*, “Facile preparation of superamphiphobic epoxy resin/modified poly (vinylidene fluoride)/fluorinated ethylene propylene composite coating with corrosion/wear-resistance,” *Appl. Surf. Sci.*, vol. 357, pp. 229–235, 2015.
[57] Z. Chu and S. Seeger, “Superamphiphobic surfaces,” *Chem. Soc. Rev.*, vol. 43, no. 8, pp. 2784–2798, 2014.
[58] T. Li, M. Paliy, X. Wang, B. Kobe, W.-M. Lau, and J. Yang, “Facile One-Step Photolithographic Method for Engineering Hierarchically Nano/Microstructured Transparent Superamphiphobic Surfaces,” *ACS Appl. Mater. Interfaces*, vol. 7, no. 20, pp. 10988–10992, 2015.
[59] J. Li *et al.*, “Facile fabrication of translucent superamphiphobic coating on paper to prevent liquid pollution,” *Chem. Eng. J.*, vol. 246, pp. 238–243, 2014.
[60] A. K. Kota, W. Choi, and A. Tuteja, “Superomniphobic surfaces: design and durability,” *MRS Bull.*, vol. 38, no. 5, pp. 383–390, 2013.
[61] K. Liu, Y. Tian, and L. Jiang, “Bio-inspired superoleophobic and smart materials: design, fabrication, and application,” *Prog. Mater. Sci.*, vol. 58, no. 4, pp. 503–564, 2013.
[62] Z. Xue, M. Liu, and L. Jiang, “Recent developments in polymeric superoleophobic surfaces,” *J. Polym. Sci. Part B Polym. Phys.*, vol. 50, no. 17, pp. 1209–1224, 2012.
[63] B. Ge, Z. Zhang, X. Men, X. Zhu, and X. Zhou, “Sprayed superamphiphobic coatings on copper substrate with enhanced corrosive resistance,” *Appl. Surf. Sci.*, vol. 293, pp. 271–274, 2014.
[64] S. Pourhashem, M. R. Vaezi, and A. Rashidi, “Investigating the effect of SiO2-graphene oxide hybrid as inorganic nanofiller on corrosion protection properties of epoxy coatings,” *Surf. Coat. Technol.*, vol. 311, pp. 282–294, 2017.
[65] A. Ghanbari and M. Attar, “A study on the anticorrosion performance of epoxy nanocomposite coatings containing epoxy-silane treated nano-silica on mild steel substrate,” *J. Ind. Eng. Chem.*, vol. 23, pp. 145–153, 2015.
[66] G. Shen, Y. Chen, L. Lin, C. Lin, and D. Scantlebury, “Study on a hydrophobic nano-TiO2 coating and its properties for corrosion protection of metals,” *Electrochimica Acta*, vol. 50, no. 25–26, pp. 5083–5089, 2005.
[67] X. Wang, X. Qi, Z. Lin, J. Wang, and N. Gong, “Electrochemical Characterization of the Soils Surrounding Buried or Embedded Steel Elements,” in *Pipelines 2016*, pp. 110–116.

[68] S. Ammar, K. Ramesh, B. Vengadaesvaran, S. Ramesh, and A. K. Arof, "A novel coating material that uses nano-sized SiO2 particles to intensify hydrophobicity and corrosion protection properties," *Electrochimica Acta*, vol. 220, pp. 417–426, 2016.
[69] S. Qiu, C. Chen, W. Zheng, W. Li, H. Zhao, and L. Wang, "Long-term corrosion protection of mild steel by epoxy coating containing self-doped polyaniline nanofiber," *Synth. Met.*, vol. 229, pp. 39–46, 2017.
[70] L. Yin, Y. Wang, J. Ding, Q. Wang, and Q. Chen, "Water condensation on superhydrophobic aluminum surfaces with different low-surface-energy coatings," *Appl. Surf. Sci.*, vol. 258, no. 8, pp. 4063–4068, 2012.
[71] C.-H. Xue, S.-T. Jia, J. Zhang, L.-Q. Tian, H.-Z. Chen, and M. Wang, "Preparation of superhydrophobic surfaces on cotton textiles," *Sci. Technol. Adv. Mater.*, vol. 9, no. 3, p. 035008, 2008.
[72] A. Das, T. A. Farnham, S. Bengaluru Subramanyam, and K. K. Varanasi, "Designing Ultra-Low Hydrate Adhesion Surfaces by Interfacial Spreading of Water-Immiscible Barrier Films," *ACS Appl. Mater. Interfaces*, 2017.
[73] J. Dong *et al.*, "Colorful superamphiphobic coatings with low sliding angles and high durability based on natural nanorods," *ACS Appl. Mater. Interfaces*, vol. 9, no. 2, pp. 1941–1952, 2017.
[74] Y. Wang and B. Bhushan, "Wear-resistant and antismudge superoleophobic coating on polyethylene terephthalate substrate using SiO2 nanoparticles," *ACS Appl. Mater. Interfaces*, vol. 7, no. 1, pp. 743–755, 2014.
[75] K. Jagadish, S. Srikantaswamy, K. Byrappa, L. Shruthi, and M. R. Abhilash, "Dispersion of multiwall carbon nanotubes in organic solvents through hydrothermal supercritical condition," *J. Nanomater.*, vol. 16, no. 1, p. 320, 2015.
[76] M. Kaszuba, D. McKnight, M. T. Connah, F. K. McNeil-Watson, and U. Nobbmann, "Measuring sub nanometre sizes using dynamic light scattering," *J. Nanoparticle Res.*, vol. 10, no. 5, pp. 823–829, 2008.
[77] Y.-J. Wan *et al.*, "Improved dispersion and interface in the graphene/epoxy composites via a facile surfactant-assisted process," *Compos. Sci. Technol.*, vol. 82, pp. 60–68, 2013.
[78] D. Liu, W. Zhao, S. Liu, Q. Cen, and Q. Xue, "Comparative tribological and corrosion resistance properties of epoxy composite coatings reinforced with functionalized fullerene C60 and graphene," *Surf. Coat. Technol.*, vol. 286, pp. 354–364, 2016.
[79] B. Ramezanzadeh, Z. Haeri, and M. Ramezanzadeh, "A facile route of making silica nanoparticles-covered graphene oxide nanohybrids (SiO2-GO); fabrication of SiO2-GO/epoxy composite coating with superior barrier and corrosion protection performance," *Chem. Eng. J.*, vol. 303, pp. 511–528, 2016.
[80] A. Alizadeh Sahraei, M. Ayati, M. Baniassadi, D. Rodrigue, M. Baghani, and Y. Abdi, "AC and DC electrical behavior of MWCNT/epoxy nanocomposite near percolation threshold: Equivalent circuits and percolation limits," *J. Appl. Phys.*, vol. 123, no. 10, p. 105109, 2018.
[81] B. Ramezanzadeh, M. Attar, and M. Farzam, "A study on the anticorrosion performance of the epoxy–polyamide nanocomposites containing ZnO nanoparticles," *Prog. Org. Coat.*, vol. 72, no. 3, pp. 410–422, 2011.
[82] M. May, H. Wang, and R. Akid, "Effects of the addition of inorganic nanoparticles on the adhesive strength of a hybrid sol–gel epoxy system," *Int. J. Adhes. Adhes.*, vol. 30, no. 6, pp. 505–512, 2010.

[83] L. Yue, G. Pircheraghi, S. A. Monemian, and I. Manas-Zloczower, “Epoxy composites with carbon nanotubes and graphene nanoplatelets–Dispersion and synergy effects,” *Carbon*, vol. 78, pp. 268–278, 2014.
[84] D. Xiang, L. Wang, Y. Tang, E. Harkin-Jones, C. Zhao, and Y. Li, “Processing-property relationships of biaxially stretched binary carbon nanofiller reinforced high density polyethylene nanocomposites,” *Mater. Lett.*, vol. 209, pp. 551–554, 2017.
[85] K. Yu, M. Wang, K. Qian, X. Lu, and J. Sun, “The synergy effect of Graphene/SiO 2 hybrid materials on reinforcing and toughening epoxy resin,” *Fibers Polym.*, vol. 17, no. 3, pp. 453–459, 2016.
[86] J. Li *et al.*, “Facile fabrication of translucent superamphiphobic coating on paper to prevent liquid pollution,” *Chem. Eng. J.*, vol. 246, pp. 238–243, 2014.
[87] K. Yang, M. Gu, and Y. Jin, “Cure behavior and thermal stability analysis of multiwalled carbon nanotube/epoxy resin nanocomposites,” *J. Appl. Polym. Sci.*, vol. 110, no. 5, pp. 2980–2988, 2008.
[88] W. Fan, W. Du, Z. Li, N. Dan, and J. Huang, “Abrasion resistance of waterborne polyurethane films incorporated with PU/silica hybrids,” *Prog. Org. Coat.*, vol. 86, pp. 125–133, 2015.
[89] M. Daniels and L. Francis, “Silane adsorption behavior, microstructure, and properties of glycidoxypropyltrimethoxysilane-modified colloidal silica coatings,” *J. Colloid Interface Sci.*, vol. 205, no. 1, pp. 191–200, 1998.
[90] J. Yu, W. Zhao, G. Liu, Y. Wu, and D. Wang, “Anti-corrosion mechanism of 2D nanosheet materials in waterborne epoxy coatings,” *Surf. Topogr. Metrol. Prop.*, vol. 6, no. 3, p. 034019, 2018.
[91] Y. Tong, S. Bohm, and M. Song, “The capability of graphene on improving the electrical conductivity and anti-corrosion properties of Polyurethane coatings,” *Appl. Surf. Sci.*, vol. 424, pp. 72–81, 2017.
[92] A. C. C. de Leon, R. B. Pernites, and R. C. Advincula, “Superhydrophobic colloidally textured polythiophene film as superior anticorrosion coating,” *ACS Appl. Mater. Interfaces*, vol. 4, no. 6, pp. 3169–3176, 2012.
[93] X. Wang, M. Pearson, H. Pan, M. Li, Z. Zhang, and Z. Lin, “Nano-modified functional composite coatings for metallic structures: Part I-Electrochemical and barrier behavior,” *Surf. Coat. Technol.*, p. 126286, 2020, doi: https://doi.org/10.1016/j.surfcoat.2020.126286.
[94] X. Wang, F. Tang, X. Qi, Z. Lin, D. Battocchi, and X. Chen, “Enhanced Protective Coatings Based on Nanoparticle fullerene C60 for Oil & Gas Pipeline Corrosion Mitigation,” *Nanomaterials*, vol. 9, no. 10, p. 1476, 2019.
[95] E. Alishahi, S. Shadlou, S. Doagou-R, and M. R. Ayatollahi, “Effects of carbon nanoreinforcements of different shapes on the mechanical properties of epoxy-based nanocomposites,” *Macromol. Mater. Eng.*, vol. 298, no. 6, pp. 670–678, 2013.
[96] H. Wagner, O. Lourie, Y. Feldman, and R. Tenne, “Stress-induced fragmentation of multiwall carbon nanotubes in a polymer matrix,” *Appl. Phys. Lett.*, vol. 72, no. 2, pp. 188–190, 1998.
[97] P. Mukhopadhyay, R. K. Gupta, and others, “Trends and frontiers in graphene-based polymer nanocomposites,” *Plast. Eng.*, vol. 67, no. 1, pp. 32–42, 2011.